

IN VITRO 3-DIMENSIONAL MODELLING OF THE FLOW IN A HYPERTROPHIC OBSTRUCTIVE CARDIOMYOPATHIC HEART

25/06/2021

University of Twente.

Technical Medicine, Bachelor thesis

Authors:

M. Baarsma - s2113473

A. Fennema - s2113732

E. H. M. Graus - s2090481

C. B. van der Poel - s2107732

Supervisors:

Dr. F.R. Halfwerk (Technical Medicine supervisor)

Dr. M. A. Koenrades (Technical Medicine supervisor)

K. C. Smits, BSc (Technical Medicine supervisor)

Dr. R.G.H. Speekenbrink (Medical supervisor)

Ir. E.E.G. Hekman (Technical supervisor)

M. van Ochten, BSc (Personal supervisor)

In vitro 3-dimensional modelling of the flow in hypertrophic obstructive cardiomyopathic heart

M. Baarsma¹, A. Fennema¹, E. H. M. Graus¹, C. B. van der Poel¹, Dr. F.R. Halfwerk^{2,3}, Ir. E.E.G. Hekman³, Dr. M.A. Koenrades⁴, K.C. Smits², Dr. R.G.H. Speekenbrink²

Background: A Morrow procedure is performed in order to relieve the symptoms of hypertrophic obstructive cardiomyopathy (HOCM) patients. The desired thickness of the interventricular septum (IVS) is 10-11 mm, however, this is not patient-specific. Also, intraoperative determination of the IVS-thickness (IVSt) is challenging. Both factors can contribute to the over- and undertreatment of HOCM patients.

Aim: To create a set-up to determine the ideal patient-specific IVSt based on the optimal left ventricular outflow tract pressure gradient (LVOT PG) using an *in vitro* left ventricle (LV) model from a HOCM patient.

Materials and Methods: In this research segmented magnetic resonance images of the LV and aorta of a HOCM patient with an IVSt of 19 mm were used to create a mould in 3-Matic. Three virtual Morrow procedures were performed on this mould creating models with IVSt's of respectively 9, 12, and 15 mm. Afterwards, the moulds were 3-dimensional (3D) printed using a 1 mm thick Polylactic Acid layer and Ultimaker S5 3D printer. Silicone, Dragon Skin 10 NV, was used for casting the models. Next, the moulds were removed and the models were connected to a centrifugal cardiopulmonary bypass pump. A 65/35 volumetric water-glycerol mixture was used to mimic blood. A pulsatile flow was set to 4.0, 5.5, and 6.2 L/min. The LVOT PG was measured for each model using continuous-wave ultrasound. Measurements were conducted at the Medisch Spectrum Twente, Enschede, the Netherlands.

Results:

The average LVOT PGs in the models for the different thicknesses of the IVS of 9, 12, 15, and 19 mm were respectively 16.7 ± 0.87 , 17.2 ± 0.90 , 18.0 ± 0.97 , and 17.4 ± 0.76 mmHg using a flow of 4.0 L/min, 26.7 ± 0.98 , 30.7 ± 1.74 , 26.9 ± 1.68 , and 31.5 ± 2.29 mmHg using flow of a 5.5 L/min and 34.7 ± 1.78 , 32.8 ± 1.31 , 33.3 ± 2.43 , and 37.3 ± 3.43 mmHg using a flow of 6.2 L/min.

Conclusion: This research is the first step in creating a patient-specific model to determine how much tissue needs to be resected when performing the Morrow procedure based on the optimal flow. Even though early results are not yet evidential, it does show that an *in vitro* model can simulate the blood flow in HOCM patients. In future research adjustments to the model should be made with respect to the inclusion of the mitral valve, pulse settings and heart contractions.

Key words: hypertrophic obstructive cardiomyopathy, Morrow procedure, *in vitro* 3D model, left ventricular outflow tract, pressure gradient

¹ Bachelor Technical Medicine (s211343), (s2113732), (s2090481), (s2107732), TechMed Centre, University of Twente., Technohal Building, Hallenweg 5, 7522NH Enschede, The Netherlands

² Thorax Centre Twente, department of cardio-thoracic surgery, Medisch Spectrum Twente, Enschede, The Netherlands

³ Faculty of Engineering Technology (ET) and Biomechanical Engineering (BE), University of Twente, Horstring West Building, Enschede, The Netherlands

⁴ Medical 3D laboratory, Medisch Spectrum Twente, Enschede, The Netherlands

Abbreviations

3D	=	3-dimensional
ANOVA	=	Analysis of Variance
CFD	=	computational fluid dynamics
CI	=	confidence interval
CO	=	cardiac output
CPB	=	cardiopulmonary bypass
CWD	=	continuous wave doppler
DUS	=	doppler ultrasound
HCM	=	hypertrophic cardiomyopathy
HOCM	=	hypertrophic obstructive cardiomyopathy
IVS	=	interventricular septum
IVSt	=	interventricular septum thickness
LV	=	left ventricle
LVOT	=	left ventricular outflow tract
MRI	=	magnetic resonance imaging
MV	=	mitral valve
PG	=	pressure gradient
SAM	=	systolic anterior motion
SPSS	=	statistical package for the social sciences
US	=	ultrasound

Introduction

Hypertrophic obstructive cardiomyopathy (HOCM) is a genetic condition resulting in asymmetrical hypertrophy of the interventricular septum (IVS) obstructing the left ventricular outflow tract (LVOT) [1,2] (appendix I, II and III) (figure 1). This affects 1 in 500 people. Obstruction of the LVOT may result in a systolic anterior motion (SAM) of the mitral valve (MV) [1]. The anterior leaflet of the MV is pulled towards the LVOT resulting in a decreased blood flow into the aorta. Symptoms caused by the altered blood flow are dyspnoea, angina pectoris, and syncope [2] (appendix IV). HOCM is initially treated with medication, but in case this is not sufficient, a Morrow procedure (septal myectomy), or in fewer cases a septal ablation, is performed [3] (appendix V). During a Morrow procedure, the cardio-thoracic surgeon resects the IVS to a thickness of 10-11 mm [4]. However, the procedure is not optimal, because it is challenging to translate intraoperative imaging measurements of the IVS to a real-life situation [4] (appendix VI). Therefore it is difficult for the surgeon to determine the thickness intraoperatively. Also, the IVS thickness of 10-11 mm is not patient-specific, possibly resulting in over- or undertreatment.

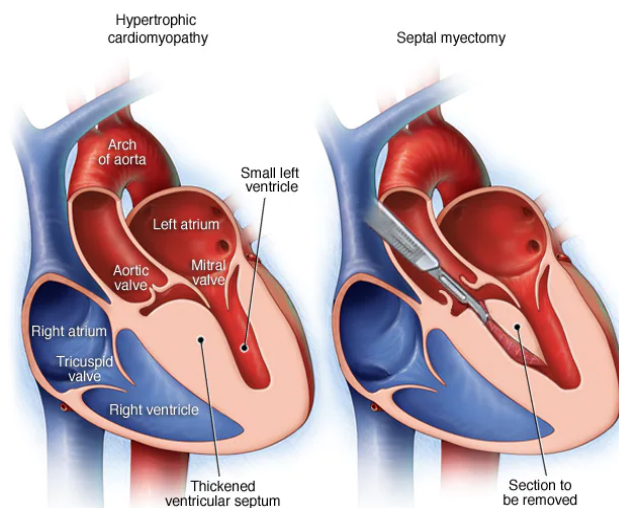


Figure 1: Left: normal IVS. Right: clinical manifestation of HOCM displaying the resection of the IVS to a thickness of 10-11 mm [5].

Overtreatment may lead to conduction abnormalities. According to research, approximately 40% of patients who underwent a Morrow procedure developed a left bundle branch block and 3% a complete heart block [6]. Overtreatment can also cause a ventricular septal defect or injury to the aortic valve in respectively 1% and 5% of the patients [7–9]. Undertreatment results in the persistence or recurrence of the complaints.

Nowadays, in some cases, a preoperatively patient-specific 3-dimensional (3D) heart model is used to reduce over- and undertreatment. A 3D model gives the surgeon better insight into the anatomy and helps planning the Morrow procedure both pre- and intraoperatively. Application of 3D models in the clinic for checking the amount of resected tissue intraoperatively [4], practising purposes [10,11], and virtual 3D planning [12], is already being researched (appendix VII).

Despite the use of patient-specific 3D heart models, it has not been investigated yet whether and how the IVS thickness should be adjusted to the specific situation of a patient. To optimize the Morrow procedure, the ideal thickness of the IVS can be determined by analyzing at which thickness the blood flow is optimal (appendix VII).

The aim of this research is to make a setup to determine what the ideal patient specific IVSt is, based on the LVOT PG using an *in vitro* left ventricle (LV) model of a HOCM patient and continuous-wave Doppler (CWD). To answer this research question, several sub-questions are formulated (appendix VIII).

Materials and method

Four in vitro LV models were connected to a flow set-up to simulate the blood flow (appendix IX). The LVOT PG in the models was measured with CWD. Values of the LVOT PG of the different models were compared and statistically analysed. The data was stored according to the data management plan (appendix X). Also troubleshooting during performing the method is described. (appendix XI)

Making the model

Four LV moulds were designed using segmented magnetic resonance imaging (MRI) images of a patient with HOCM, provided by Medisch Spectrum Twente (appendix XII). The patient was a middle-aged male who suffered from progressive dyspnoe d'effort. His IVSt was 19 mm and he had an LVOT PG of 20 mmHg at rest and 85 mmHg during exercise.

The mould designs were made in Materialise 3-Matic 15.0 (Materialise, Leuven, Belgium) and adjusted to connect the models to the Maquet HL-30 cardiopulmonary bypass (CPB) pump (Maquet, Hirrlingen, Germany) tubing (appendix XIII). A virtual Morrow procedure was executed on three moulds, reducing the IVS at its thickest point to 15, 12, and 9 mm. The moulds were then printed using an Ultimaker S5 (Ultimaker, Utrecht, The Netherlands) and Formlabs Form 3 (Formlabs, Somerville, United Kingdom) 3D printer (appendix XIV). Subsequently, the silicone models were created by casting Dragon Skin 10NV (Smooth-On Inc., Macungie, United States) silicone into the 3D-printed moulds at room temperature (23°C). The moulds were then cured for at least 24 hours at the same temperature (appendix XV). After removing the moulds, the four LV models were used for the measurements of the LVOT PG (figure 2). To test whether Dragon Skin 10 NV is suitable for casting, echoing, and to determine which thickness of silicone was optimal for the LV models, a cylinder test model was made before the heart models were designed (appendix XV).



Figure 2: The casted Dragon skin 10 NV LV model with an IVSt of 9 mm. Using coupling pieces the model is connected to $\frac{3}{8}$ tubes of the flow set-up.

Building the set-up

To simulate the blood flow in the LVOT, a set-up was used containing the LV models and a Maquet HL30 CPB pump to generate a flow (appendix XVI and XVII) (figure 3). In this research, only the centrifugal pump of the CPB pump was used.

The set-up consists of a reservoir with one litre of 65/35 volumetric water-glycerol (Thermo Fisher Scientific Inc, Waltham, US) mixture which was connected to the centrifugal pump. Here, the liquid was pumped into the system consisting of a built-in flowmeter and the LV model. This was then again connected to the reservoir. In the whole set-up, $\frac{3}{8}$ inch diameter tubes (Raumedic AG, Helmbrechts, Germany) were used. The flowmeter needed to be validated before performing any measurements (appendix XVI and XVIII).

A constant volumetric flow rate was obtained by setting the number of rotations per unit of time on the CPB pump. To mimic a physiological situation, consisting of a peak flow, the pump was set to give a pulsatile flow. This was done by setting the heart rate, and pulse height and width (appendix XIX). The LVOT PG was measured for three different conditions; a flow of 4.0, 5.5, and 6.2 L/min.

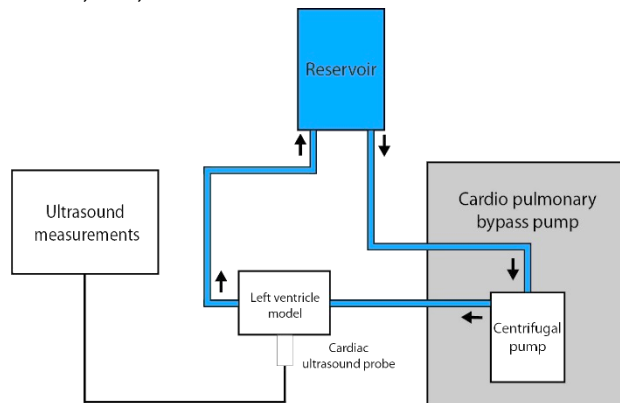


Figure 3: Schematic representation of the set-up. An HL-30 CPB pump was used to generate a pulsatile flow. Liquid, consisting of a 65/35 volumetric water-glycerol mixture, was collected in a reservoir. The LV model was connected to the CPB pump with $\frac{3}{8}$ inch tubes. LVOT PG was measured using a cardiac probe of a Philips CX50 ultrasound device.

Measuring the LVOT PG

As the degree of obstruction in the LVOT varies between the different models and with it the resistance, differences in flow could be measured. Therefore a Philips CX50 ultrasound device (Philips Ultrasound Systems, Bothell, Washington) with an S5-1 cardiac ultrasound probe was used (appendix XX). The parameter which was measured in this research is the LVOT PG. Measurements were performed on the LV model opposite to the LVOT close to the apex (appendix XIX). Colour doppler was used for locating the flow in the LVOT and CWD was then used to measure the velocities and calculate the LVOT PG (figure 4 and 5). Each researcher performed three measurements for each condition, relocating the probe in between each measurement. Each time a researcher

had performed three contiguous measurements, the LV model was disconnected and reattached to the set-up.

Data from the measurements was compared and statistically analysed with a confidence interval of 95% using IBM Statistical Package for the Social Sciences (SPSS) Statistics Version 26 (IBM, New York, United States) (appendix XXI). To check whether the data has a normal distribution the Shapiro-Wilk test was used. A paired-sample T-test test was used to calculate if a statistically significant difference between the results of the different models could be found. Additionally, one-way analysis of variance (ANOVA) tests were done to check for inter- and intraobserver variability. Results were processed in Microsoft Excel (Microsoft, Redmond, United States) to visualize the data.

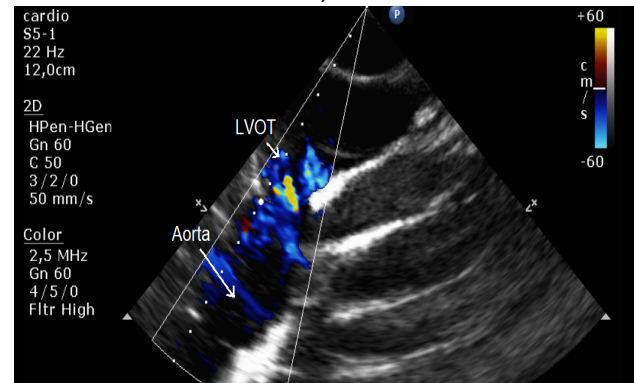


Figure 4: A colour Doppler measurement of the LV model with an IVSt of 19 mm using a flow of 6.2 L/min. It can be seen that the highest flow is present in the LVOT in comparison to the aorta.

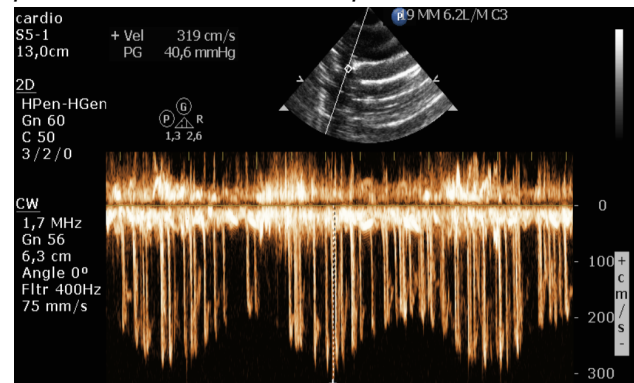


Figure 5: A continuous-wave Doppler measurement of the LV model with an IVSt of 19 mm using a flow of 6.2 L/min.

Results

Doppler ultrasound (DUS) was used to measure the LVOT PG in the different models (appendix XIX). In total, 144 measurements were performed (appendix XXII) (figure 6). The average LVOT PGs in the models for the different thicknesses of the IVS of 9, 12, 15, and 19 mm were respectively 16.7 ± 0.87 , 17.2 ± 0.90 , 18.0 ± 0.97 , and 17.4 ± 0.76 mmHg using a flow of 4.0 L/min. Using a flow of 5.5 L/min the average LVOT PGs were respectively 26.7 ± 0.98 , 30.7 ± 1.74 , 26.9 ± 1.68 , and 31.5 ± 2.29 mmHg. For a flow of 6.2 L/min average LVOT PGs of respectively 34.7 ± 1.78 , 32.8 ± 1.31 , 33.3 ± 2.43 , and 37.3 ± 3.43 mmHg were measured.

For the flow of 4.0 L/min a statistically significant difference was found between the LV models with an IVSt of 9 and 15 mm ($p=0.005$) (figure 7a). However, no statistically significant difference was found between the LV models with an IVSt of respectively 9 and 12, 9 and 19, 12 and 15, 12 and 19, and 15 and 19 mm ($p=0.235$, $p=0.066$, $p=0.062$, $p=0.409$ and $p=0.096$).

Using a flow of 5.5 L/min a statistically significant difference was found between the LV models with an IVSt of respectively 9 and 12, 9 and 19, 12 and 15, and 15 and 19 mm ($p<0.001$, $p<0.001$, $p=0.001$ and $p<0.001$) (figure 7b). However, no statistically significant difference was found between the LV models with an IVSt of respectively 9 and 15 and 12 and 19 mm this flow of 5.5 L/min ($p=0.788$ and $p=0.485$).

For the flow of 6.2 L/min, a statistically significant difference was found between respectively the LV models with an IVSt of 9 and 12, 12 and 19 and 15 and 19 mm ($p=0.016$, $p=0.001$, $p=0.001$) (figure 7c). No statistically significant difference was found between the LV models with an IVSt of respectively 9 and 15, 9 and 19 and 12 and 15 mm ($p=0.231$, $p=0.061$ and $p=0.593$).

SPSS was used to check for inter- and intraobserver variability (appendix XXIII). This resulted in no statistically significant difference in inter- and intraobserver variability for the measurements using a flow of 4.0 and 6.2 L/min. However, using a flow of 5.5 L/min a statistically significant difference could be found for the LV models with an IVSt of 12 and 15 mm.

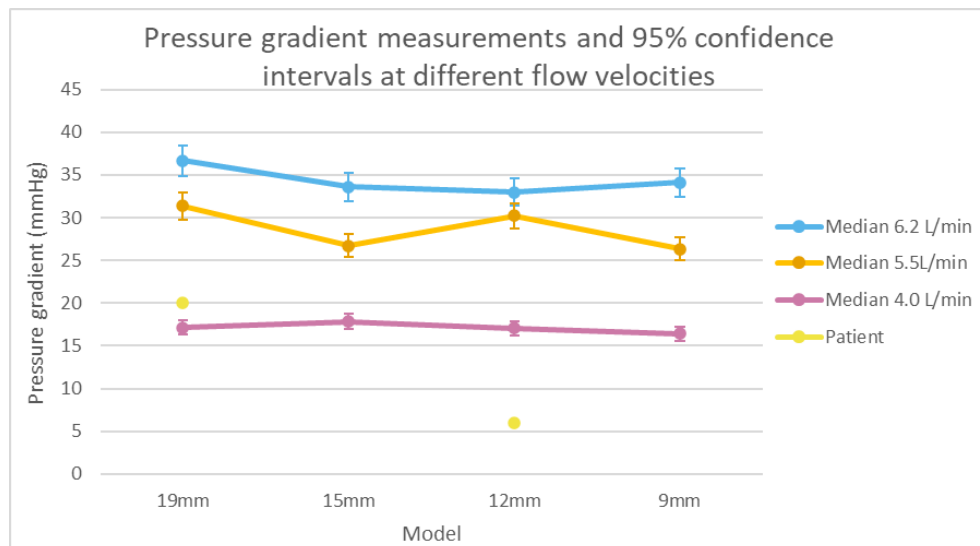


Figure 6: The median of the measured LVOT PG's of the LV models with IVSt of 19, 15, 12, and 9 mm using flows of 6.2, 5.5. and 4.0 L/min. Also, the measured LVOT PG's of the included patient pre- and post-operative are given. The 95% confidence interval (CI) is given (vertical interval at each box).

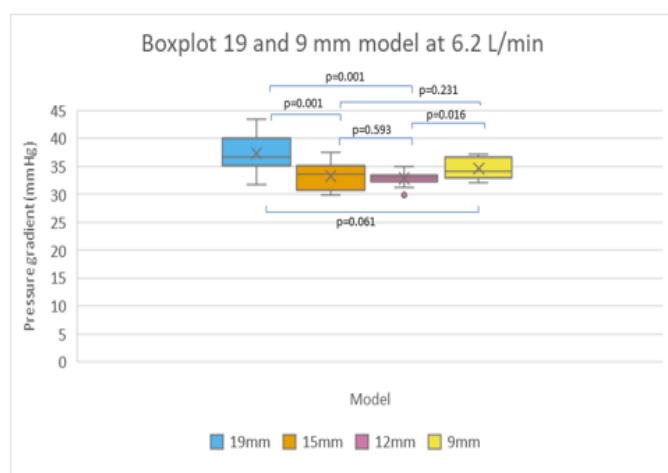
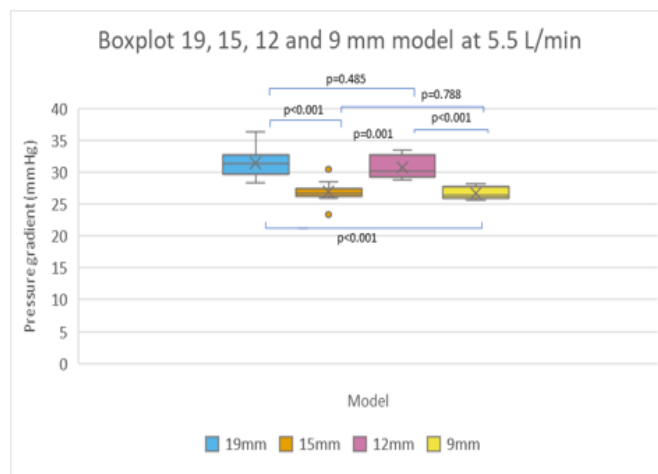
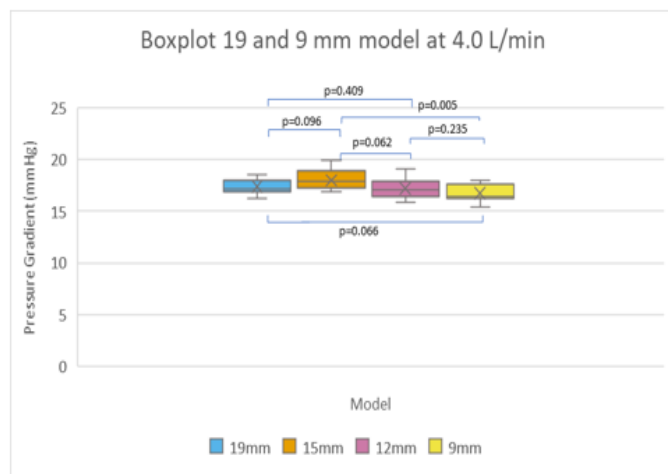


Figure 7: Boxplots of the different models used in the set-up. The plots show the standard deviation (vertical interval at each box), mean (cross in the box), median (horizontal line in the box), and outliers (dots outside of the box) of the LVOT PG measurements. a. Using a flow of 4.0 L/min b. Using a flow of 5.5 L/min. c. Using a flow of 6.2 L/min.

Discussion

Determining the optimal flow in a patient-specific model can be of great value in the treatment of HOCM. This way, the cardiothoracic surgeon can resect the amount of tissue that is optimal for the blood flow of the patient. This study can be the first step in realising this method of preoperative planning. The LV models with different IVSts have the potential to determine the optimal flow by measuring the LVOT PG.

Expectations

The LVOT PG between respectively the 15, 12, and 9 mm LV models did not decrease as much as expected. It was hypothesized that the LV models which underwent a Morrow procedure and thus have a smaller remaining IVSt would

show a lower flow velocity and lower LVOT PG. When a Morrow procedure is performed, the diameter of the LVOT will increase due to the resection of tissue.

When increasing the area of the LVOT (A_1) (m^2) the velocity in the LVOT (V_1) (m/s) and with it the LVOT PG will decrease linearly since the area (A_2) and velocity (V_2) in the LV remain constant (formula 1).

$$A_1 \cdot V_1 = A_2 \cdot V_2 \quad (\text{formula 1})$$

The clinical results of the patient show a decline in PG from 20 till 6 mmHg after the Morrow procedure. The septum was resected from 19

mm to a thickness of 12 mm. It would thus be expected that the 15, 12, and 9 mm LV models show a decrease in LVOT PG of 14 mmHg.

Explanation results

A statistical analysis was performed by making the assumption the data has a normal distribution (appendix XXII). A statistically significant difference was found between the LVOT PGs of the LV models with an IVSt of 9 and 15 mm using a flow of 4.0 L/min, 9 and 12, 9 and 19, 12 and 15, and 15 and 19 mm using a flow of 5.5 L/min and 9 and 12, 12 and 19, and 15 and 19 mm using a flow of 6.2 L/min (figure 7). This shows there is a relevant change between these models that can not be attributed to coincidence. Furthermore, errors were reduced as the protocol is strictly followed and the models are the same aside from the different Morrow incisions. However, no statistical difference was found between the measurements of the other LV models.

Reduction of the LVOT PG differed between the Morrow procedure performed by the patient and the virtual performed Morrow procedure by the LV models. The IVSt of the patient was reduced from 19 to 12 mm which caused a diminishing of the LVOT PG of 14 mmHg. Average LVOT PG diminishing between the LV models with an IVSt of 19 and 12 mm were respectively 0.18 ± 1.661 , 0.72 ± 4.029 and 4.49 ± 4.739 mmHg for a flow of 4.0, 5.5 and 6.2 L/min.

The LVOT PG of the 15, 12, and 9 mm LV models did not decrease as much as expected in comparison to the 19 mm LV model. The *in vivo* LVOT PG after a Morrow procedure normally changes, on average from 80.77 ± 40.69 to 12.33 ± 8.49 mmHg [13]. However, the results from the *in vitro* measurements at 5.5 L/min only show a decrease of 4.7 ± 3.27 mmHg. Also, at 4.0 and 6.2 L/min, no significant difference was found between the 9 and 19 mm model which showed a decrease of respectively 0.65 ± 1.63 and 2.64 ± 5.21 .

This difference between the measurements and the expected results is possibly caused by, among others, the absence of SAM in the LV models. The patient used in this research, mainly had an obstruction due to SAM instead of the thickened IVS solely so the elevated LVOT PG was mainly caused by SAM (appendix XII). In the clinical US-images from this specific patient, an elevated LVOT PG is primarily seen when performing squats or the Valsalva manoeuvre. These conditions are not included in our set-up. The lower values of LVOT PG in the 19 mm models obtained in this research are thus mainly explainable by these limitations. To overcome this problem, the cardiac output, heart rate and pressure around the heart should be changed. This can be done by changing the values on the CBP-pump to similar patient-specific *in vivo* values, or using a set-up in which the pressure around the heart is controlled.

However, the limitations named above do not explain the high values of the LVOT PG of the 9 mm LV model. The expectation was that the flow velocity would decrease, with an increased diameter of the LVOT. The flow, however, is not only related to the diameter of the LVOT. Other factors influencing the velocity are the characteristics of the fluid, the compliance of the material, the flow waveform shape, and the shape of the surface [14]. The first three factors were kept the same in every model. The latter factor is different because of the incision made by the virtual Morrow procedure. These incisions contain sharp edges which can create turbulence in the LVOT and thereby increase the LVOT PG, thus explaining the high values in the 9 mm model. To check if this is indeed the cause, in further research a model should be created in which the edges are smoothed.

Another aspect that may have created errors in the measurement is the choice to measure the LVOT PG. This variable is commonly used in clinical practice to diagnose HOCM. However, the measurement of LVOT PG is not fully representative of the physical reality. This is caused by multiple factors. Firstly, the PG is calculated using a simplified Bernoulli equation. This equation, however, is only applicable when the flow is laminar, steady and behaves like a Newtonian fluid. As discussed before, the elevated LVOT PG is partly created by the turbulence that occurs in HOCM hearts. Also, the heart contracts, giving a pulsatile and thus unsteady flow. The error created by the assumption of a Newtonian fluid will not be significant because the diameter of the LV and aorta are bigger than the critical value of 1 mm below which non-Newtonian effects have to be taken into account [15].

The calculations performed are, as stated above, not entirely accurate and do not give the actual pressure in the LVOT [16]. When comparing DUS and the simplified Bernoulli equation to catheter-based measurements, a difference of 5 ± 12 mmHg can be seen [17]. Although measurements using DUS are not comparable to the in vivo situation, it can be of use in clinical diagnosis of HOCM. The measurements are a reference for the severity of the obstruction and therefore it is not needed to know the actual pressure. Measuring the LVOT PG makes it easier to compare the results to the clinical outcomes of the patient. Research is already done on improving the Bernoulli equation for DUS LVOT PG measurements [16,17].

Another deviation in our measurements is created by the use of the simplified Bernoulli equation. This equation states that the pressure difference ΔP (Pa), and thus the LVOT PG, is equal to 4 times the squared velocity v (m/s) (formula 2).

$$\Delta P = 4v^2 \quad (\text{formula 2})$$

The value 4 in this equation is an approximated value after integrating the value of the density of blood. Because a mixture of glycerol and water is used, instead of blood, the density is different. When a value of 4 is used in the equation this will result in an error in the DUS measurements. The newly calculated value should be 4.127 creating a difference in measurements of approximately 1 mmHg (appendix IX). In the future, a correction needs to be applied to the results to minimize this effect.

Furthermore, the measurements are not entirely accurate since the measurement of the peak flow is done by hand. A little difference in the placement of the cursor can result in an error of 1 mmHg or more. Therefore it would be recommended to use an algorithm for finding the peak flow. This can give a more accurate measurement as it can determine a peak at exactly the pixel it reaches. To our knowledge, this kind of software is not yet developed.

Limitations

To our knowledge, this research was the first one to investigate the flow in HOCM hearts using a flow set-up with an in vitro silicone LV. However, there are several limitations regarding the experiments.

LV Models

First of all, there are some limitations regarding the design of the models. The MRI images that were used for the model were taken during diastole [18]. The reason for this is that end-diastolic the LV resembles cardioplegia the most, which is obtained during a Morrow procedure. Also, taking images during diastole minimizes errors created by movement of the heart. However, this research focused on the ejection of the LV which happens during systole. The volume and shape of the LV change during systole. Because of this, the anatomy of our model is not fully representative which results in a flow that is not completely comparable. In

future research, MRI-images of the systolic heart should be used to minimize the impact of the different shape of the heart on the flow.

Another limitation is that cardiac tissue can only be simulated to a certain extent. The models are made from Dragon Skin 10 NV which has slightly different mechanical properties than heart tissue [19,20] (appendix XI). Among others, the wall thickness and deformability of the material will have an impact on the pressure, velocity and wall shear stress [21]. Because of this, the flow will differ from the physiological situation. Because Dragon Skin 10 NV is stiffer than myocardial tissue or aortic wall tissue, the flow velocity will increase in the model. The determination of the exact value of this change in velocity and a correction for myocardial tissue should be done in further research.

Furthermore, the flow is simulated with an external pump and the inflow is from the apex. This is not comparable to the physiological flow which normally enters the heart from the left atrium via the MV. Because of these limitations, the flow will not be entirely comparable to a physiological situation. Also, the model is static and cannot simulate the mechanical contractions of the heart which results in a lack of radial and circumferential strain. The different inlet and lack of contractions create a more laminar flow which may have induced a lower PG.

One of the main issues is that the MV is not present in the model so there is no simulation of a SAM. In HOCM patients, SAM has a significant impact on the flow and obstruction of the LVOT. Because this phenomenon is not included in the model, the velocity and therefore the LVOT PG, will be lower in the LV model with an IVSt of 19 mm than the original in vivo situation. It is out of the scope of this research to add the MV and papillary muscles into the LV models [22].

Another limitation is that the performance of the virtual Morrow procedure can not fully simulate the Morrow procedure performed by the cardiothoracic surgeon. The incision was based on precise landmarks placed on the heart determined by the angle a surgeon would be able to operate in. Even though the incision was verified by a cardiac surgeon, it is not similar to an in vivo situation (dr. R.G.H. Speekenbrink, personal communication, May 25, 2021). This is mainly because a real Morrow procedure is done during cardioplegia. Also, the incision of the virtual procedure is cylinder shaped, which is different from what the surgeon will perform, namely, multiple incisions. This different shape of the incision can result in a different flow with more turbulence which will increase the LVOT PG. The incision is not comparable to a real-life situation, but it could provide information about the difference in flow when the obstruction of the LVOT is reduced.

Flow set-up

In this research, there are some limitations regarding the setup. These can have an impact on the reliability of the measurements.

In the set-up, $\frac{3}{8}$ inch tubes are used. These tubes are physically smaller and stiffer than a normal aorta. Therefore the resistance in the tubes is higher than the resistance in the blood vessels in the body. Because the LVOT in the different models has a diameter of approximately 13 and the aorta of 30 mm, the highest point of resistance is not at the LVOT, but will be at the connector from the heart to the smaller tubes. Because the volumetric flow rate will be constant, this will not have a significant impact on the measurements.

Before performing the measurements, the flow was validated. The validation measurements of the flow deviated from the cardiac output (CO) on the CPB pump.

This could be due to the manner used to validate the CO. The validation of the flow is not

fully accurate because of human error and the unstable cardiac output caused by the resistance-dependent centrifugal pump. Nonetheless, it could be seen that the flow given by the CPB pump did not significantly differ from the validation measurements (appendix XVIII).

The experiments were done using a pulsatile flow, generated by the CPB pump. However, because of the limited capacity of the pump, this pulse is not similar to the heart cycle. The pump generates a sinusoidal flow with a wider and lower pulse than the heart. Because of this, the velocities measured are lower than in physiological situations. However, a difference in velocity between the different LV models can still be measured.

Measurements

The measurements were done using a CWD US under supervision of an experienced echocardiographer. This limits errors created by the inexperience in using DUS. Only the LVOT PG was measured which is an important factor in HOCM diagnosis. However, this measurement is not representative of the whole flow in the LVOT. Other factors like turbulence, wall shear stress or flow velocities in specific places are not measured.

Recommendation

Recommended for future research is to include more patients. This research is based on MRI data of one patient. Additionally, the MRI data would rather be based on the systole. This way, the shape of the heart has minimal impact on the measured peak flow when comparing this to an in vivo situation. Also, it is advised to include the mitral valve and papillary muscles in the model to simulate the SAM in the model. Also, the squats and Valsalva manoeuvre should be included which could be simulated by altering the settings on the CPB pump to similar in vivo values and controlling the pressure around the heart.

Furthermore, it would be advised to use a material that can contract to simulate the pulsatility of the heart better. If this is possible it would be recommended to place the inflow of the blood at the mitral valve instead of the apex. Research on simulating a beating heart in vitro is already being done, for example in research by Cohrs et al. [23].

Another recommendation is to use a different value for the quantification of the flow. A full flow analysis including turbulence and wall shear stress will give more information about the optimal flow than only measuring the LVOT PG. Since the manual measurements of the LVOT PG are not fully accurate, it would be recommended to develop an algorithm, which can automatically find the highest peak flow.

Before the patient-specific IVSt can be achieved during Morrow procedures, more research has to be conducted. The aim of this research was to demonstrate the relationship between a certain IVSt and an optimal flow. In the future, computational fluid dynamics (CFD) should be used to determine the ideal patient-specific IVSt regarding the most optimal flow. Making 3D models to determine the optimal thickness takes too much effort and time to be implemented in standard care. Because the cardio-thoracic surgeon is not able to resect the exact amount of tissue that is needed for an optimal flow, intraoperative measurements are needed to guide the surgeon. Therefore, before the implementation of a patient-specific treatment, more research regarding CFD and intraoperative IVSt measurements has to be done.

Conclusion

An in vitro LV model can provide valuable information about the optimal IVSt for HOCM patients. This research is the first step in creating a patient-specific model that can determine how much tissue needs to be resected when performing the Morrow

procedure based on the optimal flow. However early results are not yet substantiating, it does show that an in vitro model can simulate the blood flow in HOCM patients when making some adjustments to the proposed model. Even though the LVOT PG does not measure the actual pressure, it is of use as a comparative mean.

Before the model can be clinically applied, further research needs to be performed to include the mitral valve and heart contractions in the model. In the future, CFD's could be used in preoperative planning for analyzing the optimal IVSt. Intraoperative imaging is needed to guide the surgeon during surgery and to determine the amount of resected tissue. This way, over- and undertreatment can be red

Acknowledgements

We would like to thank the following people for all their time, effort, and support during our research.

First of all, thank you *Frank Halfwerk* for your guidance throughout our research. You have been of great help during the whole process by giving us useful academic feedback and introducing us to people who were willing to help.

Edsko Hekman, thank you for your (technical) input and advice especially in building our set-up and deciding how to design the moulds. You have provided us with a critical yet creative view of our ideas.

Ron Speekenbrink, we appreciate your time and enthusiasm for our research. It was great you were willing to let us observe in surgery and were willing to record the procedure for us. We have learned a lot from it.

We would also like to show our gratitude to *Maaïke Koenrades* for showing us around in the 3D lab and making time for us. You have given us useful advice on the design of the moulds and introduced us to the 3D software.

We would like to show our appreciation to *Karin Smits* for her time and effort. You have helped us tremendously throughout the process by providing us with advice on multiple aspects. It was a pleasure working with you and we wish you all the best with your research.

We are also thankful to you, *Wouter Diemer*, for your enthusiasm, printing our 3D models, advising us on the use of materials, and sending us updates even at the weekends.

We would like to thank the perfusion team MST Enschede, in particular *Guido Warkotsch* for the guidance and for allowing us to use their equipment for this research. We would also like to thank you for the opportunity to observe during surgery and the useful explanation of the CPB pump.

We would like to recognize *Joke Hurink* and *Sjoukje Lok* for showing us how to perform correct ultrasound measurements. You have been of great help in introducing us to all the functions on the US device and showing us multiple examples of HOCM US measurements.

Also, we would like to give our thanks to *Jutta Arens* for providing us with the materials needed for the casting of our moulds and the glycerol required in our set-up. We are honoured to be the first students to use the new lab.

Furthermore, thank you to our personal tutor, *Maaïke van Ochten*, for your weekly guidance. We value the time spent on discussing the collaboration between us and helping us give insight into our personal development and goals.

And last but definitely not least, we are grateful to *Jan Leerkotte* for providing us with the Cardiopulmonary Bypass pump. We appreciate your cheerful attitude and checking in on us every now and then.

Bibliography

- [1] Raj MA, Ranka S, Goyal A. Hypertrophic Obstructive Cardiomyopathy. StatPearls, Treasure Island (FL): StatPearls Publishing; 2021.
- [2] Nishimura RA, Seggewiss H, Schaff HV. Hypertrophic obstructive cardiomyopathy: surgical myectomy and septal ablation. *Circ Res* 2017;121:771–83. <https://doi.org/10.1161/CIRCRESAHA.116.309348>.
- [3] Douglas JS. Current state of the roles of alcohol septal ablation and surgical myectomy in the treatment of hypertrophic obstructive cardiomyopathy. *Cardiovasc Diagn Ther* 2020;10:36–44. <https://doi.org/10.21037/cdt.2019.07.02>.
- [4] Andrushchuk U, Adzintsov V, Niavyhlas A, Model H, Ostrovsky Y. Early results of optimal septal myectomy using 3-dimensional printed models. *Kardiochir Torakochirurgia Pol* 2019;16:74–80. <https://doi.org/10.5114/kitp.2019.86359>.
- [5] Mayo Clinic. Hypertrophic cardiomyopathy 2020. <https://www.mayoclinic.org/diseases-conditions/hypertrophic-cardiomyopathy/symptoms-causes/syc-20350198> (accessed May 4, 2021).
- [6] Talreja DR, Nishimura RA, Edwards WD, Valeti US, Ommen SR, Tajik AJ, et al. Alcohol septal ablation versus surgical septal myectomy: comparison of effects on atrioventricular conduction tissue. *J Am Coll Cardiol* 2004;44:2329–32. <https://doi.org/10.1016/j.jacc.2004.09.036>.
- [7] Singh V, Badheka AO, Bokhari SS, Ghersin E, Clark PM, O'Neill WW. Retrograde percutaneous closure of a ventricular septal defect after myectomy for hypertrophic obstructive cardiomyopathy. *Tex Heart Inst J* 2013;40:468–71.
- [8] Kim JH. Tips for Successful Septal Myectomy in Patients with Hypertrophic Cardiomyopathy. *Korean J Thorac Cardiovasc Surg* 2018;51:227–30. <https://doi.org/10.5090/kjtcs.2018.51.3.227>.
- [9] Redaelli M, Poloni CL, Bichi S, Esposito G. Modified surgical approach to symptomatic hypertrophic cardiomyopathy with abnormal papillary muscle morphology: Septal myectomy plus papillary muscle repositioning. *J Thorac Cardiovasc Surg* 2014;147:1709–11. <https://doi.org/10.1016/j.jtcvs.2013.10.085>.
- [10] Hermesen JL, Burke TM, Seslar SP, Owens DS, Ripley BA, Mokadam NA, et al. Scan, plan, print, practice, perform: Development and use of a patient-specific 3-dimensional printed model in adult cardiac surgery. *J Thorac Cardiovasc Surg* 2017;153:132–40. <https://doi.org/10.1016/j.jtcvs.2016.08.007>.
- [11] Wang Y, Guo H, Wang S, Lai Y. Effectiveness of a patient-specific 3-dimensional printed model in Septal Myectomy of hypertrophic cardiomyopathy. *Pak J Med Sci Q* 2020;36:1678–82. <https://doi.org/10.12669/pjms.36.7.2620>.
- [12] Adhyapak SM. Hypertrophic Cardiomyopathy: A Practical Guide to Diagnosis and Management . CRC Press; 2021.
- [13] Lai Y, Guo H, Li J, Dai J, Ren C, Wang Y. Comparison of surgical results in patients with hypertrophic obstructive cardiomyopathy after classic or modified morrow septal myectomy. *Medicine (Baltimore)* 2017;96:e9371. <https://doi.org/10.1097/MD.00000000000009371>.
- [14] Myers JG, Moore JA, Ojha M, Johnston KW, Ethier CR. Factors influencing blood flow patterns in the human right coronary artery. *Ann Biomed Eng* 2001;29:109–20.

- <https://doi.org/10.1114/1.1349703>.
- [15] Salsac AV, Sparks SR, Chomaz JM, Lasheras JC. Evolution of the wall shear stresses during the progressive enlargement of symmetric abdominal aortic aneurysms. *J Fluid Mech* 2006;560:19. <https://doi.org/10.1017/S002211200600036X>.
 - [16] Donati F, Myerson S, Bissell MM, Smith NP, Neubauer S, Monaghan MJ, et al. Beyond bernoulli: improving the accuracy and precision of noninvasive estimation of peak pressure drops. *Circ Cardiovasc Imaging* 2017;10. <https://doi.org/10.1161/CIRCIMAGING.116.005207>.
 - [17] Franke B, Weese J, Waechter-Stehle I, Brüning J, Kuehne T, Goubergrits L. Towards improving the accuracy of aortic transvalvular pressure gradients: rethinking Bernoulli. *Med Biol Eng Comput* 2020;58:1667–79. <https://doi.org/10.1007/s11517-020-02186-w>.
 - [18] End-Diastolic Volume Index - Cardiac MRI n.d. <https://www.cardiacmri.com/analysis-guide/lv-function/end-diastolic-volume/> (accessed June 12, 2021).
 - [19] Physical characteristics of Dragon Skin and Ecoflex. n.d. https://www.researchgate.net/figure/Physical-characteristics-of-Dragon-Skin-and-Ecoflex_tbl1_343250212 (accessed June 10, 2021).
 - [20] Riedle H, Molz P, Franke J. Determination of the mechanical properties of cardiac tissue for 3D printed surgical models. 2018 IEEE-EMBS Conference on Biomedical Engineering and Sciences (IECBES), IEEE; 2018, p. 171–6. <https://doi.org/10.1109/IECBES.2018.8626728>.
 - [21] Wolański W, Gzik-Zroska B, Jozsko K, Kawlewska E, Sobkowiak M, Gzik M, et al. Impact of vessel mechanical properties on hemodynamic parameters of blood flow. In: Gzik M, Tkacz E, Paszenda Z, Piętko E, editors. *Innovations in biomedical engineering*, vol. 623, Cham: Springer International Publishing; 2018, p. 271–8. https://doi.org/10.1007/978-3-319-70063-2_29.
 - [22] Vedula V, Seo J-H, Lardo AC, Mittal R. Effect of trabeculae and papillary muscles on the hemodynamics of the left ventricle. *Theoret Comput Fluid Dynamics* 2016;30:3–21. <https://doi.org/10.1007/s00162-015-0349-6>.
 - [23] Cohrs NH, Petrou A, Loepfe M, Yliruka M, Schumacher CM, Kohl AX, et al. A Soft Total Artificial Heart-First Concept Evaluation on a Hybrid Mock Circulation. *Artif Organs* 2017;41:948–58. <https://doi.org/10.1111/aor.12956>.

Appendix

Abbreviations	19
Appendix I: Anatomy	21
Heart valves	21
Interventricular septum	21
Conduction system	22
Appendix II: Physiology	23
Reynolds number	24
Hagen-Poiseuille's equation	24
Bernouilli's law	25
Appendix III: Pathophysiology	26
Hypertrophy	26
Systolic anterior motion	27
LVOT gradient	27
Appendix IV: Diagnosis	28
Physical examination	28
Electrocardiogram	28
Ultrasound	29
Magnetic resonance imaging	29
Appendix V: Treatment	30
Medication	30
Septal ablation	30
Morrow procedure	31
Pre- and postoperative imaging	31
Appendix VI: Challenges	33
Invasivity	33
Limited sight	33
Limited workspace	33
Determining the right amount of resected tissue	33
Not patient-specific	34
Appendix VII: State-of-the-art	35
Appendix VIII: Subquestions	38
Anatomy	38
(Patho)physiology	38
Diagnosis	38

Treatment	38
3D model	38
Appendix IX: Justification	39
Appendix X: Data management plan	43
Appendix XI: Troubleshooting	44
Appendix XII: Pre- and post-operative information patient	46
Appendix XIII: Protocol - Designing the moulds	47
Appendix XIV: Protocol - Printing the moulds	64
Appendix XV: Protocol - Casting the models	68
Appendix XVI: Protocol - Flow set-up	73
Appendix XVII: Cardiopulmonary bypass pump	77
Appendix XVIII: Validation flow results	79
Appendix XIX: Protocol - Measuring the LVOT-PG	80
Appendix XX: Doppler Ultrasound	88
Appendix XXI: Protocol - Statistical analysis	90
Appendix XXII: Statistical analysis of the different models	93
Appendix XXIII: Statistical analysis of the inter- and intraobserver variability	100
Bibliography	104

Abbreviations

3D	=	3-dimensional
ANOVA	=	Analysis of Variance
AV-node	=	atrioventricular node
AVS	=	atrioventricular septum
CPB	=	cardiopulmonary bypass
CT	=	computed tomography
CWD	=	continuous wave doppler
DUS	=	doppler ultrasound
ECG	=	electrocardiogram
HCM	=	hypertrophic cardiomyopathy
HOCM	=	hypertrophic obstructive cardiomyopathy
IN	=	inlet septum
IVS	=	interventricular septum
IVSt	=	interventricular septum thickness
LA	=	left atrium
LV	=	left ventricle
LVOT	=	left ventricular outflow tract
LVOTO	=	left ventricular outflow tract obstruction
MR	=	mitral regurgitation
MRI	=	magnetic resonance imaging
MV	=	mitral valve
MVO	=	mid-ventricular obstruction
OS	=	outlet septum
PIV	=	particle image velocimetry

PLA	=	polyactic acid
PG	=	pressure gradient
PVA	=	polyvinyl alcohol
PWD	=	pulse wave doppler
RV	=	right ventricle
RVOT	=	right ventricular outflow tract
SAM	=	systolic anterior motion
SA-node	=	sinoatrial node
SPSS	=	statistical package for the social sciences
SSFP	=	steady-state free precession
TS	=	trabecular septum
US	=	ultrasound

Appendix I: Anatomy

In order to get a better understanding of hypertrophic obstructive cardiomyopathy (HOCM), knowledge of the anatomy of the heart valves, interventricular septum (IVS), and conduction system is required.

Heart valves

The atria are separated from the ventricles by the atrioventricular valves [1,2]. Located between the right atrium and ventricle is the tricuspid valve which consists of an anterior, septal and, posterior leaflet. The mitral valve (MV) (figure 1) can be found between the left atrium and ventricle and consists of an anterior and posterior leaflet. Both valves are connected to the papillary muscles by tendinous cords. When the ventricles contract the valves close by contraction of the papillary muscles with the help of chordae tendineae.

In addition, valves can be found between the ventricles and their outlets; the semilunar valves. During relaxation of the ventricles, these valves close. Between the right ventricle (RV) and the pulmonary artery is the pulmonary valve located consisting of an anterior, left, and right leaflet. Between the left ventricle (LV) and the aorta is the aortic valve located, consisting of a left coronary, right coronary, and noncoronary leaflet. All of the valves in the heart have a passive effect. The contraction of the heart creates pressure differences in the blood flow, causing the valves to open or close.

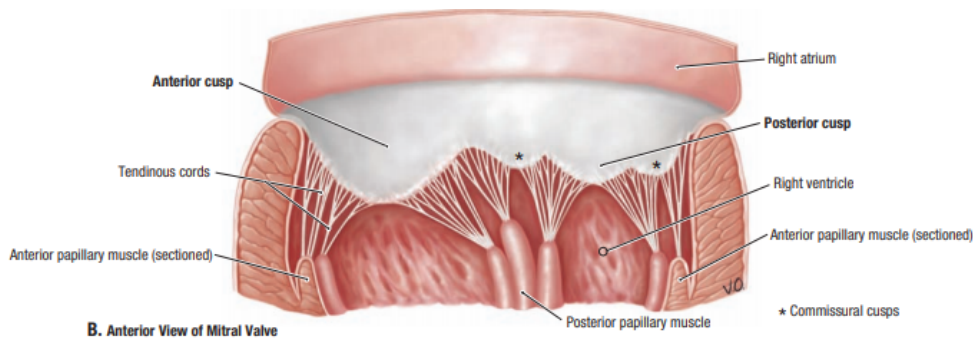


Figure 1: Anterior view of MV and its tendinous cords [2].

Interventricular septum

The IVS separates the LV and RV and is composed of a muscular and membranous part [1,2]. Normal values for the thickness of the IVS are 8.92 ± 1.14 mm for men and 8.53 ± 1.3 for women [3]. Both parts of the IVS have a separate embryonic development. The membranous part of the septum consists of a thin layer of connective tissue. The right side of the septal leaflet of the tricuspid valve is connected to the membranous part and forms the separating line between the IVS and the atrioventricular septum (AVS).

The greater part of the septum is muscular and consists of myocytes. It has a comparable thickness to the LV. The muscular part can be divided into the inlet septum (IN), trabecular septum (TS), and outlet septum (OS) [4] (figure 2). The IN extends from the atrioventricular valves to the chordal attachments. Next, the TS, the largest part of the IVS, ranges from the membranous septum to the apex and OS. At last, the OS divides the right and left ventricular outflow tracts.

Vascularisation of the IVS is provided by the anterior interventricular branch of the left coronary artery and the posterior interventricular branch of the right coronary artery or the circumflex branch of left

coronary artery. Venous blood is mostly drained by the great cardiac vein and middle cardiac vein. The IVS is innervated by the cardiac plexus.

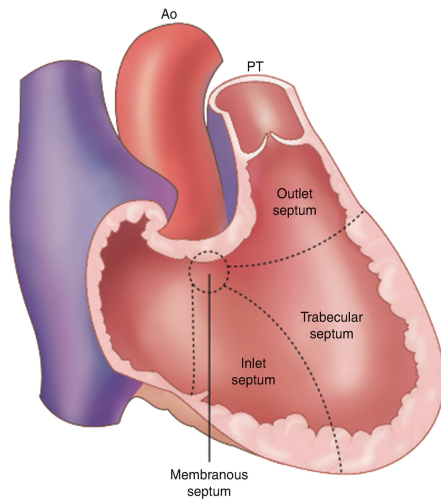


Figure 2: The different parts of the IVS; the inlet septum, trabecular septum and outlet septum. Ao = aortic, PT = pulmonary trunk [5].

Conduction system

The conduction system of the heart induces and propagates the currents that cause the contraction of heart cells [1,2] (figure 3). The sinoatrial node (SA-node) in the right atrium initiates a current which is propagated through the cardiac muscle of the atrium to the interatrial septum. In the interatrial septum the atrioventricular node (AV-node) is located. The AV-node receives the current and transmits the current through the AV bundles; a left and right bundle that both propagate through the membranous part of the IVS towards the ventricles. In the ventricles the left and right bundle divide into subendocardial branches which are distributed across the heart muscle from respectively the LV and RV. The left bundle branches stimulate the IVS, anterior, and posterior papillary muscles, and left ventricle wall. The right bundle branches stimulate the IVS, anterior papillary muscle, and RV wall.

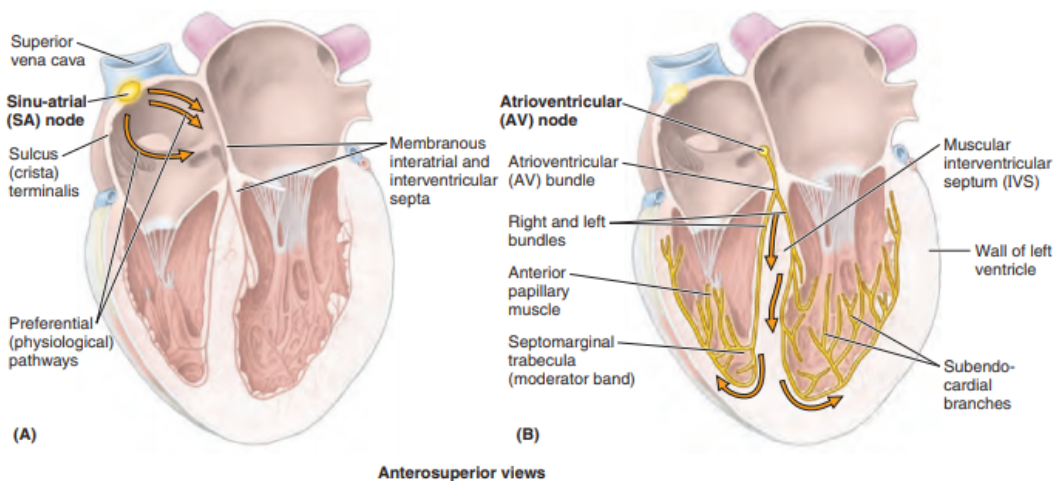


Figure 3: The conduction system of the heart. An impulse originating from the SA-node travels through the atrial myocardium to the AV-node. From the AV-node, located on the atrial septum, the impulse propagates via the left and right bundle and their branches through the ventricular myocardium. [1]

Appendix II: Physiology

The cardiac cycle begins with the diastole. The pulmonary and aortic valve are closed and the tricuspid valve and mitral valve (MV) are open [1]. When the atria contract, the pressures in the atria increase and blood flows to the ventricles [1,6]. Then, the tricuspid valve and MV close and the systole starts. The ventricles contract, creating a higher pressure in both ventricles, forcing the pulmonary and aortic valve to open [1,6]. Blood flows through both outflow tracts out of the heart. Then the cardiac cycle is repeated (figure 1).

The cardiac output in most people is 5-6 L/min at rest and can increase to more than 35 L/min during exercise [7].

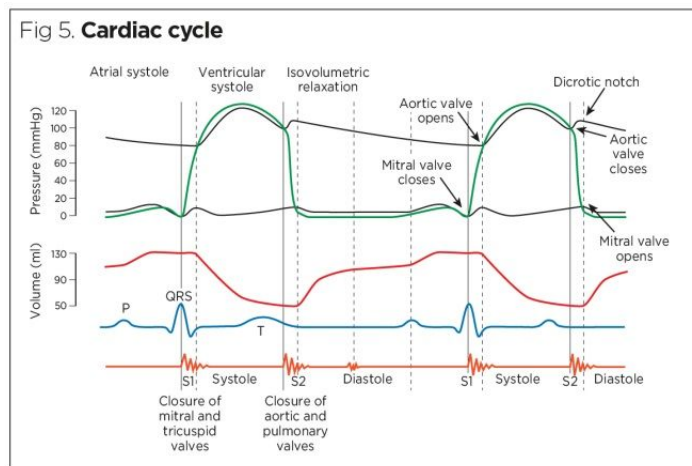


Figure 1: Pressure and volume during the cardiac cycle [6]. During diastole the ventricles fill passively with blood (red line). Atrial systole fills the ventricles completely and the end diastolic volume is reached. During systole, the blood is pushed out of the ventricles by contraction of the heart muscles initiated by the electrical impulse shown on the ECG as the QRS-complex (blue line). The pressure in the ventricle increases (green line) and blood flows into the aorta. During isovolumetric relaxation the ventricles are emptied except for the end systolic volume that remains. A slight backflow in the aorta is seen closing the aortic valves and resulting in a short pressure drop in the aorta (upper black line).

The blood flow can be laminar or turbulent [8]. In a laminar flow, the blood particles move parallel to each other. This occurs mainly in smooth tube-like structures as vessels. In case of turbulence, irregular motions develop in the flow, such as vortices. In the left ventricle (LV) during end-diastole and early systole such vortices are formed [9] (figure 2). These vortices appear to have three important roles namely: diversion of the LV inflow to the left ventricular outflow tract (LVOT), minimization of interaction between incoming, outgoing and circulating flows, and contribution to LV filling.

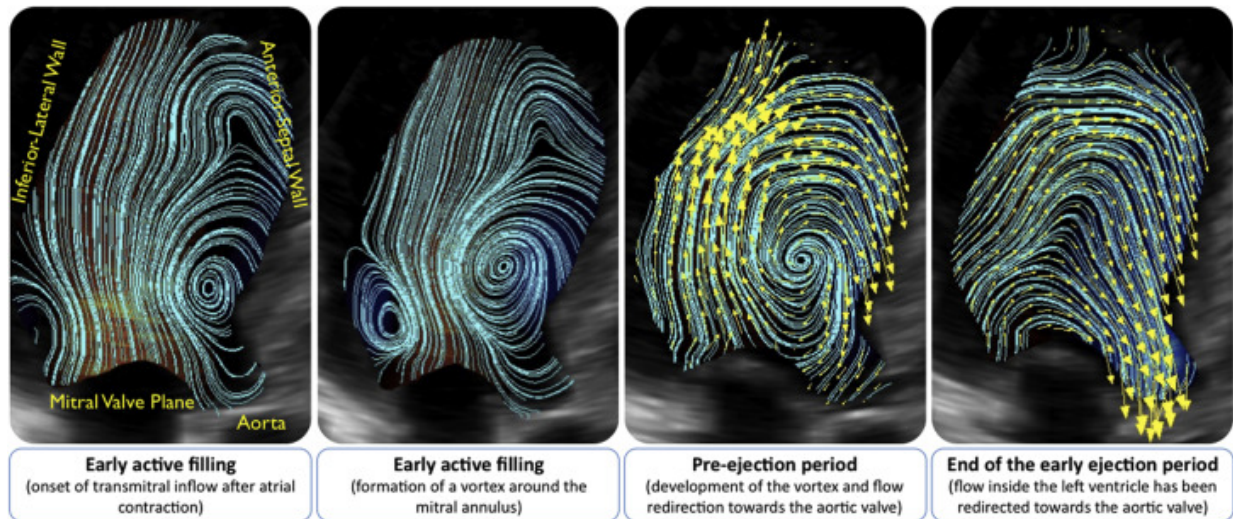


Figure 2: Vortex flow dynamics in the LV during filling and ejection. Vortex starts at the arterial contraction and moves towards the LVOT [9].

Three different equations can be used to define blood flow.

Reynolds number

Whether the flow is laminar or turbulent can be determined by the Reynold number [8]. This can be calculated by formula 1, where D is the diameter (m), v is the mean velocity (m/s), ρ is the density (kg/m^3), and η is the viscosity ($\text{N}\cdot\text{s/m}^2$). The flow is laminar if $Re < 2,000$ and turbulent if $Re > 3,000$.

$$Re = \frac{\rho D v}{\eta} \quad (\text{formula 1})$$

Hagen-Poiseuille's equation

Basic equations related to fluid flows are Bernoulli and Hagen-Poiseuille's laws [10]. Bernoulli and Poiseuille's laws are only applicable to flow through cylindrical tubes if it is a nonpulsatile and laminar flow [8,10].

Hagen-Poiseuille's equation describes the flow rate Q (m^3/s), which is the volume of the liquid V (m^3), that flows through a tube per unit of time (s) [11].

$$Q = \frac{\Delta V}{\Delta t} \quad (\text{formula 2})$$

The following equation is used for the relation between the flow rate Q and the pressure difference ΔP (Pa) between both ends of the tube.

$$\Delta P = -QR \quad (\text{formula 3})$$

The flow resistance R (Ω) in a tube can be written as:

$$R = \frac{8\eta l}{\pi r^4} \quad (\text{formula 4})$$

Where r is the radius (m) and l the length (m) of the tube.

Bernoulli's law

Bernoulli's law shows the following relationship between pressure, density, velocity (m/s), and height (m) for a gas or liquid on two different points in a streamline [10] (formula 5).

$$P_1 + \frac{1}{2}\rho v_1^2 + \rho g h_1 = P_2 + \frac{1}{2}\rho v_2^2 + \rho g h_2 \quad (\text{formula 5})$$

There is also a modified Bernoulli equation [12]. This can be used to calculate pressure gradients at certain velocities between two different points in a bloodvessel (formula 6).

$$\Delta P = -4(v_2^2 - v_1^2) \quad (\text{formula 6})$$

Formula 6 is similar to the simplified Bernoulli equation (formula 7).

$$\Delta P = 4v^2 \quad (\text{formula 7})$$

This formula is based on the fact stated in the Bernoulli equation that the energy in two different points in a streamline should be equal. Since the difference in height can be neglected, the difference in pressure is created by the change in kinetic energy (J) (formula 8).

$$K = \frac{1}{2}Dv^2 \quad (\text{formula 8})$$

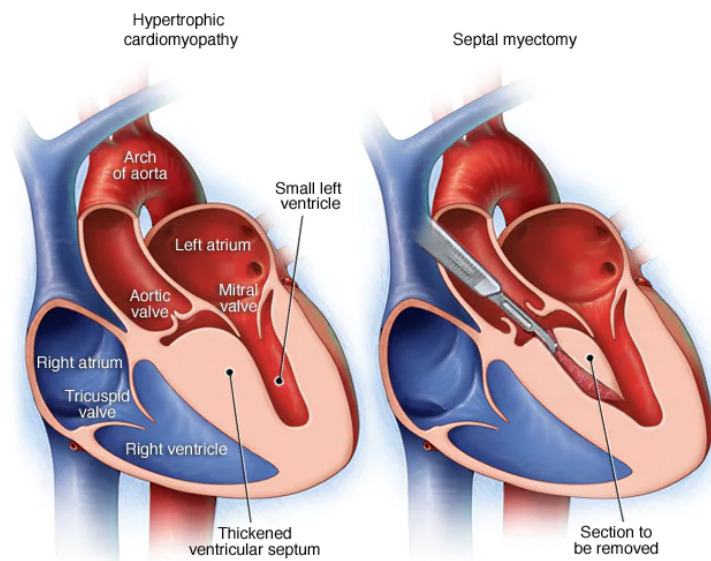
In this formula, D stands for the density of the fluid. Since in echocardiography, the working fluid is blood, the first part of the formula can be simplified by inserting the density of blood and adding a factor of 0,0075 to get an unity of mmHg. This results in an approximate value of 4. When $v_2 \gg v_1$ formula 7 can be used to calculate the LVOT PG.

Appendix III: Pathophysiology

Hypertrophic cardiomyopathy (HCM) is a genetic condition resulting in asymmetrical hypertrophy of the left ventricle [13,14]. Hypertrophy can cause an obstruction in the left ventricular outflow tract (LVOT) causing systolic anterior motion (SAM). In this case HCM is called hypertrophic obstructive cardiomyopathy (HOCM). The interventricular septum (IVS) is affected in two-thirds of the cases. The degree of hypertrophy determines the severity of the obstruction and its clinical manifestation.

Hypertrophy

Ventricular hypertrophy is caused by a mutation in one of the fourteen genes that encode for sarcomere associated proteins [15]. HOCM is an autosomal dominant disorder. Genes that are most likely to mutate are MYH7, MYBPC3, TNNT2, and TNNI3. As a result of the mutation, myocyte hypertrophy and disarray develop in patients with HOCM. [16]. The myocyte-nuclei are pleomorphic, enlarged and have hyperchromasia. Therefore they can no longer generate optimal force [13]. It is unknown how the mutations in the sarcomere associated genes lead to hypertrophy of the IVS [15]. The left ventricle (LV) has to generate more force in order to overcome the obstruction, resulting in secondary hypertrophy, mostly in the basal part of the septum, making the LVOT even narrower (figure 1). In addition, hypertrophy of the IVS may spread distally to the mid cavity region as a result of a hypertrophic papillary muscle adjacent to the septum. Creating an increased gradient in pressure between the apex and the base of the heart. High apical pressure of the LV may result in abnormal LV wall stress, even leading to myocardial ischemia. Also, apical aneurysms may develop [14]. HOCM manifests itself in the second or third decade of life. Usually, the course is asymptomatic, but there is an increased risk of sudden cardiac death, especially in younger patients.



© MAYO FOUNDATION FOR MEDICAL EDUCATION AND RESEARCH. ALL RIGHTS RESERVED.

Figure 1: Left: normal IVS. Right: clinical manifestation of HOCM displaying the resection of the IVS to a thickness of 10-11 mm [17].

Systolic anterior motion

Obstruction of the LV may result in the presence of SAM of the mitral valve (MV) [13]. Septal hypertrophy narrows the LVOT which results in an increased flow in the LVOT and causes a lower pressure according to the Venturi effect. Due to the low pressure the leaflets, in particular the anterior leaflet, are dragged towards the LVOT resulting in a dynamic obstruction and thus an altered blood flow (figure 2). In seventy percent of patients the obstruction can only be detected while performing provoking manoeuvres. In a quarter of the patients, the obstruction is also present while resting. During physical examination of HOCM patients, a SAM can be heard by a holosystolic murmur at the apex. A Valsalva manoeuvre decreases the preload causing an increased systolic ejection crescendo-decrescendo murmur. SAM of the MV may lead to secondary mitral regurgitation (MR). The severity of the regurgitation is determined by the degree of obstruction and the blood outflow [14].

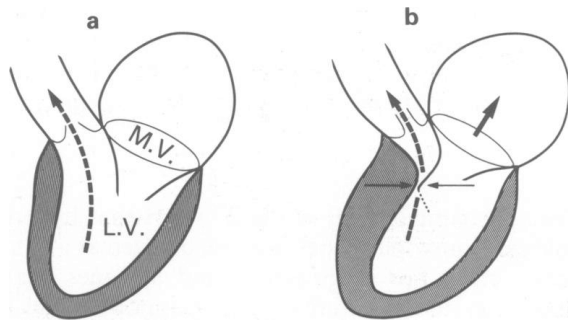


Figure 2: Left: Outflow in healthy LV. Right: SAM results in obstruction Outflow [18].

LVOT gradient

To measure the degree of obstruction in the LVOT, the pressure gradient (PG) can be used [12]. This is the difference between the pre-orifice and post-orifice pressure and is a quantitative measurement for the severity of the obstruction. PG can be calculated using Bernoulli's equation and measurements of the flow velocities. In most physiological situations v_1 is significantly less than v_2 and can thus be ignored. In HOCM, v_1 is the flow at the level of the aortic valve and v_2 is the flow at the LVOT. In HOCM v_1 is extremely high and should be taken into account when calculating the PG. According to Bernoulli's law, when the velocity increases, the pressure decreases, creating a greater difference in pressure. The PG can be measured using Doppler ultrasound (DUS). The flow velocity is measured parallel to the blood flow through the LVOT. A PG higher than 30 mmHg is defined as LVOT obstruction and higher than 50 mmHg is a clinical indication for the Morrow procedure or septal ablation [19]. PG is thus an important quantification in the diagnosis and clinical follow-up of HOCM.

Appendix IV: Diagnosis

Hypertrophic obstructive cardiomyopathy (HOCM) can be diagnosed by analyzing the symptoms and performing physical examination. In addition, an electrocardiogram, echocardiogram and magnetic resonance imaging (MRI) are made.

Physical examination

In order to diagnose a patient with HOCM, the physician first looks at the symptoms. Patients with HOCM show symptoms of dyspnoea, angina pectoris, and syncope [13]. Auscultation of the heart may show a holosystolic murmur at the apex, abnormal precordial impulse, and regurgitation at the mitral valve (MV). Also a S4 heart sound, split-second heart sound, double carotid pulse, and systolic ejection crescendo-decrescendo murmur might be heard. It is necessary to perform additional tests, to be able to properly diagnose HOCM.

Electrocardiogram

An electrocardiogram (ECG) can be made to look for specific abnormalities that indicate an enlarged IVS [20]. A shortened PR-interval and a delta wave at the origin of the QRS complex are indications of ventricular pre-excitation which is seen in HOCM (figure 1). Other abnormalities that can indicate HOCM are pathological Q-waves, ST-T segments and QT prolongation [21,22]. Nowadays ECG is performed less frequently for HOCM diagnosis, as imaging tests have more advantages in comparison to ECG.

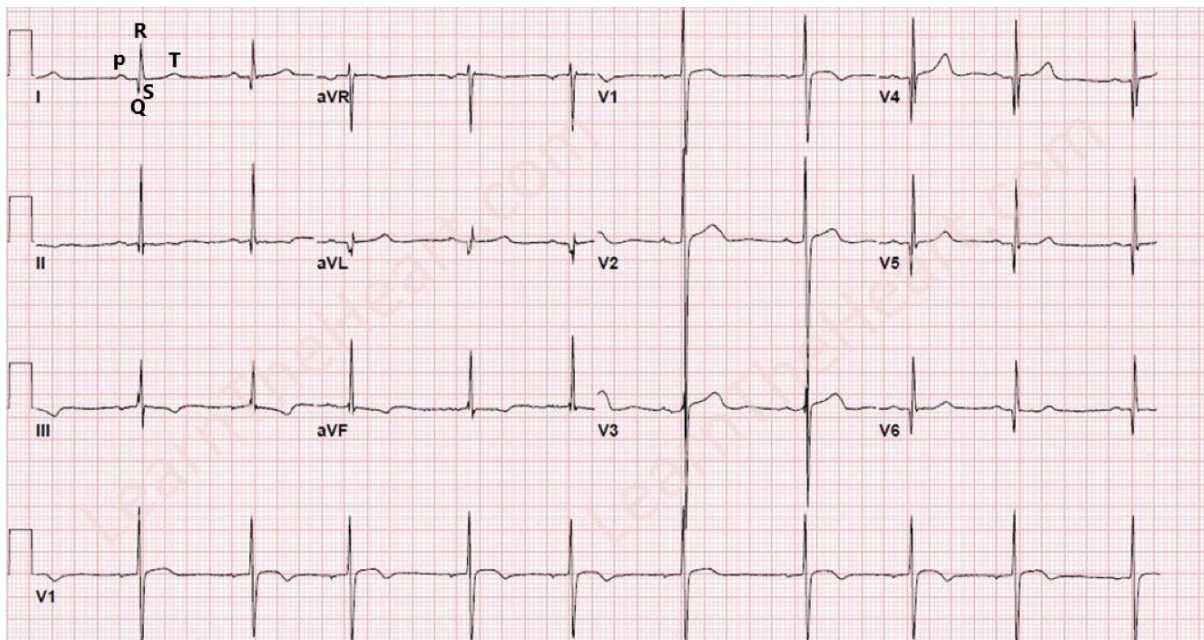


Figure 1: ECG of HOCM based on [23]. A pathological Q wave can be seen at V6 having a 'dagger' like shape.

Ultrasound

Diagnosis of HOCM can be made by performing an ultrasound (US) [24]. This has an 80% diagnostic accuracy for HOCM [13]. With a 2D M-mode transthoracic US, the thickness of the interventricular septum (IVS) can be measured at different places at the end-diastole [24]. If the septal thickness is larger than 15 mm it is referred to as HCM in which the thickest part of the septum is a marker for the degree of hypertrophy. Besides the thickness measurement of the IVS, the left ventricle (LV) systolic and diastolic function, left atrium (LA) volume, left ventricular outflow tract (LVOT), right ventricular outflow tract (RVOT), mid-ventricular obstruction (MVO), apical morphology, MV plus systolic anterior motion (SAM), and pulmonary pressure can be examined using US [25]. Different kinds of US can be used to increase the accuracy of the diagnosis of HOCM. Examples are contrast-enhanced US, tissue Doppler imaging, and speckle tracking echocardiography, which are useful tools to detect differences in strain in a thickened IVS. 3-dimensional (3D) US is also a much investigated technology gaining relevance in the imaging of HOCM, giving a much more realistic image of the IVS [26]. However, improvement of the quality, standardisation and software development is needed before it can be applied clinically.

Besides a transthoracic US, a transesophageal echography (TEE) can be used for the imaging of HOCM and MR [27]. This method of US uses a probe that is inserted into the esophagus to get a better view of the heart. Because the esophagus is close to the heart, a detailed image and precise measurement of the IVS can be made. TEE is mainly done in the operating room before the surgery. The surgeon and cardiologist can then form a final surgical plan. The best views for IVS evaluation are the midesophageal long-axis view (135°), transgastric midpapillary short-axis view (0°), and midesophageal four-chamber view (0°). TEE is also used for intraoperative guiding of a septal ablation [28]. TEE is currently the most important imaging technique to determine the surgical planning of the Morrow procedure in patients with HOCM.

Magnetic resonance imaging

Another technique to diagnose HOCM is MRI [29]. The most suitable form for this is steady-state free precession imaging (SSFP). By using cine SSFP MRI a movie of the heart can be made to get a clear vision of the morphology of the IVS. This can determine all phenotypes of HOCM. Late Gadolinium Enhancement is a form of MRI which displays the fibrosis of the heart tissue. It can be used to distinguish HOCM from other heart conditions. There are more MRI techniques like T2-weighted imaging, phase contrast or perfusion MRI, that can show specific areas or functions of the heart.

Appendix V: Treatment

The first step in treating hypertrophic obstructive cardiomyopathy (HOCM) is the use of medicine. In case medication does not resolve the symptoms, septal ablation or the Morrow procedure might be considered.

Medication

Medicines that are used are beta blockers, calcium channel blockers, heart rhythm drugs, and anticoagulants [30]. Beta blockers and calcium channel blockers are used to slow the heart rate. Heart rhythm drugs control the heartbeat and reduce the obstruction and anticoagulants prevent blood clotting.

Septal ablation

Septal ablation is a procedure which uses ethanol to reduce the hypertrophied interventricular septum (IVS). At the beginning of this procedure a balloon catheter, guiding catheter and guidewires are inserted in the groin and propagated in the direction of the heart [31]. Targetted is the part of the septum at the level of the left ventricular outflow tract (LVOT) which is most commonly accessed using the first septal branch of the left anterior descending coronary artery. When the septal artery is reached guided by echocardiography, the balloon is inflated which minimises ethanol leakage to other places (figure 1). When placed correctly, 1 to 4 mL ethanol is administered during a period of 3 to 5 minutes causing regional cell death [32]. Acute efficacy of the administration is based on the LVOT pressure gradient (PG) [28]. The injection is followed by a saline flush. During treatment the heart is monitored using ultrasound.

Instead of a septal ablation a myomectomy can be performed. Indications favouring [33] septal ablation in comparison to the Morrow procedure are patients with comorbid noncardiac conditions, higher ages, pre-existing right bundle branch blocks, and the use of a pacemaker. On the other hand, indications favouring the Morrow procedure are patients with lower ages, higher weights, and pre-existing left bundle branch blocks. Septal ablation is associated with higher reoperation rates in comparison to the Morrow procedure [34].

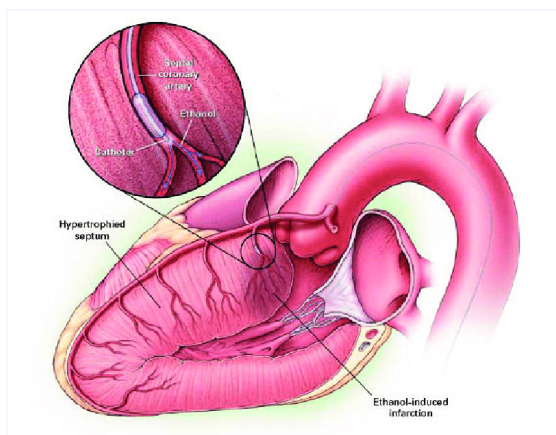


Figure 1: A balloon is inflated in the septal artery during septal ablation to treat HOCM [35].

Morrow procedure

A septal myectomy, also known as the Morrow procedure (figure 2), is often performed as treatment for HOCM [36]. The surgeon removes part of the hypertrophic septum in the left ventricle (LV), which eliminates the flow obstruction. First, the patient is attached to a cardiopulmonary bypass pump. This allows the myectomy to be performed on a static heart [37]. During the procedure, the surgeon makes an incision in the ascending aorta to access the LV [36]. In the classic myectomy, an incision of 2 to 3 cm long is made, which begins at the center of the right coronary leaflet and extends to the right and left mitral-septal contacts, expanding to the basal septum [38]. Nowadays, the modified myectomy is used, adding a midventricular resection, making an incision of 5 to 6 cm long. With the modified myectomy, the anatomy of the IVS and the LVOT PG are further improved, eliminating the complaints of HOCM.

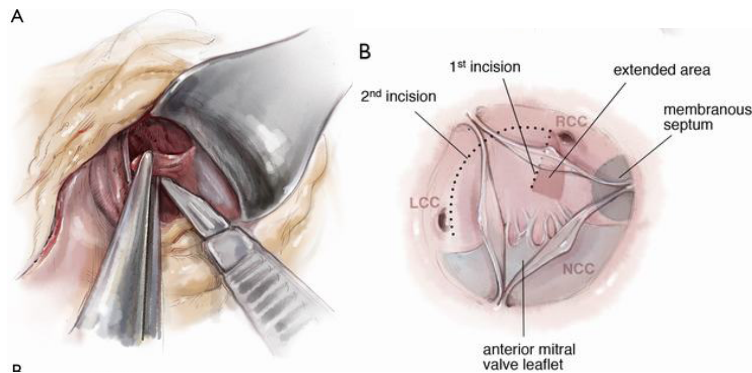


Figure 2: Morrow procedure [39] 11 blade scalpel is used to make multiple incisions in the septum removing it using an Argentine Forceps.

Pre- and postoperative imaging

Currently, 3-dimensional (3D) printed models of the individual patient can be used for the Morrow procedure [40]. The patient's heart can be imaged pre-operatively by means of magnetic resonance imaging (MRI), which then can be made into a 3D model. This gives the surgeon a better view of the anatomy, allowing him to plan and perform a more precise Morrow procedure. It is also possible to make a model of the heart including the post-operative thickness of the IVS by placing pins that indicate the original thickness of the hypertrophic septum (figure 3). The resected tissue can, intra-operatively, be placed in the 3D for better determination of the amount of already removed tissue (figure 3).

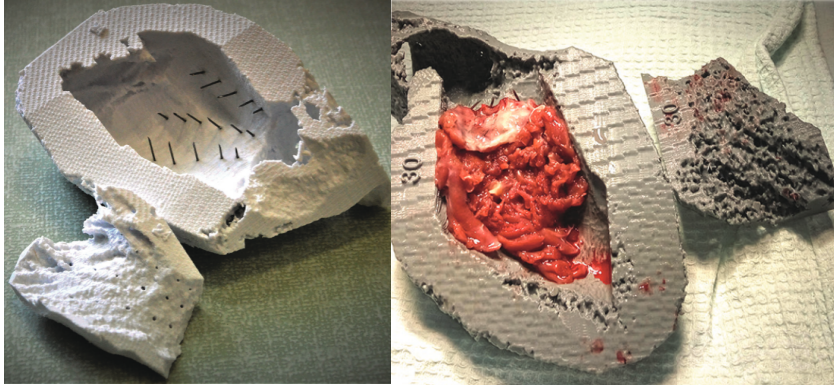


Figure 3: 3D heart models of the LV containing needles, used to determine the amount of tissue that is removed [40].

Appendix VI: Challenges

Several challenges can be found when performing the Morrow procedure to treat hypertrophic obstructive cardiomyopathy (HOCM). This research will focus on finding a solution to the challenges discussed below.

Invasivity

First of all, the procedure is invasive, consisting of cutting the sternum and dividing it to access the pericard [39]. Even though mortality after the Morrow procedure rates less than 1%, recovery times can vary from 6 to 8 weeks [41,42]. A less invasive procedure, like the right anterior minithoracotomy, can improve the recovery of patients undergoing the Morrow procedure.

Limited sight

During the procedure the right coronary cusp is distracted to the aortic wall to expose the left ventricular outflow tract (LVOT) and protect the aortic valve cusps [39]. However, the sight is still limited to make a precise resection of the interventricular septum (IVS). The surgeon has to make an incision parallel to the LVOT to a particular depth (figure 1). This act is difficult because only the anterior part of the IVS is visible. The vision is also troubled because of the cardioplegia during the procedure which increases the risk of complications

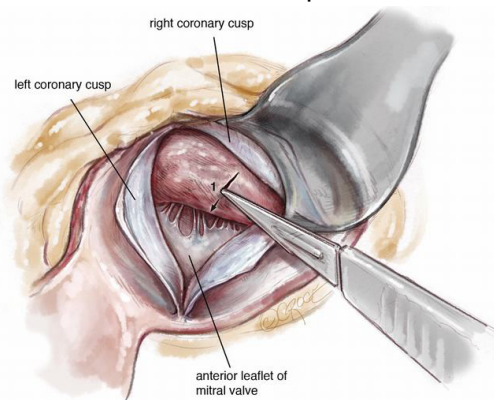


Figure 1: The surgeon makes an incision in the IVS by approaching the IVS through the aortic valve [39].

Limited workspace

The Morrow procedure has to be performed precisely which is difficult because of the limited workspace [43]. The instruments have to be inserted through the aortic valve to perform the procedure, which is a small opening, about 20-31 mm [44].

Determining the right amount of resected tissue

One of the main problems in the Morrow procedure is to determine the amount of tissue that is resected [39]. Preoperative, the amount of septum that needs to be removed is measured using ultrasound (US) or other imaging techniques. During the surgery, 3-dimensional (3D) models of the heart and intraoperative imaging can help to determine if sufficient tissue is resected. However, it remains a

challenge to resect the right amount of tissue, which may result in over- or undertreatment. Undertreatment results in the persistence of complaints. Overtreatment may lead to conduction abnormalities. According to research, approximately 40% of the patients who underwent the Morrow procedure developed a left bundle branch block and 3% a heart block after the procedure [45]. Also overtreatment can cause a ventricular septal defect, 1% of the patients, or injury to the aortic valve or mitral valve [46,47].

Not patient-specific

Pre-operative planning can be improved by a more personalized approach. Via 3D-imaging the exact thickness and localization of the hypertrophy can be measured. This way the surgeon can determine how much of the IVS needs to be resected to get an 'ideal' wall thickness of 10-11 mm [40]. However, this thickness is not based on personalized data. Because of this, over- and undertreatment can occur.

Appendix VII: State-of-the-art

In this overview, different currently used or developed methods are given for 3-dimensional (3D) planning of hypertrophic obstructive cardiomyopathy (HOCM) treatments, making an *in vitro* heart model, building a flow set-up to simulate the left ventricle (LV) and measuring the blood flow in the heart.

3D planning

In order to improve the outcome of septal myectomy a reduction of over- and undertreatment of HOCM patients is required. Nowadays, more and more hospitals use the possibility to print a 3D model from magnetic resonance imaging (MRI) images of a HOCM patient. A 3D model gives the surgeon better insight into the anatomy and helps planning the septal myectomy both pre- and intraoperative. In some hospitals, 3D models are already part of standard care [48].

More precise and objective intraoperative monitoring of the interventricular septum (IVS) thickness and the amount of resected tissue would further contribute to the minimization of over- and undertreatment.

Recently, researchers have created an experimental method for monitoring the resected tissue intraoperatively [40]. A 3D model with needles outlining the targeted excision site is used to check whether the aimed thickness is achieved (figure 1). The weighting of the resected tissue can be used as an additional measurement. Although the model is patient-specific, it does not take into account that the set IVS thickness of 10-11 mm is a general measure.

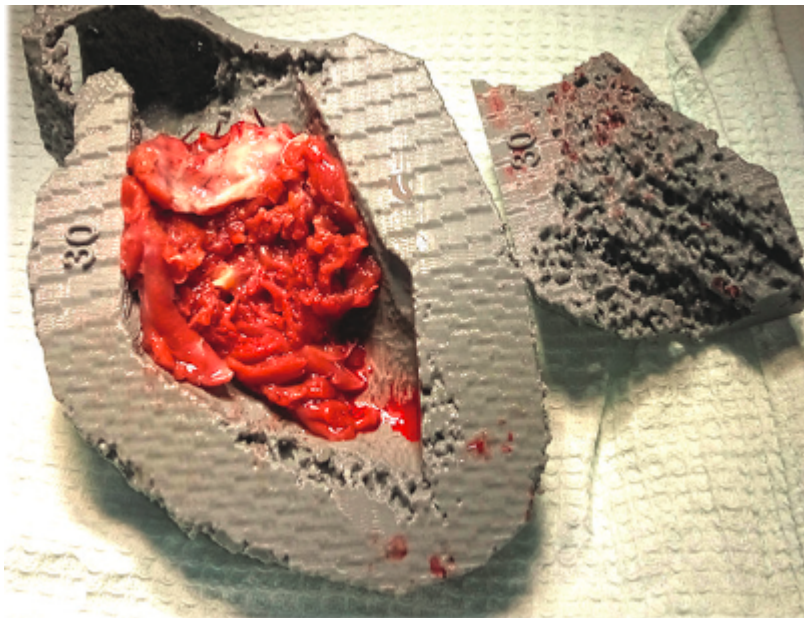


Figure 1: 3D model in which the depth and dimensions of the tissue to be resected are indicated with needles. The resected tissue is laid on these needles until the top is reached. [40]

Another way to improve the Morrow procedure is by making a 3D heart model for practising purposes [49,50]. The model is printed using hydrogel materials, therefore, creating a model with similar tissue characteristics in which the surgeon can practice the excision. By rehearsing the procedure the surgeon is less likely to resect too little or too much tissue reducing over- and undertreatment. The volume of the resected tissue is measured by liquid displacement [50]. Intraoperatively, the tissue is measured again using the same method. In this way, the surgeon can objectively determine if the volume of resected tissue is similar to that of the practice model.

Besides in vitro heart models, virtual 3D planning of the Morrow procedure can be done to better visualize the anatomical situation [51]. Either MRI or computed tomography (CT) scans from the end-diastolic phase are used to mimic the cardioplegic situation. A height colour map can be added to the virtual heart model thereby precisely indicating the degree of hypertrophy of the IVS. Next, a virtual Morrow procedure is performed by using pre-surgical planning software [52]. Unlike the method above, the surgeon does not get a hands-on simulation and measurements of the resected tissue can not be validated.

Despite the use of patient-specific 3D heart models stated above, there has not yet been research on whether and how the IVS thickness should be adjusted to the specific situation of a patient. Determining a patient-specific ideal IVS thickness could also contribute to a reduction of over- and undertreatment. The ideal thickness can be analysed by looking at which IVS thickness there is an optimal blood flow in the left ventricular outflow tract (LVOT). To achieve this a set-up with an in vitro 3D heart model and a flow is required.

In vitro heart model

There are different ways to design an in vitro heart model. To echo the flow in a heart model, an ultrasound compatible material is needed. In 3D printing different types of material are used, mostly Polylactic acid (PLA) (Ultimaker, Utrecht, The Netherlands), however, this is not suitable for ultrasound measurements [53]. Various materials are used to mimic cardiac tissue. Silicone is the most commonly used material for pouring a 3D model. It is also possible to print with hydrogels [49]. As a silicone material, Dragon Skin (Smooth-on, Macungie, United states) can be used. Dragon Skin has been used in research to mimic human tissue. Dragon Skin has a similar compliance as heart tissue [54]. Besides, it has the same speed of sound as human tissue making it a suitable material for ultrasound-guided experiments [55].

Flow set-up

To be able to measure the flow in a heart model, a flow setup is required. There are multiple methods to create a (pulsatile) flow. This can be done by either setting a constant pressure, constant flow or constant volumetric flow rate. For example, constant pressure is created by connecting two reservoirs at a fixed height difference [56]. However, it is easier to use a piston pump or a cardiopulmonary bypass (CPB). The piston pump uses a piston cup and an oscillating mechanism which moves the fluid in and out of the pump. [57] This way it can create a consistent pressure or volumetric flow rate [58]. The CPB can provide both a constant flow rate as well as a constant pressure as there are two kinds of pumps available. A roller pump provides a (pulsatile) constant volumetric flow rate and a centrifugal pump a constant pressure, both by setting the pump on a fixed number of rotations per minute. Besides, a centrifugal pump can provide a pulsatile flow by setting a pulse [59,60].

Flow measurements

Once a flow setup using 3D in vitro heart models is built, there are multiple methods to quantify and measure the flow. One option is to measure the flow using a flowmeter. However, with a flowmeter, it is challenging to measure the flow inside of the heart model at the height of the LVOT. Therefore optical particle image velocimetry (PIV) or ultrasound can provide a useful tool for flow quantifications. Optical PIV is a technique that uses a high speed camera for the detection of laser illuminated contrast in the fluid. It is a very accurate method for quantifying flow characteristics [61]. Color Doppler, continuous wave Doppler and pulsed wave Doppler are ultrasound methods used for measuring the flow [62]. Nowadays, researchers are finding new techniques to visualize the flow in 3D. An example is echo-PIV which uses 3D spatial tracking of microbubbles. However, this is still in the testing phase and specific echo-PIV software needs to be developed [63]. Another imaging technique used to visualize flow concerns the use of 4D MRI images. With this technique it is possible to capture the 3D velocity field in both the heart and vessels during a full cardiac cycle. In spite of the accurate flow patterns, the long scanning time is a limitation [64].

Appendix VIII: Subquestions

To answer the research question several sub-questions are formulated:

Anatomy

- What is the anatomy of
 - the heart valves?
 - the interventricular septum?
 - the conduction system?

(Patho)physiology

- What is the (patho)physiology of
 - a septum?
 - a systolic anterior motion?
 - the flow in the left ventricle?

Diagnosis

- How is hypertrophic obstructive cardiomyopathy (HOCM) diagnosed?

Treatment

- How is the Morrow procedure performed?
- What are the other treatment options for patients with HOCM?
- Which imaging technique is used pre- and intraoperative?
- What are the challenges of the Morrow procedure?

3D model

- How can multiple IVS thickness be simulated in a 3-dimensional (3D) heart model?
- How can a computer 3D heart model be made using magnetic resonance imaging (MRI)-data?
- How can the flow in the left ventricular outflow tract be simulated in vitro?
- How can the flow be measured in the 3D model using ultrasound?

Appendix IX: Justification

For this research, several choices were made in order to create a simplified, yet reliable set-up. A justification of these choices is given below.

Model

In designing the different models several aspects were not taken into account. Magnetic resonance imaging (MRI) images of a hypertrophic obstructive cardiomyopathy (HOCM) patient (Medisch Spectrum Twente, Enschede Netherlands) were used which were taken during diastole. This is the part of the cardiac cycle in which the heart is mechanically still for the longest time and the left ventricle (LV) volume is largest [65]. It is thus easier to make the MRI image. Also, a diastolic heart resembles the cardioplegic state which is used during surgery [66].

As the main interest of this research is the outflow in the left ventricular outflow tract (LVOT), only the left ventricle was modelled in 3-Matic 15.0 (Materialise, Leuven Belgium). Because the model is static and cannot simulate the mechanical contraction of the heart, the inflow of the fluid was created at the apex of the heart. If the inflow were to be at the mitral valve, the model could not fully empty, resulting in a residual volume. The LV model was therefore closed at the mitral valve.

The diameter of the inflow tract of the model was set at 32 mm which is the same diameter as the aorta in this case. This is chosen to create similar resistance at both flow tracts to minimize the effect on the flow.

To be able to mimic a Morrow procedure on a segmented heart 3-Matic was used and a landmark was placed on the septum from a surgical view through the aorta. This creates a certain angle at which the excision is performed. A cylindrical shaped excision at this angle was used to be able to remove the tissue. In this way, the virtual excision was done with a similarly limited view the surgeon has. The cylinder was adjusted to be able to create the aimed thicknesses. The thickness was measured at the thickest part of the septum. For each model (9, 12, 15, and 19 mm) this was done at the same place. This way the thickness could be precisely measured. The specific thicknesses were chosen to get a significant difference in the measurements of the different models. A normal septum has an average thickness of 8.92 ± 1.14 mm for men and 8.53 ± 1.3 for women mm so it would not be necessary to go below that [3]. The remaining thickness of the models was chosen to be at 11 mm as that is approximately the average value for posterior myocardial tissue in HOCM patients [67].

Material

The heart model is casted using a 3-dimensional (3D) printed mould. Casting is done because the 3D-printer (Ultimaker S5, Utrecht Netherlands) can not print materials that are suitable for ultrasound measurements. The mould is printed using a 1 mm layer of polylactic acid (PLA) and polyvinyl alcohol (PVA) support where needed. PVA is solvable in hand warm water. Because of the thin layer PLA both the inner and outer mould can be easily removed after casting. A thin layer of PLA is easily breakable especially when being heated [68].

The casting material used is Dragon skin 10 NV silicone (Smooth-On, Inc., Macungie, United States). This material is flexible, does not tear easily, is suitable for ultrasound measurements [55] and it does not require vacuum degassing during the molding process. Besides, Dragon Skin has similar

mechanical properties compared to human tissue, only it is more flexible therefore it has a higher tensile strength and 100% modulus (table 1) [69-72]. Dragon skin has been used in research for the development of artificial heart valves for practicing purposes [73]. Compared to human tissue, Dragon Skin has a slightly higher attenuation causing a limitation in the depth of view when imaging with conventional ultrasound. For this research, the limitation in depth can be neglected as the model is only a few mm thick [55].

Table 1: Mechanical properties of both Dragon Skin and Heart tissue. [70-72]

	Dragon Skin	Heart tissue
Tensile strength	400 psi = 2758 kPa	206 kPa
Shore hardness	10A	7.5 - 18.0A
100% modulus	27 psi = 186.2 kPa	60.4 kPa

Flow set-up

For the simulation of blood, a water-glycerol mixture in ratio 65/35 is used. This creates a liquid which has a viscosity similar to blood for an optimal simulation of the flow [74].

In the set-up a HL-30 cardiopulmonary bypass pump (CPB) (Maquet, Hirrlingen, Germany), is used to mimic the flow. Only a centrifugal pump is used because a pulsatile flow can be set, a constant pressure is maintained and the tubes wear more slowly [75]. This is important as the tubes are used for a longer period of time. As the LVOT pressure gradient (PG) is measured in this research, a peak flow is needed and therefore a pulsatile flow is required. A roller pump is able to maintain a constant flow by setting a fixed amount or RPM [59]. Also, only a small roller pump, which could generate a maximum volumetric flow rate of about 2 L/min, was available. This is the reason a centrifugal pump was used.

Because the measured value is the LVOT PG, the flow, and thus cardiac output, was chosen as a constant parameter. Although the cardiac output does change in HOCM patients, the pressure also changes [76]. A constant flow was chosen because the LVOT will not increase when setting a constant pressure and the measurements would not give valuable information.

Because the centrifugal pump is resistance dependent the flow has to be measured at the pump and set to the right value at every measurement. The pressure was measured using the velocities given by the ultrasound and the simplified Bernoulli equation (appendix III, formula 7).

There is different tubing available for the CPB pump. The largest possible tubes that fit the centrifugal pump have a diameter of $\frac{3}{8}$ inch (Raumedic AG, Helmbrechts, Germany). The greatest resistance should be in the LVOT. In order to minimize the resistance caused by the in- and outflow of the model, the diameter difference should be minimal. The in- and outflow diameters of the model are 32 mm. The largest tubes of $\frac{3}{8}$ inch are therefore utilised in the set-up.

Measurements

To measure the flow in the LVOT, a Philips CX50 ultrasound device (Philips Ultrasound Systems, Bothell, WA) with an S5-1 cardiac ultrasound probe is used (appendix XVII). This is done because the same technique is used in the clinic to diagnose patients with HOCM [24]. With ultrasound it is possible

to measure the velocities in the LVOT which can be used to calculate the PG. The quantitative variable used to compare the different models is the PG. This is also done because it is the main indication in the clinic for HOCM diagnosis [24]. Also, this way the model can be easily compared to the original physiological measurements.

The LVOT PG is calculated using the simplified Bernoulli equation (appendix III). In this equation the density of blood is integrated in the shape of the value 4. Because in the set-up a glycerol-water volumetric mixture, and not blood, is used the density also varies and using the simplified Bernoulli equation creates an error. This can be corrected by calculating the right value for the simplified equation. This is done by first calculating the mass-fraction glycerol that is used for the mixture. Then, using the table from [77], the density of the mixture is determined at room temperature. This creates the following calculation:

The volumes used in the mixture were 350 ml glycerol and 650 mL water so 0.000350 and 0.000650 m³. The density of glycerol and water are respectively 1262.3 and 997 kg/m³. This means that the mass fraction is:

$$(0.000350 \times 1261.3) + (0.000650 \times 997) = 1.089505 \text{ kg} \rightarrow \frac{0.000350 \times 1261.3}{1.089505} = 0.405188595$$

By looking up this value in the table and interpolating the two values above and below it, the final density of the solution is 1100.65 kg/m³ for room temperature. This means that the value in the Bernoulli equation should be:

$$1100.65/2 \times 0.00750 = 4.127$$

This will create a difference in the measurements of about 1 mmHg.

When measuring the LVOT PG continuous wave doppler (CWD) is used. Pulsed wave doppler (PWD) is not suitable for the measurements as aliasing occurs at high velocities [24]. CWD is able to capture higher velocities without aliasing. Another reason CWD is used instead of PWD is that PWD measures the velocity on a selected location while CWD measures the highest velocity on a chosen line [12]. PWD is used to determine at which point the highest velocity occurs which is then used to determine where the CWD line should be placed in the ultrasound images. A more accurate measurement could be done using other flow imaging techniques like optical particle image velocimetry (PIV). However, using ultrasound (US) makes the step to clinical application smaller.

The average value of the cardiac output is 5-6 L/min [78]. A pulsatile flow of 5.5 L/min is therefore set to mimic a physiological cardiac output at rest. The pulse settings were set from 20-80% to simulate the systolic phase of the cardiac cycle. In order to maintain a flow of 5.5 L/min the base of the pulse is set to 40% To simulate the situation at rest, the heart rate was set to 65 bpm as this is the average heart rate of the patient.

In order to further investigate the difference between the HOCM model (19 mm) and the extreme Morrow procedure model (9 mm) the flow is altered and the LVOT PG is again measured. The minimal flow is chosen to be set at 4.0 L/min as below this value it is difficult/not possible to measure flow velocities. The maximal flow is set at 6.2 L/min because this is the maximal rate the centrifugal CPB pump can generate.

Measurements were performed in duo's. Researcher A operates the US machine while researcher B places and holds the probe in the right place. This method of measurement is chosen so the researchers can fully focus on a specific task. With inexperience comes the risk of moving the US probe while operating the US device and those artifacts are unwanted. In total there are four researchers so two duo's. Each person performs three measurements for each condition to make sure the measurements are more reliable. So each duo generates six measurements for each condition. Each time a researcher has performed three contiguous measurements, the LV model is removed from the set up. This way, the conditions under which the measurements are done, remain stable for each researcher.

Appendix X: Data management plan

General information

Students group 23

Milou Baarsma - s2113473
Arno Fennema - s2113732
Evie Graus - s2090481
Carla van der Poel - s2107732

Supervisors

Dr. F.R. Halfwerk (Technical Medicine supervisor)
Dr. M. A. Koenrades (Technical Medicine supervisor)
K. C. Smits, BSc (Technical Medicine supervisor)
Dr. R.G.H. Speekenbrink (Medical supervisor)
Ir. E.E.G. Hekman (Technical supervisor)
M. van Ochten, BSc (Personal supervisor)

Title: In vitro modelling of the flow in hypertrophic obstructive cardiomyopathy 3-dimensional heart models

Project duration: 11 weeks (19/04/2021 - 30/06/2021)

Data collection

Collected data: measured flow in 3D printed left ventricle models, regarding experimental, simulation and derived data

- i. US images → DICOM or SPF (experimental data)
- ii. MRI images of a healthy heart and a hypertrophic obstructive cardiomyopathy heart. (derived data)
- iii. 3D printed silicone heart models and moulds (simulation data)

Rights data: MRI images used for making 3D models are provided by Medisch Spectrum Twente (MST) and therefore they have the data rights. The patient has agreed that the images are used for medical research. MST gave us permission to use and process the data outside the hospital. During the research period we, as a group, have the rights over the measured US data and the 3D heart models and moulds.

Data security and storage

Data will be saved on our computers. Structural naming of all data is provided, including group name, subject and date to ensure it is understandable for secondary users. To make sure the data is secured the data is saved in an encrypted folder.

Data transfer

At the end of our research period (30/06) the data will be transferred to the University of Twente who functions as co-owner of all data. We will sign a document to give permission.

Appendix XI: Troubleshooting

During this research, several setbacks and problems were encountered. To prevent future researchers making the same mistakes and save time in solving these problems, the following document is created to show the troubles this research had to overcome.

Designing the moulds

In designing the moulds it is advised to not use pins and holes to connect different parts of the mould as it is difficult to precisely fit those two. If pins and holes are used and turn out not to fit, it can be adjusted with sandpaper and a file to make it fit.

If 3-Matic gives a pop-up stating that there are several bad edges in the design, fix this by consulting the Fix wizard tool. Follow the advised steps.

Casting the moulds

It is not recommended to use reusable beakers for mixing the Dragon Skin 10 NV as it is a sticky silicone which is difficult to remove when set. In addition, the use of a vacuum degasser is discouraged. This is due to the fact that the pot life is only 15 minutes and vacuum degassing takes more time. If the degassing is performed while the silicone is curing it will cause large gas bubbles instead of removing them.

If after the stated cure time the silicone still feels sticky, let it set for a longer period of time. It is advised not to let the silicone cure in a cold environment as this prolongs the curing process.

Set-up

If the flow cannot be increased further to achieve the desired flow of 6.2 L/min, this can be caused by a high resistance somewhere in the set-up. Using only $\frac{3}{8}$ inch or larger tubes is recommended in this research. When choosing smaller tubes, the resistance will increase causing a lower maximum flow. Additionally, it is important to not use an intravenous bag as a reservoir. The inflow and outflow diameters are relatively small compared to the $\frac{3}{8}$ inch tubes used. Again, causing a limited flow.

For connecting the model to the tubes of the Cardiopulmonary Bypass (CPB) pump, do not use coupling pieces made out of polylactic acid (PLA). PLA is not water resistant causing water to leak out of the system. Also, the relatively thick edge of the coupling pieces create an extra pressure component on the model which can cause the tubes to unlink when a flow is applied. Instead of printing the coupling pieces with an Ultimaker 3-dimensional (3D) printer and PLA and thick edges, use a Formlabs 3D printer with white resin instead and smoothen the edges.

If one of the tubes is still subject to the risk of shooting loose, seal the coupling piece with tie wraps over the model at the place where the coupling piece enters the model.

There is also a possibility that there are bubbles in the system which cause an altered flow or influence the ultrasound measurements. If this is the case, lift the reservoir to a height above the model, pump and tubes. Move the model and tubes until all the air is trapped in the reservoir. Next, remove the air from the reservoir by opening the venting tube and pushing the air out of the bag. Close the venting tube after all the air is out.

Setting pump

If the centrifugal pump is not able to generate a flow of 6.2 L/min, set the base of the puls to a minimum of 40%.

When the pump is used for a longer period of time there is a chance of overheating. The CPB pump will give a notification if this is the case. Make sure the pump is positioned in a way that the ventilator has enough room to ventilate. If this is not sufficient to cool down the pump, turn off the pump and wait till the pump is cooled down again.

Ultrasound device

When performing the ultrasound measurements, specifically the continuous wave doppler measurements, it is possible that there is (a lot of) noise. To remove most of the noise, set the gain to a lower value.

The depth of the ultrasound B-mode measurement can be adjusted to make more accurate measurements. The visualization of the left ventricular outflow tract (LVOT) is only necessary. If more structures are taken into the measurement, the pressure gradient (PG) will be influenced.

Appendix XII: Pre- and post-operative information patient

This research used magnetic resonance imaging (MRI) data of a patient with hypertrophic obstructive cardiomyopathy (HOCM). The patient was a middle aged male who suffered from progressive dyspnoe d'effort. His interventricular septum thickness (IVSt) was 19 mm and he had a left ventricular outflow tract (LVOT) pressure gradient (PG) of 20 mmHg in rest and 85 mmHg during exercise. The patient mainly suffered from the contribution of systolic anterior motion (SAM) to the obstruction instead of the thickened IVS.

He underwent a Morrow procedure after which a IVSt of 12 mm remained. The post-operative LVOT PG was reduced to 6 mmHg in rest and 13-16 mmHg when performing a Valsalva maneuver. The dyspnoea was solved. However the patient complained of jerky breathing.

Appendix XIII: Protocol - Designing the moulds

Protocol: Designing the 3D moulds

25/06/2021

Technical Medicine - Bachelor thesis

Students group 23

Milou Baarsma - s2113473
Arno Fennema - s2113732
Evie Graus - s2090481
Carla van der Poel - s2107732

Supervisors

Dr. F.R. Halfwerk (Technical Medicine supervisor)
Dr. M. A. Koenrades (Technical Medicine supervisor)
K. C. Smits, BSc (Technical Medicine supervisor)
Dr. R.G.H. Speekenbrink (Medical supervisor)
Ir. E.E.G. Hekman (Technical supervisor)
M. van Ochten, BSc (Personal supervisor)

Introduction

This protocol explains how the different moulds are designed in 3-matic 15.0 (Materialise, Leuven, Belgium). Five different moulds and two coupling pieces are designed;

- a. Cylinder for validation
- b. LV with IVSt of 19 mm
- c. LV with IVSt of 9 mm
- d. LV with IVSt of 12 mm
- e. LV with IVSt of 15 mm
- f. Coupling pieces

Method

Cylinder for validation

A test model is designed to validate the heart models. It is made by casting Dragon Skin 10 NV (Smooth-on Inc., Macungie, United States) in an inner- and outer cylindrical mould. This chapter describes the designing of the inner- and outer test model.

Inner mould

The inner mould is designed to create a tube when casting the mould with silicone. The tube will have a radius of 16 mm and a length of 200 mm. It will also have a lid so the mould can be closed.

Inner tube

- Design → Create Analytical Cylinder → $r = 16.000$ mm, $l = 200.000$ mm
→ Convert Analytical Primitive to Part → Cylinder 16 mm

Mould lid

- Design → Create Analytical Cylinder → $r = 31.000$ mm, $l = 200.000 - 210.000$ mm →
Convert Analytical Primitive to Part → Cylinder 31 mm
- Design → Boolean union → Union entities = Inner tube, Mould lid → Inner mould (figure 1)

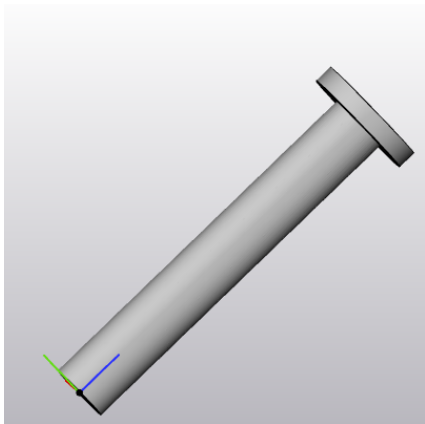


Figure 1: The inner mould of the test mould.

Mould lid pins

The lid will be connected to the outer mould using attaching pins on the inner mould that fit tightly in holes in the outer mould.

- Create points
 - *Point 1*
 - Design → Create Analytical Cylinder → $r = 2 \text{ mm}$, $l = 5 \text{ mm}$ → Convert analytical primitive to part → Point 1
 - *Point 2*
 - Design → Create Analytical Cylinder → $r = 2 \text{ mm}$, $l = 5 \text{ mm}$ → Convert analytical primitive to part → Point 2
 - *Point 3*
 - Design → Create Analytical Cylinder → $r = 2 \text{ mm}$, $l = 5 \text{ mm}$ → Convert analytical primitive to part → Point 3
 - *Point 4*
 - Design → Create Analytical Cylinder → $r = 2 \text{ mm}$, $l = 5 \text{ mm}$ → Convert analytical primitive to part → Point 4
- Duplicate points (for subtraction of outer mould)
- Design → Boolean union → Union entities = Inner mould, points 1, 2, 3 en 4 (figure 2) → Inner mould

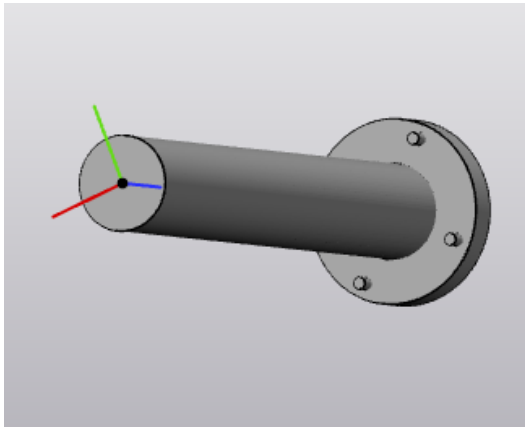


Figure 2: The inner mould of the test mould with lid pins.

Outer mould

The outer mould will determine the diameter of the testmodel. The radii are 26 and 21 mm which results in two different thicknesses of silicone after casting. The outer mould will consist of two separate parts which can be connected using pins and pinholes. This is done so that the silicone can easily be removed from the mould.

Inner part of the outer mould with a big diameter

- Design → Create Analytical Cylinder → $r = 26.000 \text{ mm}$, $l = 100.000 - 200.000 \text{ mm}$ → Convert Analytical Primitive to Part → Cylinder

Inner part of the outer mould with a small diameter

- Design → Create Analytical Cylinder → $r = 21.000 \text{ mm}$, $l = 0 - 100.000 \text{ mm}$

Outer part of the outer mould

- Design → Create Analytical Cylinder → $r = 31.000 \text{ mm}$, $l = 0 - 200.000 \text{ mm}$

Inner part and outer part connected

- Design → Boolean subtraction → Entities = Outside, Subtractions entities = small part and big part, Clearance off → Outer mould

Outer mould with lid pinholes

- Design → Boolean subtraction → Entities = Outer mould, Subtractions entities = duplicate points 1, 2, 3 en 4, Clearance on → Clearance factor = 0.300 mm (figure 3) → Outer mould

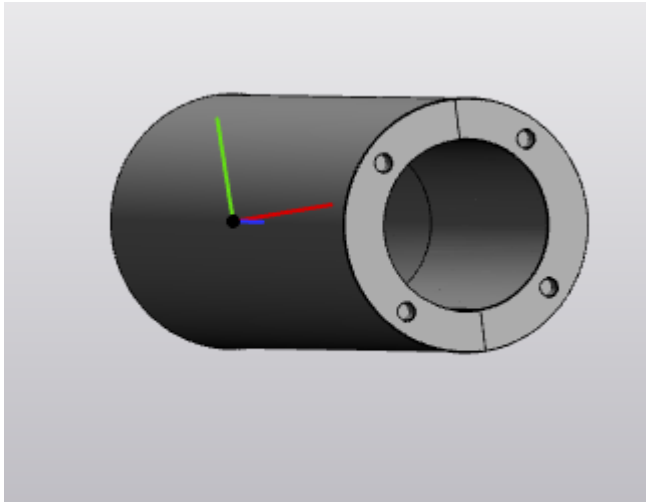


Figure 3: The outer mould of the test mould with holes for the lid pins.

Bisect outer mould

- Design → Create Datum Plane
- Design → Cut → Entities: Outer mould, Cutting Entity: Datum Plane (figure 4)

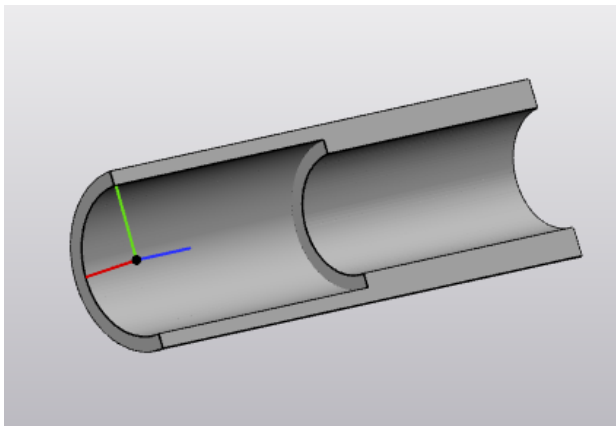


Figure 4: The bisected outer mould of the test mould.

Outer mould pins

- Create points
 - Point 5
 - Design → Create Analytical Cylinder → $r = 2 \text{ mm}$, $l = 5 \text{ mm}$ → Convert analytical primitive to part → Point 5
 - Point 6

- Design → Create Analytical Cylinder → $r = 2 \text{ mm}$, $l = 5 \text{ mm}$
→ Convert analytical primitive to part → Point 6
- Point 7
 - Design → Create Analytical Cylinder → $r = 2 \text{ mm}$, $l = 5 \text{ mm}$
→ Convert analytical primitive to part → Point 7
- Point 8
 - Design → Create Analytical Cylinder → $r = 2 \text{ mm}$, $l = 5 \text{ mm}$
→ Convert analytical primitive to part → Point 8
- Point 9
 - Design → Create Analytical Cylinder → $r = 2 \text{ mm}$, $l = 5 \text{ mm}$
→ Convert analytical primitive to part → Point 9
- Point 10
 - Design → Create Analytical Cylinder → $r = 2 \text{ mm}$, $l = 5 \text{ mm}$
→ Convert analytical primitive to part → Point 10
- Duplicate points 5, 6, 7, 8, 9 and 10
- Design → Boolean union → Union entities = Outer mould 1, points 5, 6, 7, 8, 9 and 10 (figure 5)

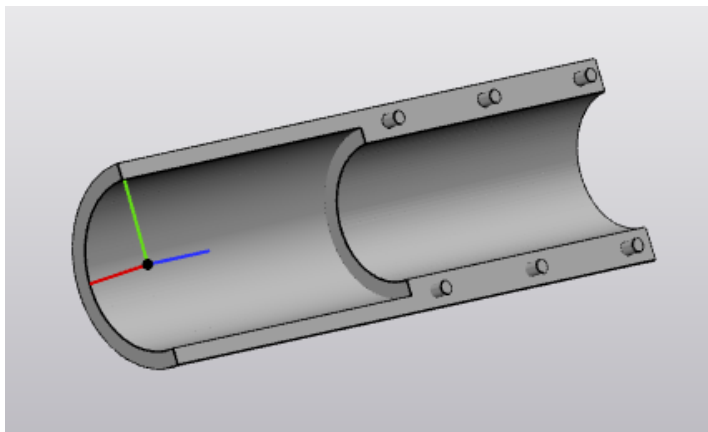


Figure 5: The bisected outer mould of the test mould with lid pins.

- Design → Boolean subtraction → Entities = Outer mould 2, Subtractions entities = duplicate points 5, 6, 7, 8, 9 and 10, Clearance on → Clearance factor = 0.300 mm

Export file

Before printing, the coupling piece is finished by fixing little mistakes.

- Fix → Fix Wizard
- File → Export STL, Entities: Mould

LV with IVSt of 19 mm

After making a test mould, the left ventricle (LV) moulds are made. First a mould is made which is based on the segmented hypertrophic obstructive cardiomyopathic (HOCM) heart which is obtained from magnetic resonance imaging (MRI) data. This heart has an interventricular septal thickness (IVSt) of 19 mm. First the outlet and inlet of the LV are prepared which forms the inner mould. After that the outer mould is designed.

Designing parts for outlet

The outlet will consist of a tube with a diameter of 16 mm.

- Import part → Aorta and Left ventricle
- Design → Create Analytical Primitive → Create Datum Plane
- Design → Cut → Entities: Aorta, Cutting Entity: Datum Plane → Upper Aorta and Lower Aorta
- Design → Create Analytical Cylinder → Method: Fit Cylinder (to Upper Aorta) → Radius: 16.0000 → Convert Analytical Primitive to Part → Cylinder
- Design → Cut → Entities: Cylinder, Cutting Entity: Datum Plane → Upper Cylinder and Lower Cylinder
- Delete → Upper Aorta and Lower Cylinder

Creating a surface on LVOT and aorta

To ensure that the aorta and left ventricular outflow tract (LVOT) will fit together correctly, surfaces need to be created on both objects.

- Design → Create Datum Plane, Method: Through 1 point, parallel to a1 plane, Parallel plane: Fit Triangle Left Ventricle → Datum Plane
- Align → Interactive translate, Main entity: Datum Plane
- Mark → Brush Mark → Wave Brush Mark → Select surface LVOT (figure 6a) → Delete (figure 6b)
- Fix → Fill hole freedom → Entities: Contour LVOT (figure 6c)

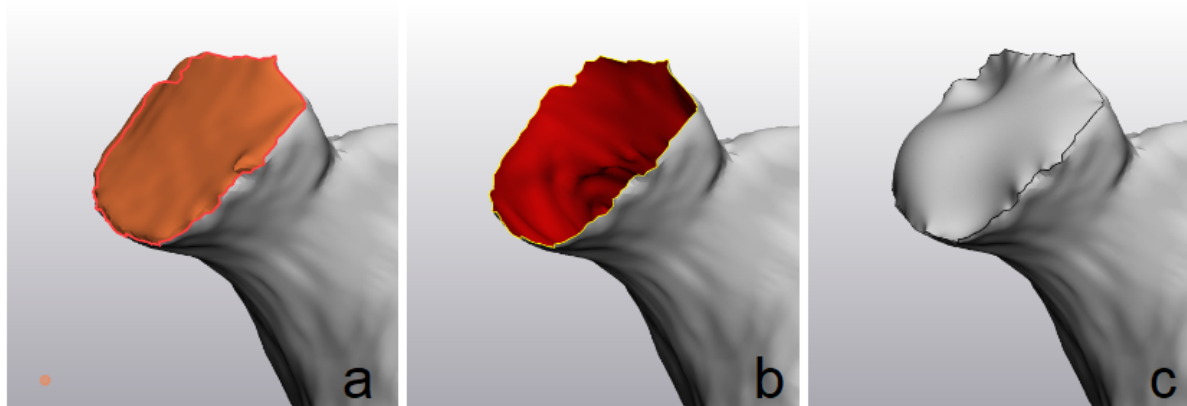


Figure 6: The created surface on the LVOT of the IVSt 19 mm mould. a. The selection of the cutted part of the LVOT. b. The selected part is deleted. c. The filled new LVOT surface.

- Align → Interactive translate, Main entity: Datum Plane

- Mark → Brush Mark → Wave Brush Mark (figure 7a) → Select surface aorta → Delete (figure 7b)
- Fix → Fill hole freedom → Entities: Contour aorta (figure 7c)

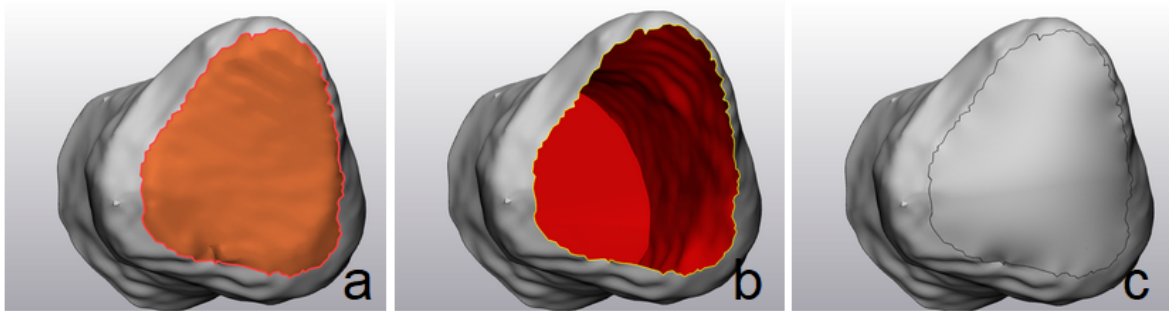


Figure 7: The created surface on the aorta of the IVSt 19 mm mould. a. The selection of the cutted part of the aorta. b. The selected part is deleted. c. The filled new aorta surface.

Designing parts for inlet

To minimize the resistance the inlet will have a radius of 16 mm. The inlet will be connected to the apex of the LV.

- Design → Create Analytical Primitive → Create Datum Plane
- Design → Cut → Entities: Left ventricle, Cutting Entity: Datum Plane → Left ventricle
- Design → Create Analytical Cylinder → Method: 2 points → Convert Analytical Primitive to Part → Lower Cylinder

Connecting outlet and inlet to LV

The inlet and outlet need to properly fit on the apex and aorta. To do this the surfaces will be gradually connected using loft.

- Design → Loft → Entity 1: Surface aorta , Entity 2: Surface LVOT → LVOT connection → Merge surface list (figure 8a)
- Design → Loft → Entity 1: Surface aorta, Entity 2: Surface cylinder → Aorta connection→ Merge surface list (figure 8b)
- Design → Loft → Entity 1: Surface Left Ventricle, Entity 2: Surface cylinder → Apex connection Merge surface (figure 8c)

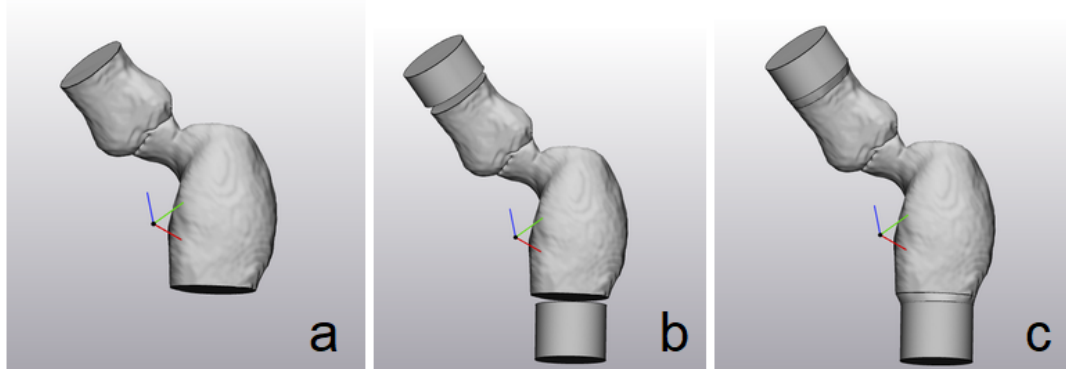


Figure 8: The connected inlet and outlet to the LV. a. The attached aorta to the LV. b. The attached outlet cylinder to the aorta. c. The attached inlet cylinder to the apex.

- Design → Boolean Union → Entities: Apex connection, Aorta connection, LVOT connection, Upper Cylinder, Lower Cylinder, Left ventricle and Lower Aorta → Inner mould (figure 9)
- Fix → Improve mesh → Entities: Inner mould

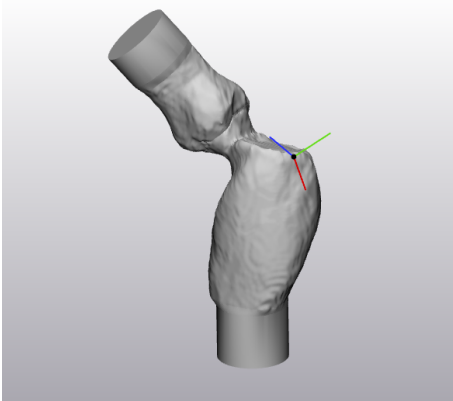


Figure 9: The merged surface sets of the IVSt 19mm mould and improved mesh.

Thicken inner mould

In order to 3-Dimensional (3D) print the inner mould, it needs to have a thickness of 1 mm. This is achieved by thickening the inner mould and subtracting the original from the thickened LV.

- Inner mould → Duplicate → Inner mould duplicate
- Design → Uniform offset → Entities: Inner mould duplicate, Internal offset, distance = 2.0000 mm → Inner mould inner inside
- Design → Uniform offset → Entities: Inner mould inner inside, External offset, distance = 1.0000 mm → Inner mould inner
- Design → Boolean subtraction → Entities: Inner mould duplicate, Subtraction: Inner mould inner → Inner mould hollow
- Fix → Fix wizard → Surface List → Merge all surfaces in set (figure 10)

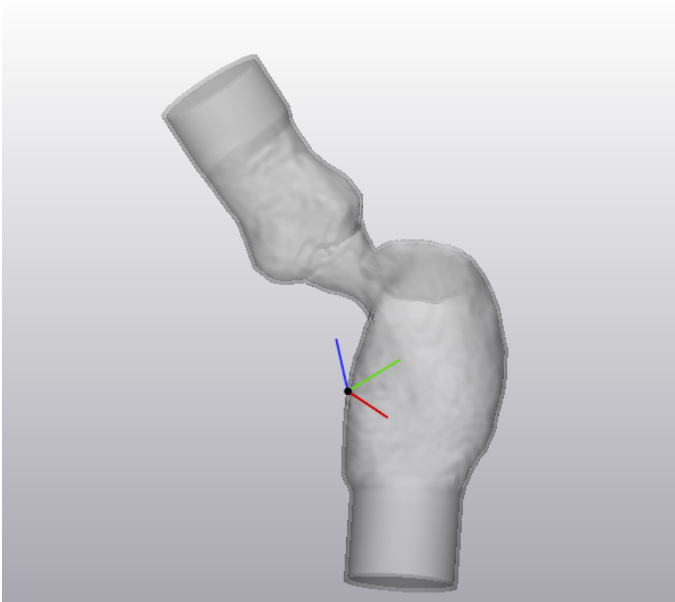


Figure 10: The thickened inner mould of the IVSt 19mm mould.

Making outer mould

The outer mould will be the outside of the LV model and therefore needs to be 11 mm bigger than the inner mould. It also needs to be 1mm thick to 3-dimensional (3D) print it after the design is finished.

- Design → Uniform offset → Entities: Inner mould duplicate, External offset, distance = 11.0000 mm → Outer mould inner (figure 11a)
- Outer mould inner → Duplicate → Outer mould inner duplicate
- Design → Uniform offset → Entity: Outer mould inner duplicate, External offset, distance = 1.0000 mm → Outer mould outer
- Design → Boolean subtraction → Entity: Outer mould outer, Subtraction: Outer mould inner → Outer mould hollow
- Fix → Fix wizard → Surface List → Merge all surfaces in set (figure 11b)

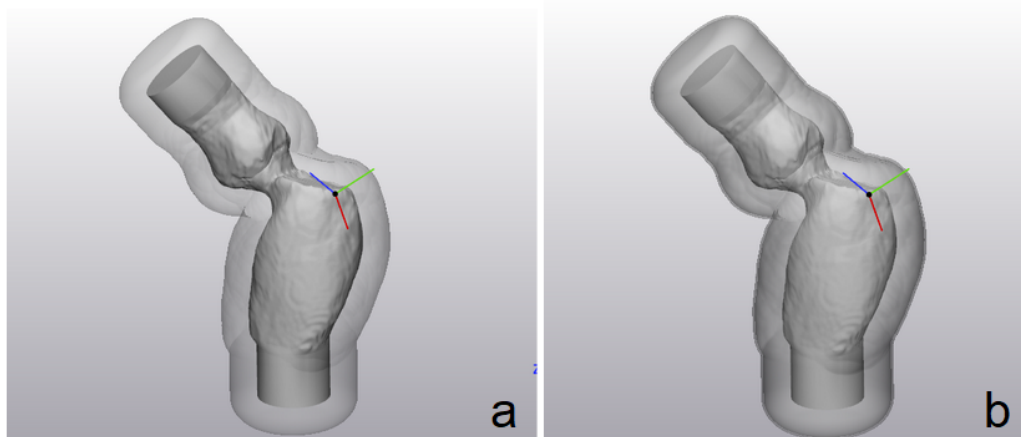


Figure 11: The outer mould of the IVSt 19mm mould. a. The created first layer of the outer mould. b. The thickened layer of the outer mould.

Adjusting outer mould to inner mould

To achieve the same lengths for the inner and outer moulds, the top and bottom of the outer mould need to be cut at the ends of the inner mould.

- Design → Create Datum Plane, Through 1 point, parallel to a plane, parallel plane: inlet side Inner mould, Fit triangle
- Align → Interactive translate, Main entity: Datum Plane (figure 12a)
- Design → Cut, Entities: Outer mould hollow & Inner mould hollow, Cutting Entity: Datum Plane (figure 12b)

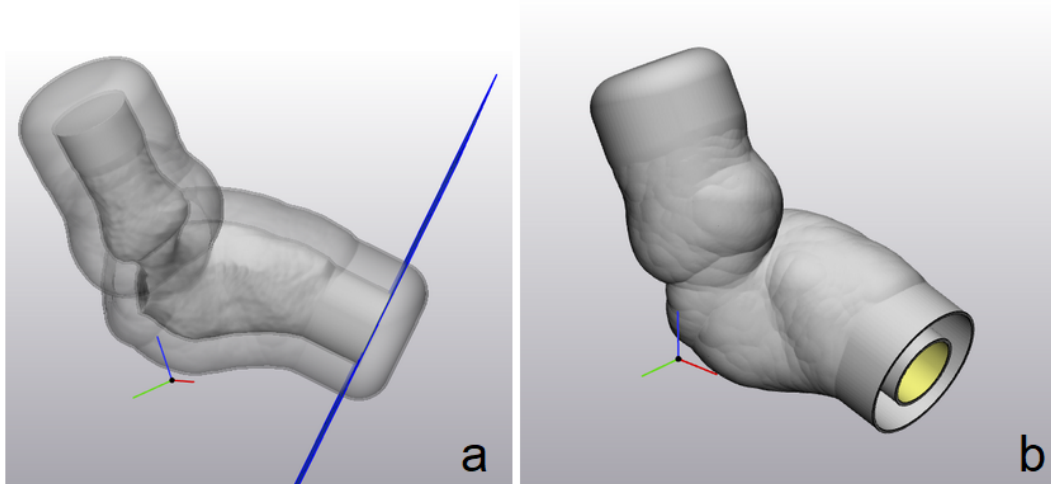


Figure 12: The cutted inlet of the initial inner and outer mould of the IVSt 19 mm mould. a. The created Datum plane. b. The cutted mould.

- Design → Create Datum Plane, Through 1 point, parallel to a plane, parallel plane: outlet side Inner mould, Fit triangle
- Align → Interactive translate, Main entity: Datum Plane (figure 13a)
- Design → Cut, Entities: Outer mould hollow & Inner mould hollow, Cutting Entity: Datum Plane (figure 13b)

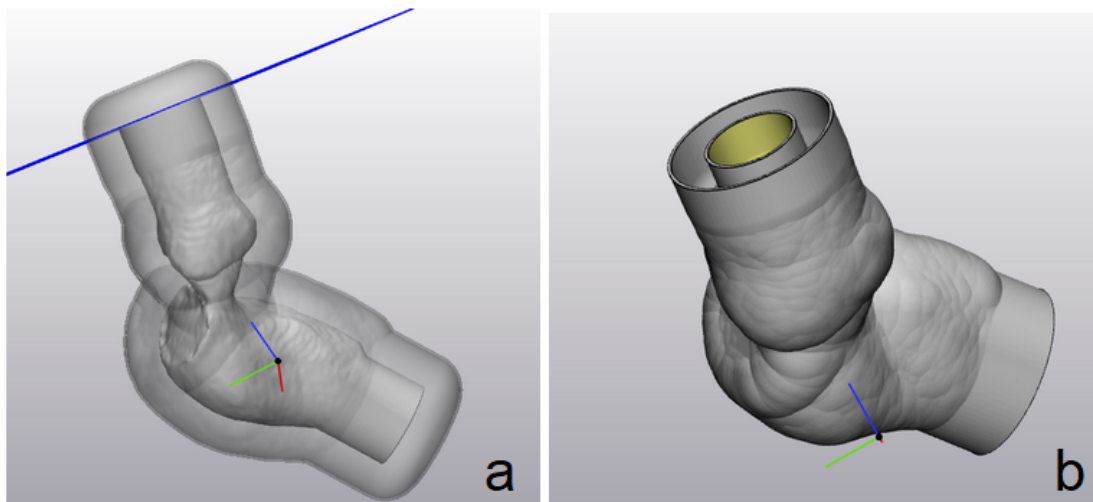


Figure 13: The cutted outlet of the initial inner and outer mould of the IVSt 19 mm mould. a. The created Datum plane. b. The cutted mould.

Closing the outer and inner mould at the apex

The inner and outer mould need to be closed to ensure silicone can be casted into it. Also, this way both moulds are connected to each other.

- Design → Create Analytical cylinder, radius = 29.000 mm, length = 1.000 mm
- Design → Convert Analytical Primitive to Part → Cylinder
- Align → Plane to Plane Align, Plane on fixed entity: Fit surface: Outer mould hollow, Plane on moving entity: Fit surface (Cylinder) Method: Coincident face to face → Lid outer mould
- Design → Boolean Union, Entities: Lid outer mould and Outer mould hollow → Merge surface list → Outer mould (figure 14)

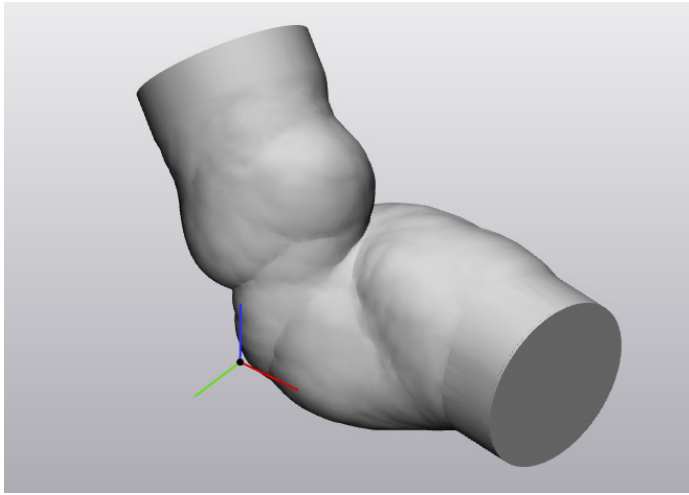


Figure 14: The closed apex of the inner and outer mould of the IVSt 19mm mould.

Connecting the outer and inner mould for printing

Before printing, the mould is finished by uniting everything and fixing little mistakes.

- Design → Boolean Union, Entities: Outer mould & Inner mould → Mould
- Fix → Fix Wizard
- File → Export STL, Entities: Mould

LV with IVSt of 9, 12, and 15 mm

Next to the LV mould of the HOCM heart, three LV models are made to simulate a performed Morrow procedure. Thicknesses of the IVSt after the Morrow procedure of 9, 12, and 15 mm are used. The protocol is described for making a mould of an IVSt of 9 mm but the protocol for making the moulds of an IVSt of 12 and 15 mm is similar.

Import IVSt mould

- File → Open project → Mould

Create a surface color map

A color map can show the thicknesses of the heart which gives insight into the degree of HOCM.

- Analysis → Create wall thickness analysis

Create landmarks

Landmarks are created to determine the angle at which a surgeon would be able to perform a Morrow procedure and to get consistency in the different virtual procedures. The landmarks are based on the length, depth and angle of an incision during a Morrow procedure.

- Design → Create Datum Plane
- Design → Cut → Entities: Left myocardium, Cutting entities: Datum Plane (figure 15) → Left myocardium 1 and Left myocardium 2
- Hide Left myocardium 2

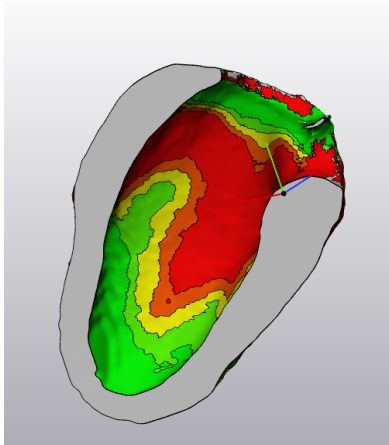


Figure 15: The myocard is cutted according to a frontal view.

Design → Create Line, method: (between thickest part of septum) → Line 1 (figure 16)

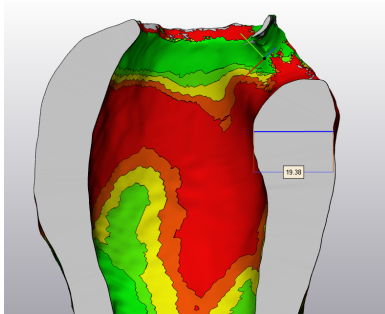


Figure 16: A line is created on the thickest part of the septum of the myocard.

- Aorta → Show
- Design → Create Point (surgical view through aorta) → Landmark 1 (figure 17)

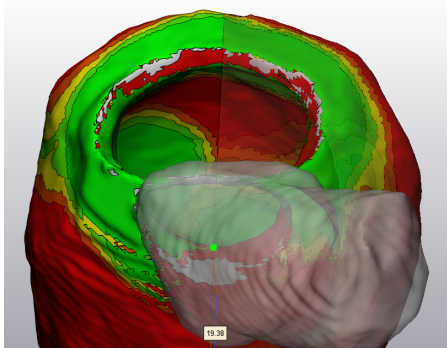


Figure 17: A landmark (landmark 1) is created on the myocardium the spot of the IVS which is visible according to the transaortic view.

- Design → Create Point (lowest Morrow procedure point) → Landmark 2
- Measure → Measure Distance (between the two landmarks for resection) → Line 2 (figure 18)

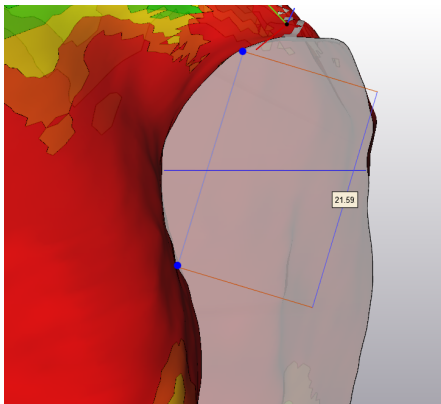


Figure 18: The distance is measured of the wanted length of the incision of the Morrow procedure. The lowest point of the incision is marked with landmark 2.

- Design → Create Point (select the thickness you want to achieve on line 1) → Landmark 3
- Performing Morrow procedure

The Morrow procedure is performed to create different models with different thicknesses of the septum. This is done using virtual cutting tools.

- Design → Create Analytical Cylinder (make a cylinder through landmark 1 and 2) → Convert Analytical Primitive to Part → Cylinder (figure 19)

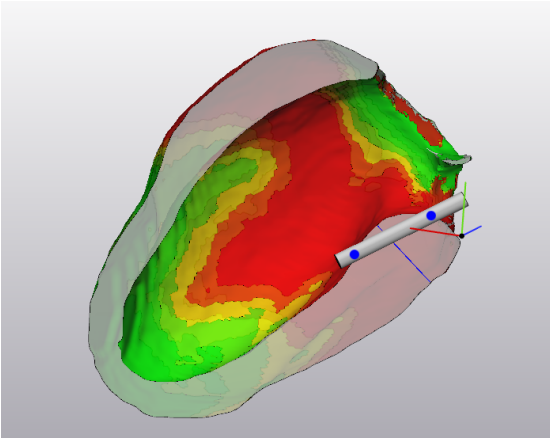


Figure 19: A cylinder is created on the septum of the myocard to be able to create a sketch which is necessary to perform the virtual Morrow procedure.

- Sketch → New sketch → Through 1 point, parallel to a plane → Parallel plane: Top Cylinder, fit surface → Cells count: 60, 60
- Import References to Sketch → Selection: sketch, Projection: Landmark 1, Landmark 2, Landmark 3 & Line 1, Outline: Left myocardium 1 → 9 mm
- Sketch → Line segment (make 3 line segments)
- Sketch → Create circle arc (figure 20)

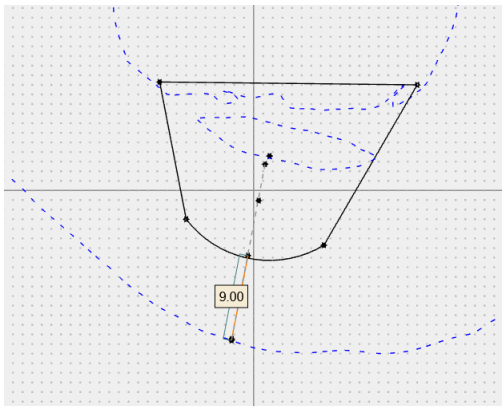


Figure 20: A sketch is created which determines the shape of the incision of the Morrow procedure.

- Design → Extrude, Entity: 9 mm, Depth: 50 mm (figure 21)

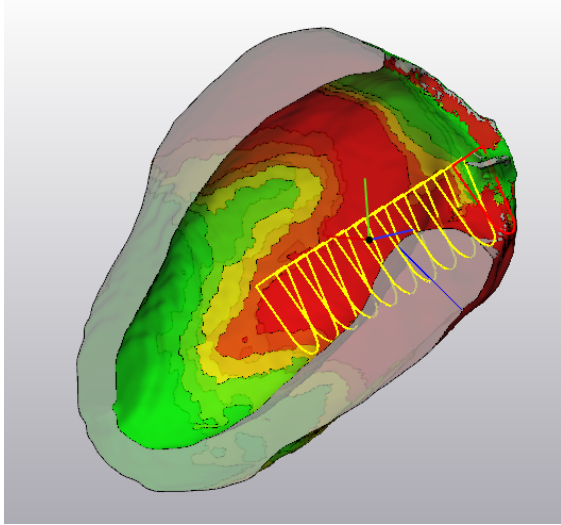


Figure 21: The virtual Morrow procedure is performed making use of the sketch.

- Design → Cut, Entities: Left myocardium, Cutting Entity: Extrude 9 mm → Morrow executed 9 mm resection (figure 22)
- Mark → Wave Brush Mark (remove excess parts)

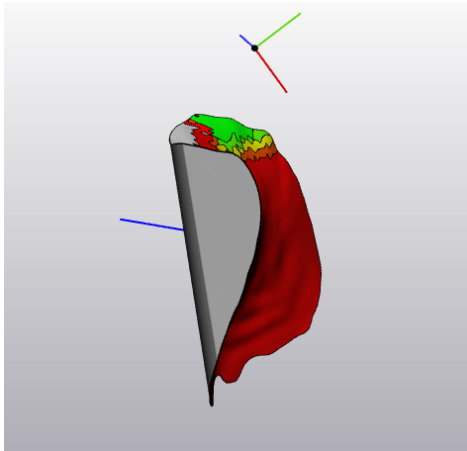


Figure 22: The resected tissue after performing the virtual Morrow procedure.

Create an inner- and outer mould

The resected part of the myocard after the virtual Morrow procedure is added to the moulds. This way, the silicone models will have a part where the septum is reduced.

- Merge all thicknesses surface list Morrow executed 9 mm resection
- Design → Uniform Offset → Entities: Morrow executed 9 mm resection → Internal Offset, 2mm → Fix → Fix wizard
- Design → Boolean Subtraction → Entities: Inner mould, Subtraction Entities: Morrow executed 9 mm resection → Inner mould 9 mm
- Surfaces → Delete surfaces (all thicknesses except for the most outer part) (merged surface) from Morrow executed 9 mm resection
- Design → Uniform Offset → Entities: Morrow executed 9 mm resection → Internal Offset, 1 mm

- Design → Boolean Subtraction → Entities: Morrow executed 9 mm resection, Subtraction Entities: Inner mould inside (imported from previous file)
- Design → Boolean Union → Entities: Morrow executed 9 mm resection and Inner mould 9 mm → Surface List → Merge all surfaces in set (figure 23)

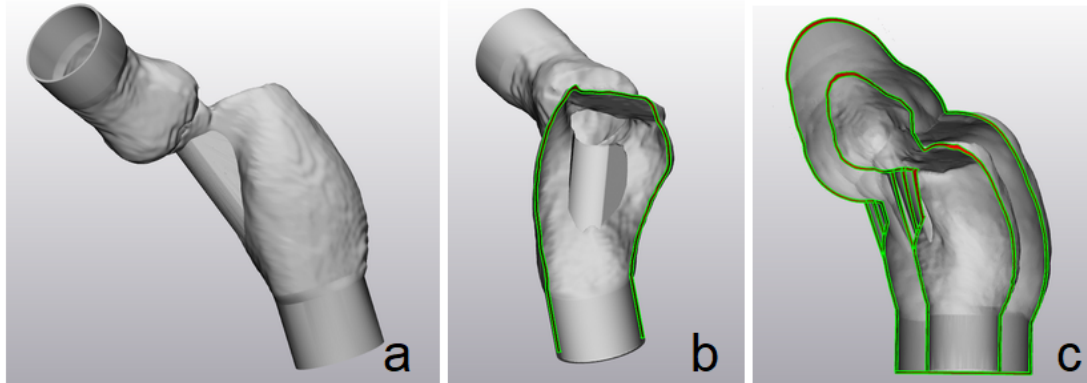


Figure 23: The mould of the IVSt 19mm mould with the resected part of the tissue after performing the Morrow procedure attached. a. Anterior view of the mould. b. Sagittal view of the mould. c. Frontal view of the mould.

For the Morrow procedure of 12 mm and 15 mm you can follow the same protocol (figure 24).

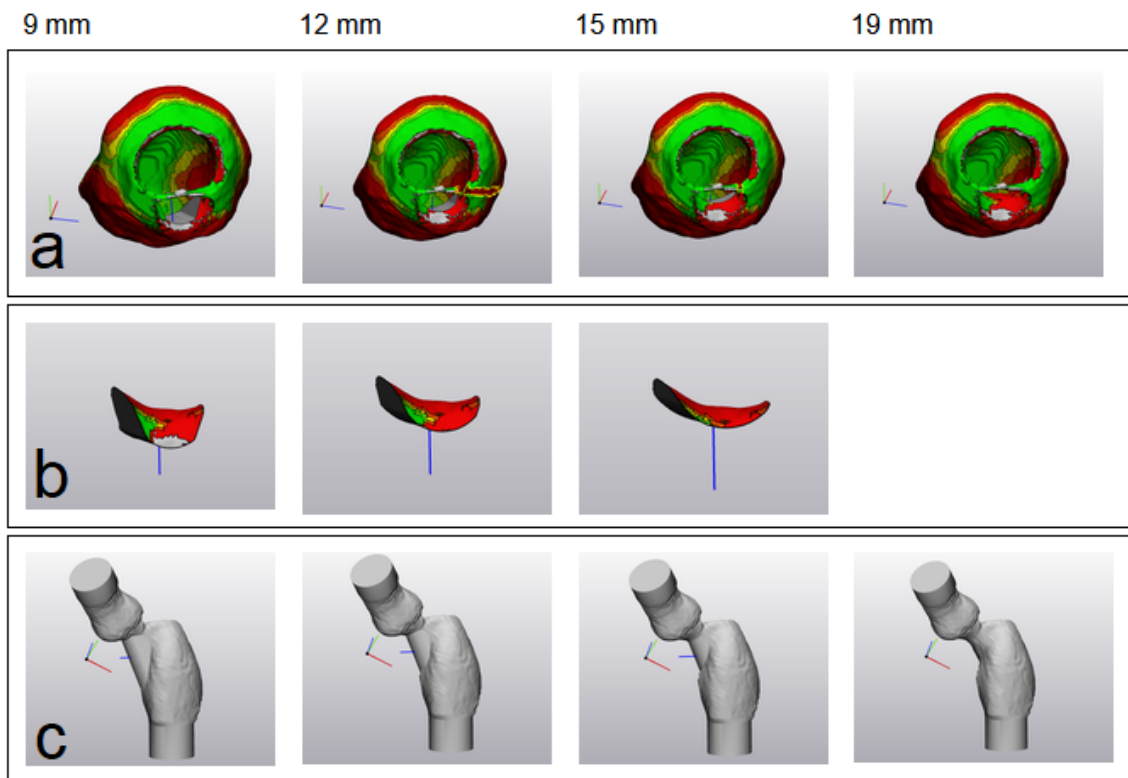


Figure 24: The IVSt 19 mm mould, IVSt 12 mm mould, IVSt 15 mm mould and IVSt 19 mm mould a. Superior view of the myocardium after performing the Morrow procedure. b. The resected parts of the IVS. c. The moulds.

Coupling pieces

Coupling pieces are designed to connect the heart model with the used tubes of the flow set-up.

LV side

The LV side of the connector needs to fit into the tube of the LV. This means that it needs an outer radius of 19 mm so that the silicone tube can fit tightly around it.

- Design → Create Analytical Cylinder → Radius 19, length 20 → Convert analytical primitive to part → Cylinder 19 mm
- Design → Create Analytical Cylinder → Radius 17, length 20 → Convert Analytical Primitive to Part → Cylinder 17 mm
- Design → Boolean subtraction → Entities: Cylinder 19mm, Subtraction entities: Cylinder 17 mm

Tube side

The tube side of the connector needs to fit on $\frac{3}{8}$ inch tubes used in a CPB-pump.

- Design → Create Analytical Cylinder → Radius 6, length 20 → Convert analytical primitive to part → Cylinder 6 mm
- Design → Create Analytical Cylinder → Radius 4, length 20 → Convert analytical primitive to part → Cylinder 4 mm
- Design → boolean subtraction → Entities: Cylinder 6mm, Subtraction entities: Cylinder 4mm

Loft both sides

Both sides are lofted to get a gradual reduction of the tubes which will optimize the flow in our set-up.

- Distance between both sides 25 mm
- Design → Loft → Entity 1: Bottom LV side, Entity 2: Top tube side (figure 25a)
- Surface list → Merge all surfaces (figure 25)

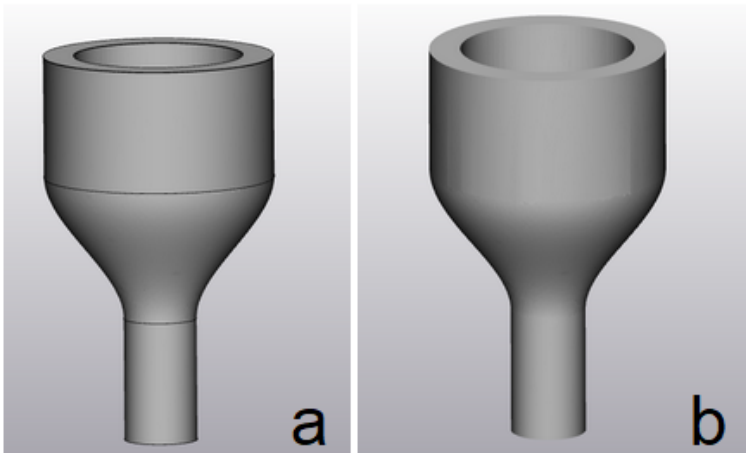


Figure 25: The coupling piece. a. Before merging all surface sets. b. After merging all surface sets.

Creating small edge on the sides

Small edges on the sides ensure that the flow of the fluid does not push the connector out of tubes. It reduces the resistance and optimizes the flow.

- Design → Create Analytical Cylinder → Radius 19, length 0.5 → Convert analytical primitive to part → Cylinder 19, 0.5mm

- Plane to Plane Align → Plane on Fixed Entity: Top one side, Plane on Moving Entity: Cylinder 19, 0.5mm
- Design → Create Analytical Cylinder → Radius 18, length 0.5 → Convert analytical primitive to part → Cylinder 18, 0.5mm
- Plane to Plane Align → Plane on Fixed Entity: Top one side, Plane on Moving Entity: Cylinder 18, 0.5mm
- Design → Boolean subtraction → Entities: Cylinder 19, 0.5mm, Subtraction entities: Cylinder 18, 0.5mm → Cylinder small edge one side
- Distance between Top LV side and Cylinder small edge one side: 3mm
- Design → Loft → Entity 1: Cylinder small edge one side; Entity 2: Top one side (figure 26)



Figure 26: The coupling piece with small edges.

- Design → Create Analytical Cylinder → Radius 6, length 0.5mm → Convert analytical primitive to part → Cylinder 6, 0.5mm
- Plane to Plane Align → Plane on Fixed Entity: Bottom other side, Plane on Moving Entity: Cylinder 6, 0.5mm
- Design → Create Analytical Cylinder → Radius 5, length 0.5mm → Convert analytical primitive to part → Cylinder 5, 0.5mm
- Plane to Plane Align → Plane on Fixed Entity: Bottom other side, Plane on Moving Entity: Cylinder 5, 0.5mm
- Design → boolean subtraction → Entities: Cylinder 6, 0.5mm, Subtraction entities: Cylinder 5, 0.5mm → Cylinder small edge other side
- Distance between Top other side and Cylinder small edge other side: 3mm
- Design → Loft → Entity 1: Cylinder small edge other side; Entity 2: Top other side
- Surface list → Merge all surfaces

Export file

Before printing, the coupling piece is finished by fixing little mistakes.

- Fix → Fix Wizard
- File → Export STL, Entities: Coupling pieces

Appendix XIV: Protocol - Printing the moulds

Protocol: Printing the moulds

25/06/2021

Technical Medicine - Bachelor thesis

Students group 23

Milou Baarsma - s2113473
Arno Fennema - s2113732
Evie Graus - s2090481
Carla van der Poel - s2107732

Supervisors

Dr. F.R. Halfwerk (Technical Medicine supervisor)
Dr. M. A. Koenrades (Technical Medicine supervisor)
K. C. Smits, BSc (Technical Medicine supervisor)
Dr. R.G.H. Speekenbrink (Medical supervisor)
Ir. E.E.G. Hekman (Technical supervisor)
M. van Ochten, BSc (Personal supervisor)

Introduction

This protocol describes how the four left ventricle (LV) moulds and coupling pieces are printed.

Materials

- Ultimaker S5 (Ultimaker, Utrecht, The Netherlands)
- Formlabs Form 3 (Formlabs, Somerville, United Kingdom)
- Formcure (Formlabs, Somerville, United Kingdom)
- Formwash (Formlabs, Somerville, United Kingdom)
- Polylactic acid (PLA) (Ultimaker, Utrecht, The Netherlands)
- Polyvinyl alcohol (PVA) (Ultimaker, Utrecht, The Netherlands)
- Standard White Resin (Formlabs, Somerville, United Kingdom)

Method

Cylinder for validation, LV moulds with IVSt of 19, 9, 12 and 15 mm

- Load the stl files of the cylinder for validation and LV moulds with interventricular septum thickness (IVSt) of 19, 9, 12 and 15 mm in Cura.
- Cura determines where and how much support is needed.
- Set the printing density to a value of 200 μm .
- Attach the polylactic acid (PLA) and polyvinyl alcohol (PVA) to the Ultimaker S5.
- Perform a test print to make sure the x-axis and y-axis correspond.
- Start the printing process.

Connecting parts

- Load the stl files of the coupling pieces in Preform.
- 'Perform' determines where and how much support is needed.
- Set the printing density to a value of 50 μm .
- Pour the White Resin into the Formlabs Form 3 reservoir.
- Start the printing process.
- After printing, wash the print with alcohol for 10 minutes using the Formwash.
- Cure the print for 60 minutes on 60 degrees using Formcure.

Result

The results of the printed models can be seen in figure 1a, b, and c. In addition, figures 2 and 3 display the 3-dimensional (3D) printers used.

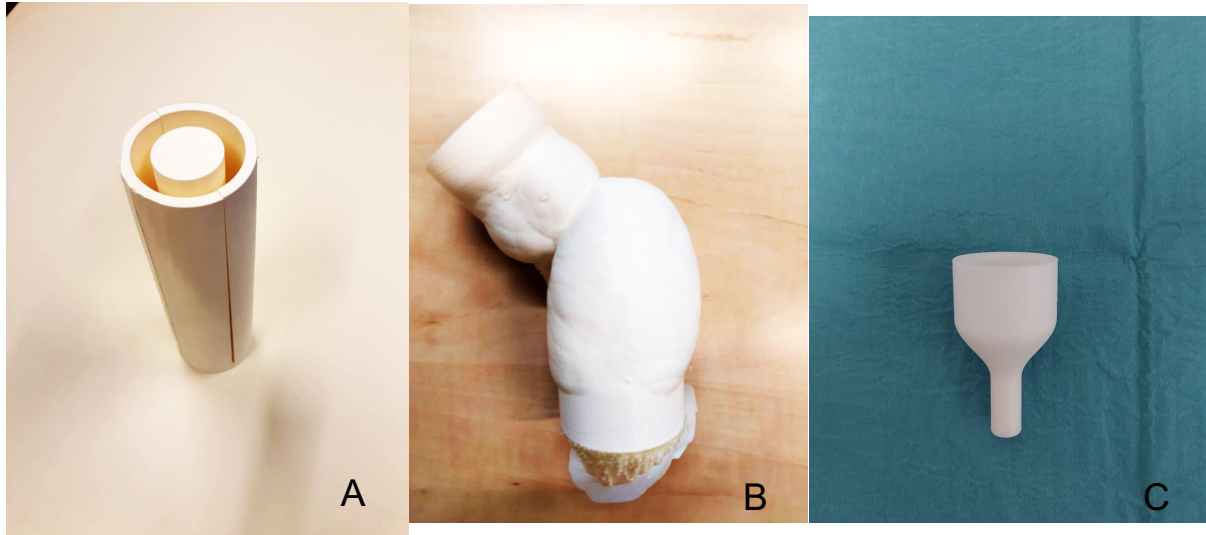


Figure 1: the printed objects. a. The printed cylinder test object. b. The printed LV mould of 19 mm. c. The printed coupling piece.



Figure 2: The used Formlabs Form 3 3D printer. [79]

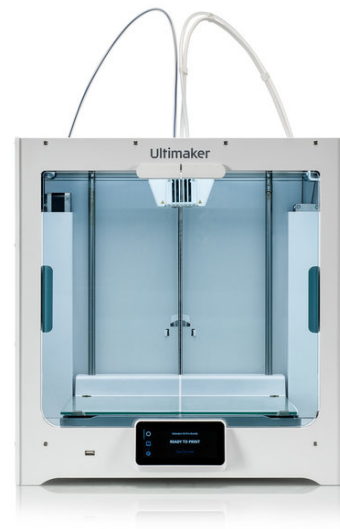


Figure 3: The used Ultimaker S5 3D printer. [80]

Appendix XV: Protocol - Casting the models

Protocol: Casting the models

25/06/2021

Technical Medicine - Bachelor thesis

Students group 23

Milou Baarsma - s2113473
Arno Fennema - s2113732
Evie Graus - s2090481
Carla van der Poel - s2107732

Supervisors

Dr. F.R. Halfwerk (Technical Medicine supervisor)
Dr. M. A. Koenrades (Technical Medicine supervisor)
K. C. Smits, BSc (Technical Medicine supervisor)
Dr. R.G.H. Speekenbrink (Medical supervisor)
Ir. E.E.G. Hekman (Technical supervisor)
M. van Ochten, BSc (Personal supervisor)

Introduction

This protocol describes how to cast Dragon skin (Smooth-On Inc., Macungie, United States) as a silicone into the 3-Dimensional (3D) printed moulds. Also, it states how to remove the moulds from the silicone.

Materials

- Reservoir (Sorin Group, Saluggia, Italy)
- 3D printed moulds (3D lab Medisch Spectrum Twente, Enschede, The Netherlands)
- Dragon skin 10 NV (Smooth-on Inc., Macungie, United States)
- 0.5 L Disposable beaker
- Mixing tools
- Gloves
- Vice
- Wire cutters
- Flat nose pliers
- Philips CX50 ultrasound device (Philips Ultrasound Systems, Bothell, United States)
- Aquasonic 100 ultrasound transmission gel (Parker, Fairfield, United States)
- Optional: Ultrasonic cleaner (VWR, Radnor, United States)
- Optional: Ethanol 80% (Orphi Farma, Dordrecht, The Netherlands)

Method

First, the polyvinyl alcohol (PVA) necessary for the 3D printing of the moulds, is dissolved by leaving the moulds in a water reservoir for ± 12 hours. If necessary, the moulds can be cleaned for about 30 minutes using an ultrasonic cleaner at 30 °C (figure 1).

The Dragon Skin 10 NV parts A and B need to be mixed in a ratio of 1:1. During mixing the use of hand gloves is recommended. For each model, we used 400 g dragon skin, which means 200 g of part A and 200 g of part B. This was measured with a measuring beaker and merged in the 0.5 L disposable beaker. Using mixing tools the dragon skin was stirred carefully, to prevent air bubbles in the silicone. After mixing, the Dragon Skin 10 NV was poured into the 3D printed mould (figure 2). The pot life of the used Dragon Skin 10 NV is 15 minutes, so it needs to be poured within this time limit otherwise it is too thick. Next, the Dragon Skin 10 NV needs to be cured for 75 minutes at room temperature (23 °C). To attain full physical properties it has to cure another 24 hours at room temperature. After that, the mould was removed by breaking it with a vice, wire cutters and flat nose pliers (figure 3 and 4).

Make sure the procedure is done on a disposable surface as spilled Dragon Skin is hard to remove. If necessary the spilled Dragon Skin on the workspace can be cleaned with ethanol 80%.



Figure 1: 3D mould in the ultrasonic cleaner at 30 °C to be able to remove all the PVA.



Figure 2: Casting the Dragon Skin into the 3D mould.

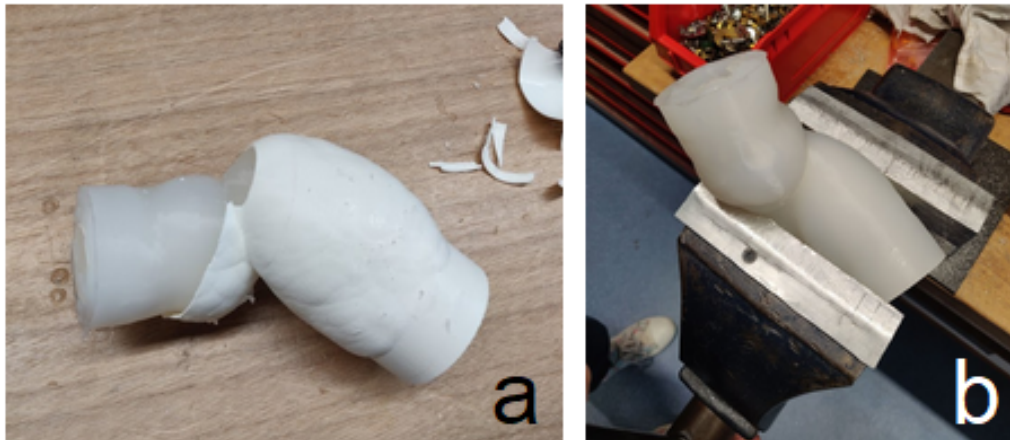


Figure 3: Removing the 3D printed mould made out of polylactic acid (PLA) from the silicone heart. a. Using wire cutters and flat nose pliers. b. Using a vice to break the inner mould.



Figure 4: The casted Dragon skin 10 NV left ventricle (LV) model.

Validation

To test whether Dragon Skin 10 NV is suitable for casting, a cylinder test model is casted before the heart models were casted (figure 5). The thickness, density and amount of air bubbles of the cylinder test model will be analysed. Also, ultrasound measurements will be performed on the cylinder test model using a Philips CX50 ultrasound device to test whether the material is suitable for ultrasound flow measurements.



Figure 5: The casted Dragon skin 10 NV cylinder test model.

Appendix XVI: Protocol - Flow set-up

Protocol: Flow set-up

25/06/2021

Technical Medicine - Bachelor thesis

Students group 23

Milou Baarsma - s2113473
Arno Fennema - s2113732
Evie Graus - s2090481
Carla van der Poel - s2107732

Supervisors

Dr. F.R. Halfwerk (Technical Medicine supervisor)
Dr. M. A. Koenrades (Technical Medicine supervisor)
K. C. Smits, BSc (Technical Medicine supervisor)
Dr. R.G.H. Speekenbrink (Medical supervisor)
Ir. E.E.G. Hekman (Technical supervisor)
M. van Ochten, BSc (Personal supervisor)

Introduction

This protocol describes how to build a flow set-up to simulate the blood flow through the heart model.

Materials

- 3 m $\frac{3}{8}$ inch tubes (Raumedic, Helmbrechts, Germany)
- 2 3-Dimensional printed coupling pieces
- Cardiopulmonary Bypass (CPB) Maquet HL30 pump (Maquet, Hirrlingen, Germany)
 - Centrifugal pump
- Glycerol (Thermo Fisher Scientific Inc, Waltham, US)
- Water
- Clamps (Achim Schulz-Lauterbach, Iserlohn, Germany)
- CPB venous reservoir (Sorin Group, Saluggia, Italy)

Method

Building the set-up

To measure the pressure gradient (PG) in the left ventricular outflow tract (LVOT), it is necessary to simulate the blood flow in the heart. This will be generated using the Maquet HL30 CPB pump. This machine has roller pumps and a centrifugal pump from which the centrifugal pump will be used (figure 1). The setup will be as follows (figure 3 and 4):

- Connect the reservoir to the inlet of the centrifugal pump using $\frac{3}{8}$ inch tubes.
 - Make sure the reservoir is properly sealed with clamps till after the set-up is built.
- Connect the outlet of the centrifugal pump to the inlet of the model using a coupling piece and a $\frac{3}{8}$ inch tube.
- Connect the outlet of the model to the reservoir using a coupling piece and a $\frac{3}{8}$ inch tube.
- Make sure the tubes are properly connected to the model and the CPB pump to prevent leakage.

Before the LVOT PG measurements can be performed validation measurements are required.

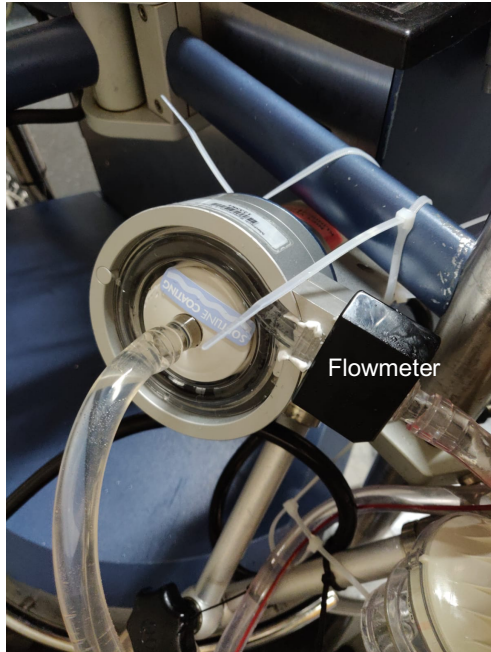


Figure 1: Connection of the centrifugal pump to the CPB device. A flowmeter is built in the pump.

Validation flow CPB

To validate the flowmeter and the ultrasound flow measurements, the flow will be measured using a beaker and will then be compared to the value of the flowmeter.

The following steps will be followed for a proper validation:

- Add 1 L water to the flow set-up.
- Disconnect the model from the set up. Make sure the flowmeter can measure the flow in the tubing properly by lubricating it using a kind of ointment. Set a constant flow somewhere between 2.5 and 3.5 L/min on the CPB pump. First, let the flow run into the tube leading to the reservoir. Then, let the flow instantly run into a measuring beaker. Start a timer and let the liquid flow for a fixed amount of time, in this case 10 seconds. Make sure to keep filling the reservoir during the measurement. After 10 seconds remove the measuring beaker and let the flow instantly run again into the tube leading to the reservoir. Stop the flow and read the total volume in the beaker. Make sure the tubes are clamped off after stopping the flow to prevent the spilling of liquids. Calculate the flow (L/min) based on the volume in the timeframe.
- Compare the calculated flow to the built-in flowmeter in the centrifugal pump.

After the validation measurements are performed, the 1 L water can be drained out of the model and 1 L of 65/35 water-glycerol can be added. After this the protocol measuring the LVOT PG can be followed.

Result

The design of the set-up is displayed in figure 2 and 3. The results of the validation of the flow can be found in appendix XVI.

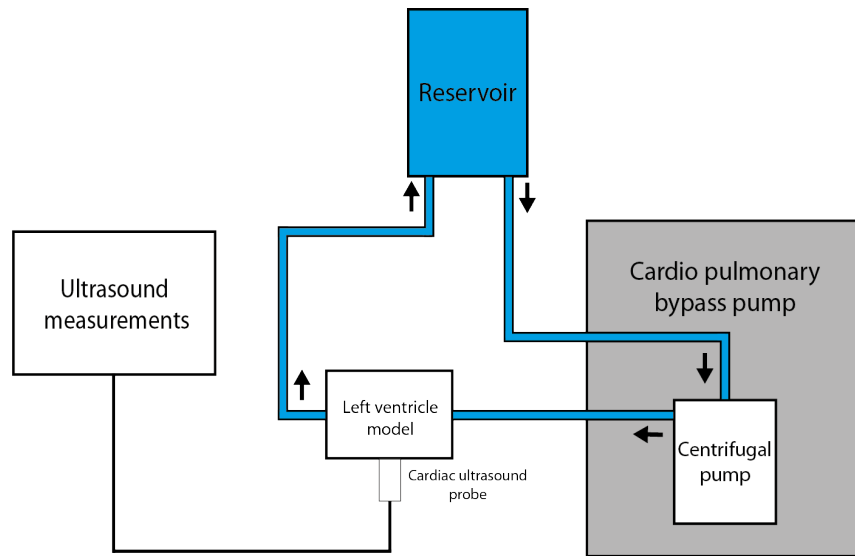


Figure 2: Schematic representation of the set-up. A HL-30 CPB pump is used to generate a pulsatile flow. Liquid, consisting of a 65/35 water-glycerol mixture, is collected in a reservoir. The LV model is connected to the CPB pump with $\frac{3}{8}$ inch tubes. LVOT PG is measured using a Philips CX50 ultrasound device.

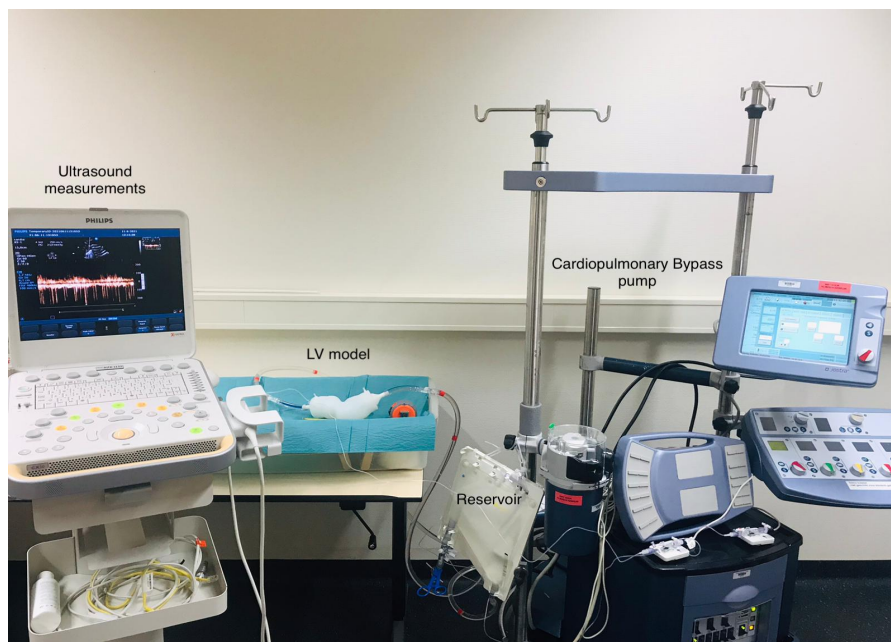


Figure 3: Set-up. A HL-30 CPB pump is used to generate a pulsatile flow. Liquid, consisting of a 65/35 water-glycerol mixture, is collected in a reservoir. The LV model is connected to the CPB pump with $\frac{3}{8}$ inch tubes. LVOT PG is measured using a Philips CX50 ultrasound device.

Appendix XVII: Cardiopulmonary bypass pump

A cardiopulmonary bypass (CPB) pump is used to take over the function of the heart and lungs [81]. It is used when cardioplegia is necessary to perform heart surgery.

The CPB pump has two different kinds of pumps, the roller pump and the centrifugal pump. A roller pump consists of a bent tube inside a curved wall and two or more rollers [59] (figure 1). The rollers are constantly rotating, thereby compressing the tube against the wall, beginning where the tube enters the pump and rolling to where the tube leaves the pump. Hereby the fluid in the tube moves along with the rollers creating a flow. There is no fluid at the place where the roller presses the tube, so at the end when the pressure releases, the empty space is filled with fluid from both sides of the system, resulting in a minimal pulsatile flow.

In the set up a centrifugal pump is used. This kind of pump uses, as the name suggests, centrifugal forces to move the liquid in the system [60]. In the pump there is an impeller and a suction pipe which is connected to the center of this impeller. The motor can rotate the impeller, because it contains magnets [82]. The rotations create a centrifugal force, resulting in the liquid to be flung towards the side of the pump and then leaving the pump via the delivery pipe (figure 2). This also creates a vacuum at the center of the impeller, causing the liquid to rush through the suction pipe into the pump. The pump is thus resistance dependent and will give a constant pressure. That is how the flow is generated. The flow of both kinds of pumps can be changed by setting the number of rotations. It is also possible to create a pulsatile flow with both pumps.

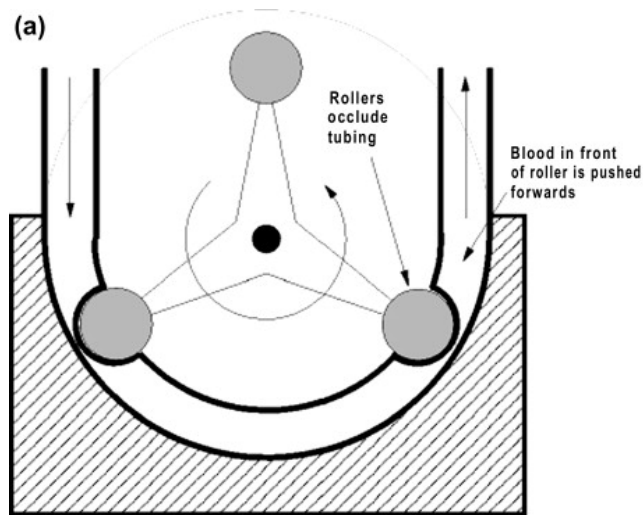


Figure 1: Roller pump. Flow is generated by multiple rollers pushing the fluid along the pump. [83]

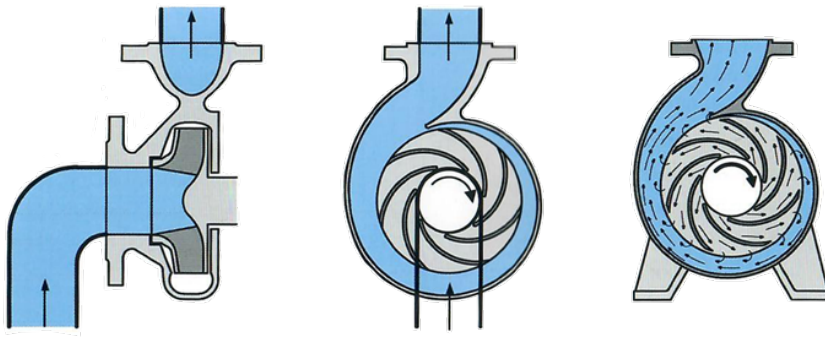


Figure 2: The principle of a centrifugal pump. The motor rotates the impeller causing a centrifugal force resulting in the movement of fluids. [84]

Appendix XVIII: Validation flow results

To validate the flowmeter and the ultrasound flow measurements, the flow will be measured using a beaker and will then be compared to the value of the flowmeter (appendix XIV). Table 1 shows the results of the validation of the flow.

Table 1: The results of the validation of the flow of the cardiopulmonary bypass pump. Difference in measured flow between the CPB flowmeter and beaker are given in absolute (mL/min) and relative differences (%).

Measurement	CPB flow (mL/min)	Beaker (mL)	Time (s)	Beaker flow (mL/min)	Difference in flow (mL/min)	Relative difference (%)
1	2770	500	11	2639	131	4.7
2	2700	565	13	2582	118	4.4
3	2860	570	12	2776	84	2.9
4	3000	595	12	2965	35	1.2
5	3010	600	12	2915	95	3.2
				Mean error	93	3.3

Appendix XIX: Protocol - Measuring the left ventricle outflow tract pressure gradient

Protocol: Measuring the left ventricle outflow tract pressure gradient

25/06/2021

Technical Medicine - Bachelor thesis

Students group 23

Milou Baarsma - s2113473
Arno Fennema - s2113732
Evie Graus - s2090481
Carla van der Poel - s2107732

Supervisors

Dr. F.R. Halfwerk (Technical Medicine supervisor)
Dr. M. A. Koenrades (Technical Medicine supervisor)
K. C. Smits, BSc (Technical Medicine supervisor)
Dr. R.G.H. Speekenbrink (Medical supervisor)
Ir. E.E.G. Hekman (Technical supervisor)
M. van Ochten, BSc (Personal supervisor)

Introduction

This protocol explains how the cardiopulmonary bypass (CPB) pump and ultrasound are set and how the left ventricular outflow tract pressure gradient (LVOT PG) is measured and saved.

Materials

- Philips CX50 ultrasound device (Philips Ultrasound Systems, Bothell, United States)
- Aquasonic 100 ultrasound transmission gel (Parker, Fairfield, United States)
- Materials needed for the flow set-up (appendix XIV)

Method

CPB pump settings

To generate a pulsatile flow, the CPB pump is set to a pulse and a heart rate.

- Turn the HL-30 CPB pump on and start the monitor and centrifugal pump (In this case pump 1).
- Go to the arterial master pump settings on the monitor (figure 1).
- Press safety and pulse int. at the same time.
- Go to 'general', Rota flow calibration and press safety and set zero at the same time, to calibrate the flow (figure 2).
- Set the pulse base to 40%, start to 20% and stop to 80% (figure 1).
- Go to 'heart rate' and set 'Sim HR' to 65 bpm, for a heart rate at rest (figure 3).

Running pump

A cardiac output of 5.5 L/min is set to mimic a physiological condition.

- Change the pump settings in the panel to get a flow of 5.5 L/min for the measurement to simulate the situation at rest (figure 4).
- Now the pump is running and the ventricle starts to pulsate.

Probe

The ultrasound probe needs to be positioned at a certain angle to perform doppler measurements.

- First, put some ultrasound transmission gel on the S5-1 cardiac ultrasound probe or the spot on the ventricle where you place the probe. Make sure that you use enough gel.
- Place the probe on the ventricle at a horizontal position, opposite to the LVOT (figure 5), so that you have a view through the LVOT.

Settings ultrasound

In order to correctly measure the LVOT PG in the heart models, the ultrasound measurements need to be performed in the same way with the same settings.

- First, make sure the 2-Dimensional (2D) ultrasound is on (the button on the panel has to be green). For a description of all the buttons see figure 6.
- Press 'Color' on the panel in order to see the direction of the velocities. You can change the box position with the cursor on the panel, so that you can view the velocities in the LVOT (figure 7)
- Press 'CW' on the panel, to activate the Continuous Wave (CW) Doppler. Make sure that the CW line goes through the LVOT.
- Press 'Freeze' on the panel, you can now see the measurements you made and scroll through it with the cursor on the panel.

- The button at the top of the panel, second from the left, allows you to change the level of the Baseline. Make sure that you can see the bottom of the biggest pulse.
- The Button at the top, second from the right, allows you to change the Sweep Speed. With it you can compress and stretch the velocity chart.
- Press 'Caliper' on the panel. Now, move the pointer with the cursor to the highest velocity. At the upper left corner you can read the velocity and the PG (figure 8).

Saving the measurements

Before analysing the results, the data needs to be saved and transferred from the ultrasound machine to a computer.

- Before performing any measurements, press 'End Exam'. A pop-up window will appear. Choose 'Manual Entry' and fill in the title of the study.
- After a measurement is performed, press 'Acquire' to take a screenshot.
- Take a screenshot of every measurement.
- Connect a USB stick in the ultrasound device. (On the right side are USB portals)
- Press 'Review' (on the top of the panel). All screenshots taken are visible.
- Click on the pictures you want to save.
- Go to 'Export Selected Images' at the top of the screen. Then choose at 'Selected DICOM Format' the 'Modify' button and select the option 'Palette color' as format'.
- Press 'Start Export' at the bottom of the screen.
- The pictures are now transferred to the USB stick.

Measurements of the different researchers

The measurements were performed in duos. One person (researcher A) operates the ultrasound (US) machine and the other person (researcher B) places and holds the probe in the right place.

- Follow the previous stated 'CPB pump settings' & 'running pump' to start the CBP pump and set the right pulse.
- Researcher A creates a new folder following 'saving the measurements' protocol
- Researcher B places the pump in the right position, see 'probe'.
- Researcher A operates the US measurements according to 'Settings ultrasound'.
- The duo performs three consecutive measurements in this setting.
- After the three measurements are done, turn off the pump and remove the model. Make sure the reservoir is below the heart model to prevent spilling.
- Reconnect the same heart model again.
- Researchers A en B switch roles and again do three measurements.
- Repeat the stated steps above for each model (9, 12, 15, and 19 mm).

Measurements at different flow rates

In order to further investigate the LVOT PG between the HOCM model (19 mm) and the most extreme Morrow procedure model (9 mm) different flow rates are set.

- Connect the 19 mm heart model.
- Follow all the steps from the previously stated protocols except, set the flow of the pump to 4.0 L/min instead of 5.5 L/min.
- Remove the heart model from the set up.
- Connect the 9 mm heart model.

-
- The screenshot shows the Jostra HL30 V2.4 control panel interface. At the top, there are status bars for Bypass (00:00:00), X Clamp (00:00:00), Add (00:00:00), and the time (09:55:48). Below these, there are several status indicators: Art. Flow (-0.04 l/min), a wrench icon, a floppy disk icon, Analog, a clock icon, a red circle with a percentage sign, a wrench icon, and a status indicator showing 'S' and 'Priming Mode Off'.
- The main display area is titled 'Arterial Master Pump Settings'. It is divided into several sections:
- Left Column (Status Indicators):**
 - Art. Flow: -0.04 l/min
 - CplgSlv Flow: Offline ml/min
 - CplgMst Flow: Offline ml/min
 - T 2: Offline °C
 - P 1: Offline mmHg
 - P 2: Offline mmHg
 - P 3: Offline mmHg
 - P 4: Offline mmHg
 - Central Settings Area:**
 - Art. Flow:** -0.04 l/min
 - Speed:** 0 rpm
 - Heart Rate:** 0 bpm
 - Regulation:** RPM and LPM buttons.
 - Right Section (Op. Modes):**
 - Op. Modes:** Continuous (selected), Puls. Int., Puls. Ext.
 - Assist Rate:** 1: 1, with left and right arrow buttons.
 - Pulsatile Pumping Curve:** A graph showing a square wave pulse. The y-axis has markers for 40 % (Base), 20 %, and 80 %. The x-axis has markers for Start and Stop.
 - Bottom Right:**
 - CI [l/min/m²]: ---
 - Art.Flow [%]: ---
- At the bottom of the screen, there is a configuration bar showing 'Config: StdUser / StdConfig' and 'Rel. 000904 HL30 V2.4'.

83

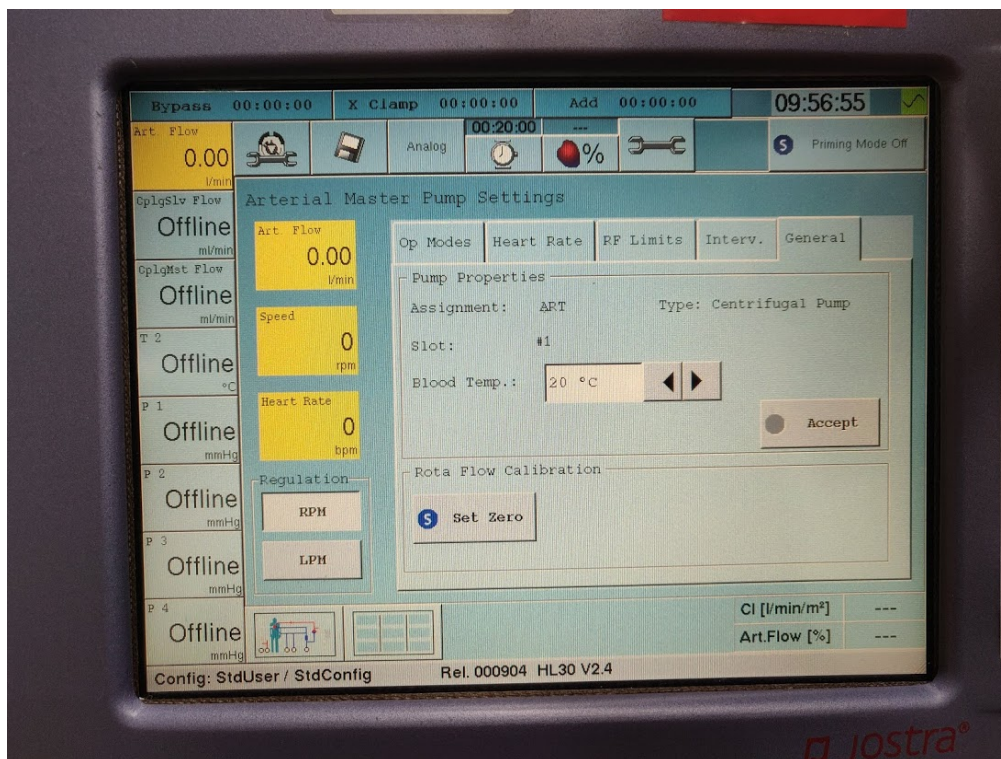


Figure 2: Menu in which the flow sensor can be calibrated. This is done by pressing the safety button and the 'Set Zero' button at the same time.

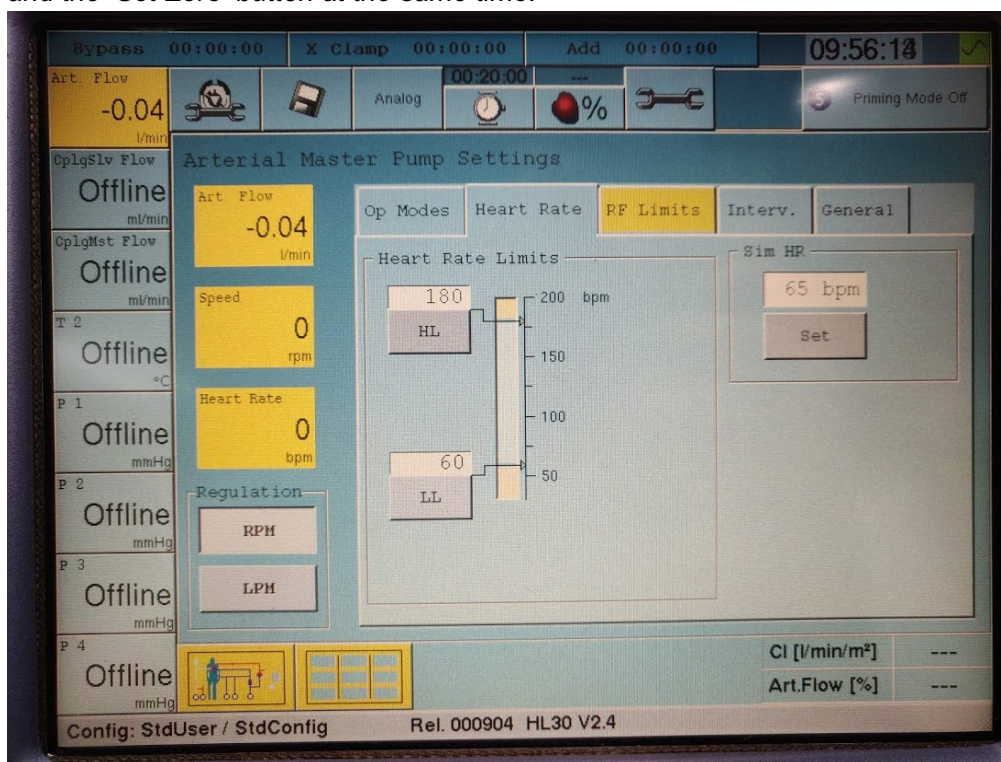


Figure 3: Menu in which the heart can be adjusted. Heart rate is set at 65 bpm by rotating the button on the monitor and pressing the 'Set' button.



Figure 4: Display of the setting menu of the arterial pump. The rotary knob is used to adjust the rpm.



Figure 5: Placement of the S5-1 cardiac ultrasound probe on the LV model. Placement of the probe should be on the ventricle at a horizontal position, opposite to the apex.

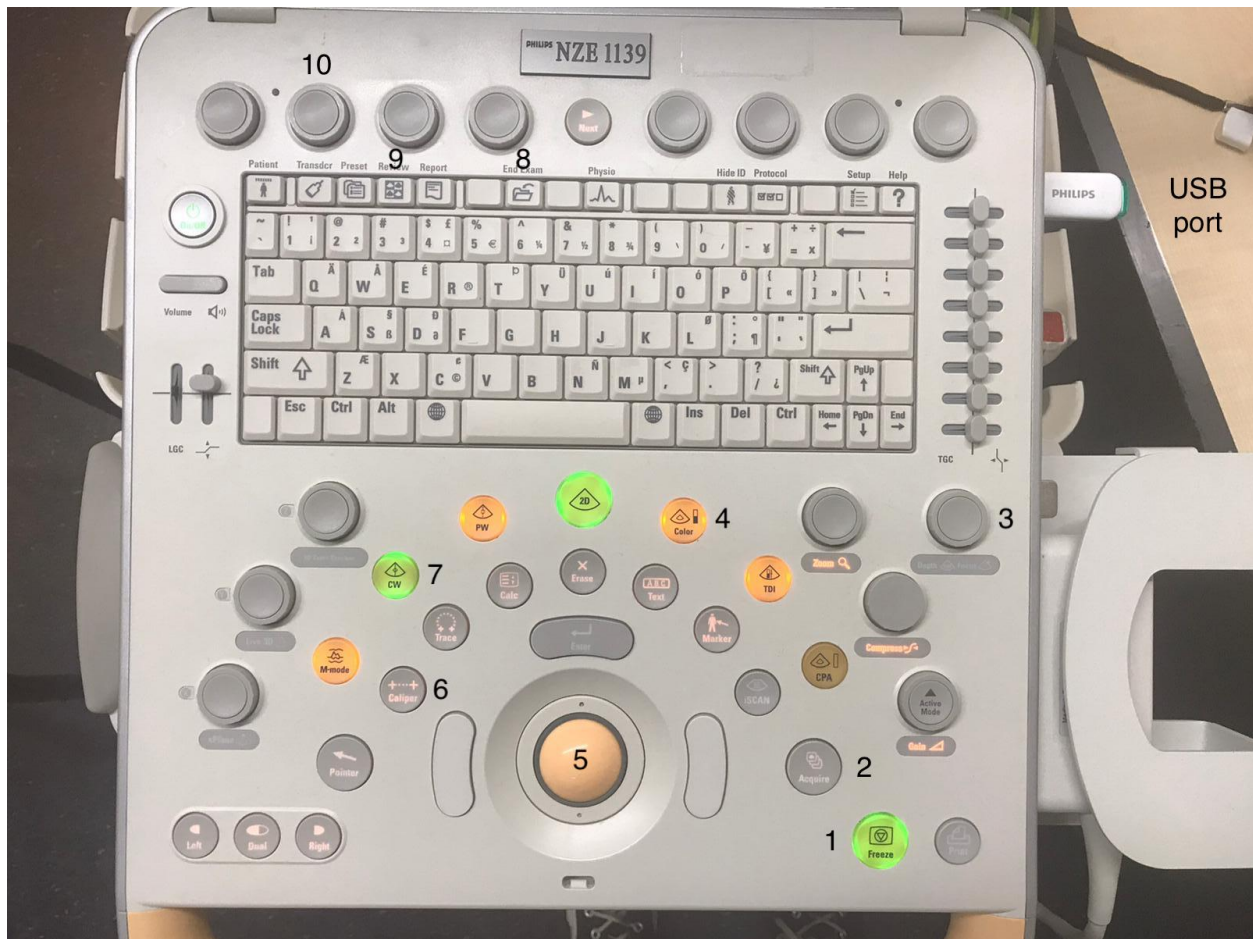


Figure 6: 1 = Freeze, used to freeze the measurement at a specific time, 2 = Acquire, takes a screenshot of the frozen image, 3 = Depth, used to set the depth for measurement, 4 = Color, enables color Doppler function which visualizes the (direction of the) velocities, 5 = cursor, 6 = Caliper, used to measure in the ultrasound images, 7 = CW, enables continuous wave doppler which displays the maximum speed in the time on a specified line, 8 = End Exam, creates a folder in which measurements can be saved, 9 = Review, displays all screenshots taken, 10 = baseline, button used to set the baseline of the CW measurements.

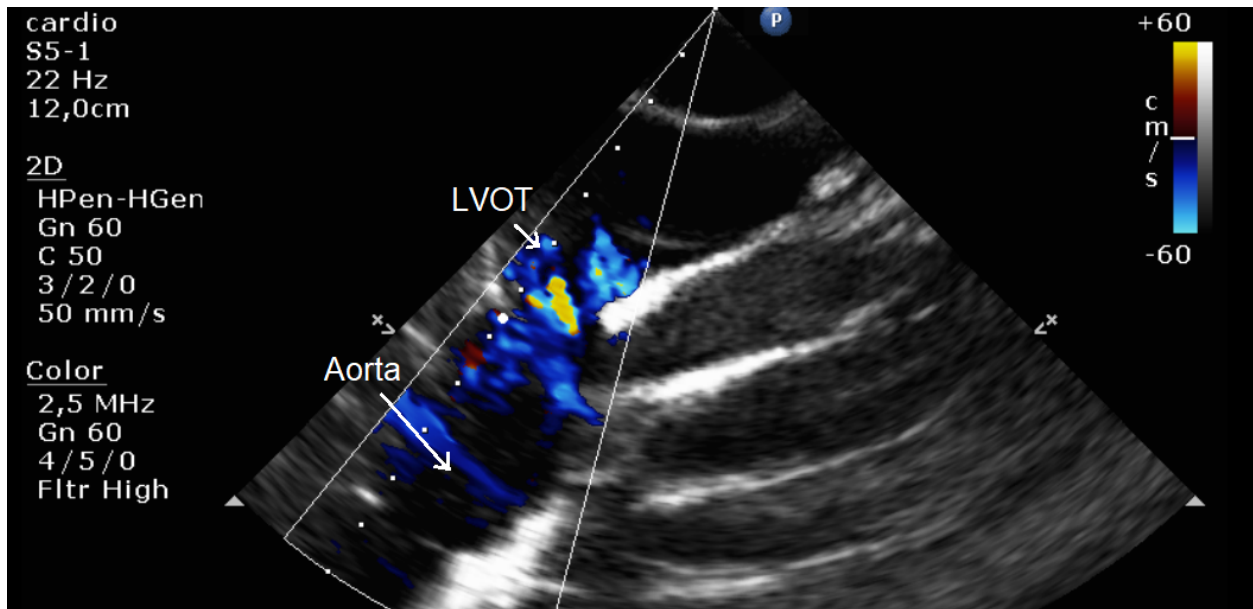


Figure 7: A color Doppler measurement of the LV model with an IVSt of 19 mm using a flow of 6.2 L / min. It can be seen that the highest flow is present in the LVOT in comparison to the aorta.

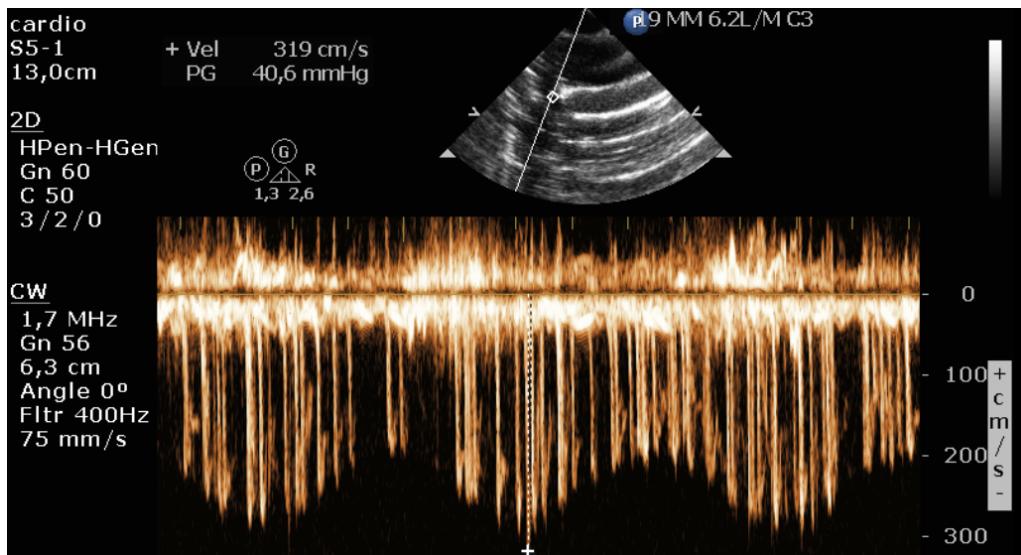


Figure 8: A continuous wave Doppler measurement of the LV model with an IVSt of 19 mm using a flow of 5.5 L / min. The LVOT PG is calculated and has a value of 40.6 mmHg.

Appendix XX: Doppler Ultrasound

To measure the blood flow in the left ventricular outflow tract (LVOT), doppler echography can be used. Using this technique the velocity, direction, and characteristics of the flow can be determined. Doppler ultrasound (DUS) is based on the frequency-shift of the US pulse caused by the velocity of blood particles. By measuring this shift, the blood flow velocity can be determined using the Doppler equation [62]. This equation states that the frequency shift Δf (Hz) is related to the speed of the blood v , the speed of sound in tissue c (m/s), and the angle at which the sound is emitted and detected $\cos(\varphi)$.

$$\Delta f = \frac{2f v \cos(\phi)}{c} \quad (\text{formula 1})$$

After the velocity of the blood flow is measured, it can be used to calculate the pressure gradient using the modified Bernoulli's equation (appendix II, formula 6) [12,62]. There are two different ways to calculate the PG between the aorta and the left ventricle (LV). These are the maximal instantaneous gradient and the peak-to-peak gradient. To calculate the maximal instantaneous gradient, the maximal aortic jet velocity through the aortic valve is used. In order to get the peak-to-peak gradient (Peak-Peak Δp), the maximal LV pressure is subtracted from the maximal aortic pressure [85].

There are two types of Doppler that can be used to measure the velocity of the blood flow. Firstly, pulsed wave Doppler (PWD) is available [62]. This method emits an US pulse and detects the shifted pulse reflected by the bloodstream. After detecting the reflected pulse, it can send a new pulse. Continuous wave Doppler (CWD) does not wait for the signal to come back but keeps emitting US pulses and detecting the reflected signals using two different crystals. The disadvantage of this kind of US is that it can not measure where the signal is coming from. However, it can measure higher velocities than PWD [12]. This is because PWD is limited by the Nyquist limit which states that the maximum Doppler shift that can be measured is half the pulse repetition frequency. CWD is not limited by a Nyquist limit and thus more useful for measuring peak velocities.

To visualize the pulsed DUS, a color map can be used which shows the velocities of the blood using colors, combined with the US image of the surrounding tissue [62]. This technique is also known as color Doppler. Continuous wave Doppler can only be visualized using a 2-dimensional graph, plotting time and velocity.

Figure 1 shows a Doppler examination of a patient with hypertrophic obstructive cardiomyopathy (HOCM). The CWD-echo of HOCM patients is characterized by a dagger shaped curve, or more like a lobster claw in cases of severe obstruction [86].

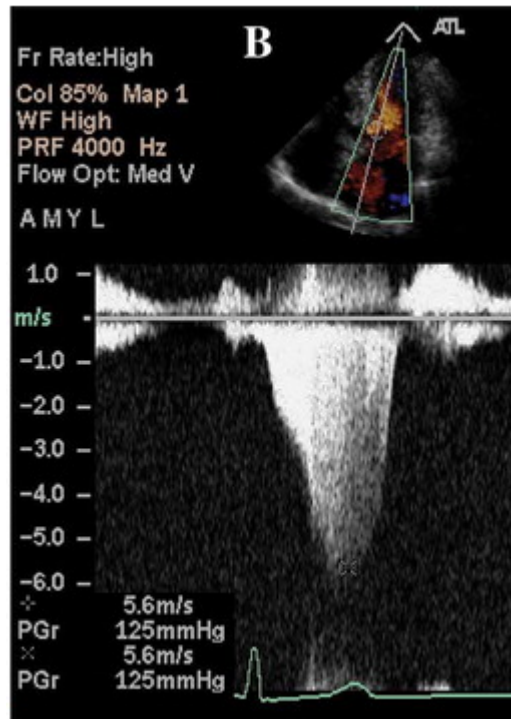


Figure 1: A Doppler examination from a HOCM patient [87]. The characteristic 'dagger shaped' curve can clearly be seen.

Appendix XXI: Protocol - Statistical analysis

Protocol: Statistical analysis with IBM SPSS Statistics Data Editor

25/06/2021

Technical Medicine - Bachelor thesis

Students group 23

Milou Baarsma - s2113473
Arno Fennema - s2113732
Evie Graus - s2090481
Carla van der Poel - s2107732

Supervisors

Dr. F.R. Halfwerk (Technical Medicine supervisor)
Dr. M. A. Koenrades (Technical Medicine supervisor)
K. C. Smits, BSc (Technical Medicine supervisor)
Dr. R.G.H. Speekenbrink (Medical supervisor)
Ir. E.E.G. Hekman (Technical supervisor)
M. van Ochten, BSc (Personal supervisor)

Introduction

To validate the measurements, a statistical analysis is performed. This is done using Social Sciences (SPSS) Statistics Version 26 (IBM, New York, USA). The analysis can indicate if the results have a significant difference and if there is inter- or intraobserver variability. This gives valuable information about the confidence level of the measurements.

Method

- Start IBM Statistical Package for the Social Sciences (SPSS) Statistics Version 26 (IBM, New York, USA).
- Make a new file and give it the following name: 'Statistical analysis of all models with a flow of 5.5 L/min'.
- First, go to the 'Variable View' tab at the bottom of the program.
- Add the following variables:
 - Researchers
 - Model_19mm
 - Model_15mm
 - Model_12mm
 - Model_9mm
- Set the decimals for the variable 'Researchers' to zero and for the models to one.
- Set the measure for the variable 'Researchers' to 'Ordinal' and for each of the models to 'Scale'.
- Add the following values to 'Researchers':
 - Value: 1, Label: A
 - Value: 2, Label: B
 - Value: 3, Label: C
 - Value: 4, Label: D
- Go to the 'Data View' tab at the bottom of the program.
- Put the measurements and the values of the researchers (see two steps back) in the program.

Paired-Samples T-Test

A Paired-Samples T-Test is done to compare the measurements between the different researchers.

- Go to 'Analyze' → 'Compare Means' → 'Paired-Samples T Test'
- Set the following Paired variables:
 - Pair 1, variable1: 'Model_19mm', variable2: 'Model_15mm'
 - Pair 2, variable1: 'Model_19mm', variable2: 'Model_12mm'
 - Pair 3, variable1: 'Model_19mm', variable2: 'Model_9mm'
 - Pair 4, variable1: 'Model_15mm', variable2: 'Model_12mm'
 - Pair 5, variable1: 'Model_15mm', variable2: 'Model_9mm'
 - Pair 6, variable1: 'Model_12mm', variable2: 'Model_9mm'
- Press 'OK'.

Figures

Histograms and boxplots can provide visual insight into the results.

- Go to 'Analyze' → 'Descriptive Statistics' → 'Explore'
- Set 'Model_19mm', 'Model_15mm', 'Model_12mm', and 'Model_9mm' as Dependent List and 'Researchers' as a factor.

- Set the Display to 'Both'.
- Go to 'Plots' → set Descriptive: Histogram, also set Normality plots with tests on → 'Continue'
- Press 'OK'.

One-way ANOVA

An one-way analysis of variance (ANOVA) test is done to do a statistical analysis of the inter- and intraobserver variability.

- Go to 'Analyze' → 'Compare Means' → 'One-way ANOVA'
- Set 'Model_19mm', 'Model_15mm', 'Model_12mm', and 'Model_9mm' as Dependent list and 'Researchers' as Factor
- Go to 'Post Hoc' → set Equal Variances assumed: Bonferroni → 'Continue'
- Go to 'Options' → set statistics: Descriptive, Fixed and random effects, also set Means plot on → 'Continue'
- Press 'OK'

Save the file. Make also files for the flows of 4 L/min and 6.2 L/min. Do the same test as with the 5.5 L/min.

Appendix XXII: Statistical analysis of the different models

In total, 96 measurements were done (table 1, 2, and 3). Four models were used with thicknesses of 19, 15, 12, and 9 mm. All the models were measured using a flow of 4.0 L/min, 5.5 L/min and 6.2 L/min. Every researcher performed three consecutive measurements in all the different situations.

Table 1: Left ventricular outflow tract pressure gradient (LVOT PG) values in mmHg for measurements of the left ventricle (LV) models with an interventricular septum thickness (IVSt) of 9, 12, 15, and 19 mm using a flow of 4.0 L/min.

Researcher	19mm	15mm	12mm	9mm
A	16.2	16.9	15.9	18.0
A	16.9	16.9	16.4	15.7
A	16.4	17.2	16.4	15.4
B	18.0	18.0	18.0	17.7
B	18.2	18.2	17.2	16.7
B	18.0	17.7	18.0	16.2
C	18.0	19.1	16.9	16.2
C	17.4	17.4	19.1	16.4
C	16.9	19.9	17.2	16.4
D	18.5	17.2	17.7	17.4
D	16.9	18.0	16.9	16.4
D	16.9	19.1	16.4	18.0
Average:	17.36±0.76	17.97±0.96	17.18±0.90	16.71±0.87

Table 2: LVOT PG values in mmHg for measurements of the LV models with an IVSt of 9, 12, 15, and 19 mm using a flow of 5.5 L/min.

Researcher	19mm	15mm	12mm	9mm
A	30.4	26.2	31.6	26.2
A	28.4	26.5	30.9	27.8
A	30.1	26.2	33.0	27.5

B	33.0	23.4	33.0	26.2
B	28.8	26.2	31.6	28.2
B	29.5	25.9	33.4	28.2
C	31.5	26.9	28.8	25.6
C	32.0	27.5	28.8	25.6
C	36.4	27.2	29.5	26.5
D	32.0	30.5	29.2	26.9
D	31.2	27.5	29.5	25.9
D	34.1	28.5	29.5	25.9
Average:	31.45±2.29	26.88±1.68	30.73±1.74	26.71±0.98

Table 3: LVOT PG values for measurements in mmHg of the LV models with an IVSt of 9, 12, 15, and 19 mm using a flow of 6.2 L/min.

Researcher	19mm	15mm	12mm	9mm
A	35.8	30.2	34.9	36.9
A	33.9	33.4	29.9	36.9
A	31.7	29.9	33.0	34.1
B	35.6	34.1	32.3	32.0
B	41.9	33.8	31.2	34.1
B	35.2	32.0	32.3	35.6
C	43.5	35.2	33.0	33.0
C	35.2	35.6	32.7	34.1
C	40.6	37.5	33.4	33.0

<i>D</i>	38.7	34.9	34.1	33.0
<i>D</i>	37.9	32.7	33.4	37.1
<i>D</i>	37.5	29.9	33.4	36.0
Average:	37.29±3.43	33.27±2.43	32.80±1.31	34.65±1.78

A statistical analysis is performed to prove if there is a statistically significant difference between the different models. Several situations are compared:

- LV models with an IVSt of 9, 12, 15, and 19 mm using a flow of 4.0 L/min
- LV models with an IVSt of 9, 12, 15, and 19 mm using a flow of 5.5 L/min
- LV models with an IVSt of 9, 12, 15, and 19 mm using a flow of 6.2 L/min

A paired sample T-test is performed for all situations a, b and c with a confidence interval of 95%.

Situation a

Looking at the results of the statistical analysis it can be concluded that a statistically significant difference can be found between the following models (figure 1) :

- LV models with an IVSt of 9 and 15 mm ($p=0.005$)

No statistically significant differences can be found between the other models:

- LV models with an IVSt of 9 and 12 mm ($p=0.235$)
- LV models with an IVSt of 9 and 19 mm ($p=0.066$)
- LV models with an IVSt of 12 and 15 mm ($p=0.062$)
- LV models with an IVSt of 12 and 19 mm ($p=0.409$)
- LV models with an IVSt of 15 and 19 mm ($p=0.096$)

Paired Samples Test									
		Paired Differences							
		Mean	Std. Deviation	Std. Error Mean	95% Confidence Interval of the Difference		t	df	Sig. (2-tailed)
					Lower	Upper			
Pair 1	Model_19mm - Model_15mm	-,6083	1,1572	,3340	-1,3436	,1269	-1,821	11	,096
Pair 2	Model_19mm - Model_12mm	,1833	,7396	,2135	-,2866	,6532	,859	11	,409
Pair 3	Model_19mm - Model_9mm	,6500	1,1017	,3180	-,0500	1,3500	2,044	11	,066
Pair 4	Model_15mm - Model_12mm	,7917	1,3222	,3817	-,0484	1,6317	2,074	11	,062
Pair 5	Model_15mm - Model_9mm	1,2583	1,2413	,3583	,4696	2,0470	3,512	11	,005
Pair 6	Model_12mm - Model_9mm	,4667	1,2858	,3712	-,3503	1,2836	1,257	11	,235

Figure 1: A paired sample T-test is performed to prove if there is a statistically significant difference between the LV models with an IVSt of 9, 12, 15, and 19 mm using a flow of 4.0 L/min.

The lack of statistically significant differences may partly be caused by a questionable normal distribution of the data. This can be concluded by looking at the kurtosis of the different measurements (table 4) and the Shapiro-Wilk test (figure 2). Data is normally distributed if the skewness and kurtosis

have a value between -1 and 1. The skewness indicates a normal distribution. The kurtosis shows a normal distribution for the LV models with an IVSt of 12 and 15 mm, however, not for the LV models with an IVSt of 9 and 19 mm. Therefore also a Shapiro-Wilk test is done (figure 2). By looking at the p-value it can be seen that for all models there is a normal distribution. So it is assumed that the data is normally distributed.

Table 4: The skewness and kurtosis of the statistical analysis of the LV models with an IVSt of 9, 12, 15, and 19 mm using a flow of 4.0 L/min.

IVSt of the LV model (mm)	Skewness	Kurtosis
9	0.331	1.041
12	0.730	0.390
15	0.808	-0.252
19	0.014	1.418

Tests of Normality

	Kolmogorov-Smirnov ^a			Shapiro-Wilk		
	Statistic	df	Sig.	Statistic	df	Sig.
Model_19mm	,227	12	,089	,913	12	,231
Model_15mm	,154	12	,200 [*]	,907	12	,197
Model_12mm	,156	12	,200 [*]	,944	12	,554
Model_9mm	,222	12	,106	,914	12	,237

*. This is a lower bound of the true significance.

a. Lilliefors Significance Correction

Figure 2: A test of normality is performed to determine if the data of the different models using a flow of 4 L/min is normally distributed.

Situation b

Looking at the results of the statistical analysis it can be concluded that a statistically significant difference can be found between the following models (figure 3) :

- LV models with an IVSt of 9 and 12 mm ($p < 0.001$)
- LV models with an IVSt of 9 and 19 mm ($p < 0.001$)
- LV models with an IVSt of 12 and 15 mm ($p = 0.001$)
- LV models with an IVSt of 15 and 19 mm ($p < 0.001$)

No statistically significant differences can be found between the other models:

- LV models with an IVSt of 9 and 15 mm ($p = 0.788$)
- LV models with an IVSt of 12 and 19 mm ($p = 0.485$)

Paired Samples Test									
		Paired Differences							
		Mean	Std. Deviation	Std. Error Mean	95% Confidence Interval of the Difference		t	df	Sig. (2-tailed)
					Lower	Upper			
Pair 1	Model_19mm - Model_15mm	4,5750	2,5320	,7309	2,9662	6,1838	6,259	11	,000
Pair 2	Model_19mm - Model_12mm	,7167	3,4380	,9925	-1,4677	2,9011	,722	11	,485
Pair 3	Model_19mm - Model_9mm	4,7417	2,9904	,8633	2,8416	6,6417	5,493	11	,000
Pair 4	Model_15mm - Model_12mm	-3,8583	3,1762	,9169	-5,8764	-1,8403	-4,208	11	,001
Pair 5	Model_15mm - Model_9mm	,1667	2,0943	,6046	-1,1640	1,4973	,276	11	,788
Pair 6	Model_12mm - Model_9mm	4,0250	1,3532	,3906	3,1652	4,8848	10,304	11	,000

Figure 3: A paired sample T-test is performed to prove if there is a statistically significant difference between the LV models with an IVSt of 9, 12, 15, and 19 mm using a flow of 5.5 L/min.

The lack of statistically significant differences may partly be caused by a questionable normal distribution of the data. This can be concluded by looking at the kurtosis of the different measurements (table 5). The skewness indicates a normal distribution. The kurtosis shows a normal distribution for the LV model with an IVSt of 19 mm, however, not for the LV models with an IVSt of 9, 12, and 15 mm. By looking at the p-value of the Shapiro-Wilk test, it can be seen that for all models there is a normal distribution (figure 4). So it is assumed that the data is normally distributed.

Table 5: The skewness and kurtosis of the statistical analysis of the LV models with an IVSt of 9, 12, 15, and 19 mm using a flow of 5.5 L/min.

IVSt of the LV model (mm)	Skewness	Kurtosis
9	0.504	1.380
12	0.412	-1.543
15	0.196	2.377
19	0.781	0.616

Tests of Normality

	Kolmogorov-Smirnov ^a			Shapiro-Wilk		
	Statistic	df	Sig.	Statistic	df	Sig.
19	,155	12	,200 [*]	,955	12	,718
15	,198	12	,200 [*]	,923	12	,315
12	,261	12	,024	,868	12	,061
9	,197	12	,200 [*]	,882	12	,093

This is a lower bound of the true significance.

Lilliefors Significance Correction

Figure 4: A test of normality is performed to determine if the data of the different models using a flow of 5.5 L/min is normally distributed.

Situation c

Looking at the results of the statistical analysis it can be concluded that a statistically significant difference can be found between the following models (figure 5) :

- LV models with an IVSt of 9 and 12 mm ($p=0.016$)
- LV models with an IVSt of 12 and 19 mm ($p=0.001$)
- LV models with an IVSt of 15 and 19 mm ($p=0.001$)

No statistically significant differences can be found between the other models:

- LV models with an IVSt of 9 and 15 mm ($p=0.231$)
- LV models with an IVSt of 9 and 19 mm ($p=0.061$)
- LV models with an IVSt of 12 and 15 mm ($p=0.593$)

Paired Samples Test

		Paired Differences					t	df	Sig. (2-tailed)
		Mean	Std. Deviation	Std. Error Mean	95% Confidence Interval of the Difference				
					Lower	Upper			
Pair 1	Model_19mm - Model_15mm	4,0250	2,9610	,8548	2,1437	5,9063	4,709	11	,001
Pair 2	Model_19mm - Model_12mm	4,4917	3,5259	1,0178	2,2514	6,7319	4,413	11	,001
Pair 3	Model_19mm - Model_9mm	2,6417	4,3775	1,2637	-,1397	5,4230	2,090	11	,061
Pair 4	Model_15mm - Model_12mm	,4667	2,9367	,8478	-1,3992	2,3326	,550	11	,593
Pair 5	Model_15mm - Model_9mm	-1,3833	3,7755	1,0899	-3,7822	1,0155	-1,269	11	,231
Pair 6	Model_12mm - Model_9mm	-1,8500	2,2625	,6531	-3,2875	-,4125	-2,832	11	,016

Figure 5: A paired sample T-test is performed to prove if there is a statistically significant difference between the LV models with an IVSt of 9, 12, 15, and 19 mm using a flow of 6.2 L/min.

The lack of statistically significant differences may partly be caused by a questionable normal distribution of the data. This can be concluded by looking at the kurtosis of the different measurements (table 6). However the skewness indicates a normal distribution. The kurtosis shows a normal distribution for the LV model with an IVSt of 12 and 19 mm, however, not for the LV models with an

IVSt of 9 and 15 mm. By looking at the p-value of the Shapiro-Wilk test, it can be seen that for all models there is a normal distribution (figure 6). So it is assumed that the data is normally distributed.

Table 6: The skewness and kurtosis of the statistical analysis of the LV models with an IVSt of 9, 12, 15, and 19 mm using a flow of 6.2 L/min.

IVSt of the LV model (mm)	Skewness	Kurtosis
9	0.158	-1.485
12	-0.050	-0.758
15	-0.815	1.401
19	0.367	0.383

Tests of Normality

	Kolmogorov-Smirnov ^a			Shapiro-Wilk		
	Statistic	df	Sig.	Statistic	df	Sig.
Model_19mm	,168	12	,200 [*]	,968	12	,891
Model_15mm	,147	12	,200 [*]	,947	12	,592
Model_12mm	,184	12	,200 [*]	,941	12	,510
Model_9mm	,205	12	,177	,903	12	,175

*. This is a lower bound of the true significance.

a. Lilliefors Significance Correction

Figure 6: A test of normality is performed. By looking at the Shapiro-Wilk test it can be determined if the data of the different models using a flow of 6.2 L/min is normally distributed.

Appendix XXIII: Statistical analysis of the inter- and intraobserver variability

A statistical analysis is performed to prove if there is inter- and intraobserver variability. Several situations are compared:

- Left ventricle (LV) models with an interventricular septum thickness (IVSt) of 9, 12, 15, and 19 mm using a flow of 4.0 L/min
- LV models with an IVSt of 9, 12, 15, and 19 mm using a flow of 5.5 L/min
- LV models with an IVSt of 9, 12, 15, and 19 mm using a flow of 6.2 L/min

An one-way analysis of variance (ANOVA) test is performed for all situations a, b and c with a confidence interval of 95%.

Situation a

Looking at the results of the statistical analysis it can be concluded that there is no statistically significant difference within groups (intraobserver variability) and between groups (interobserver variability) for all the LV models (figure 1) .

ANOVA						
		Sum of Squares	df	Mean Square	F	Sig.
Model_19mm	Between Groups	3,749	3	1,250	3,845	,057
	Within Groups	2,600	8	,325		
	Total	6,349	11			
Model_15mm	Between Groups	4,940	3	1,647	2,501	,133
	Within Groups	5,267	8	,658		
	Total	10,207	11			
Model_12mm	Between Groups	4,623	3	1,541	2,867	,104
	Within Groups	4,300	8	,538		
	Total	8,923	11			
Model_9mm	Between Groups	1,782	3	,594	,726	,564
	Within Groups	6,547	8	,818		
	Total	8,329	11			

Figure 1: An one-way ANOVA test is performed to prove if there is inter- and intraobserver variability between the LV models with an IVSt of 9, 12, 15, and 19 mm using a flow of 4.0 L/min.

Situation b

Looking at the results of the statistical analysis it can be concluded that there is no statistically significant difference within groups and between groups for the LV models with an IVSt of 9 and 19 mm (figure 2). It can be seen that there is a statistically significant difference for the LV models with an IVSt of 12 and 15 mm.

ANOVA						
		Sum of Squares	df	Mean Square	F	Sig.
Model_9mm	Between Groups	5,309	3	1,770	2,661	,119
	Within Groups	5,320	8	,665		
	Total	10,629	11			
Model_19mm	Between Groups	26,170	3	8,723	2,217	,164
	Within Groups	31,480	8	3,935		
	Total	57,650	11			
Model_15mm	Between Groups	21,569	3	7,190	5,971	,019
	Within Groups	9,633	8	1,204		
	Total	31,202	11			
Model_12mm	Between Groups	28,847	3	9,616	17,248	,001
	Within Groups	4,460	8	,558		
	Total	33,307	11			

Figure 2: An one-way ANOVA test is performed to prove if there is inter- and intraobserver variability between the LV models with an IVSt of 9, 12, 15, and 19 mm using a flow of 5.5 L/min.

Looking at the comparisons between the researchers of the LV model with an IVSt of 15 mm it can be concluded that researchers B and D show much interobserver variability (figure 3).

Multiple Comparisons

Dependent Variable: Model_15mm

Bonferroni

(I) Researcher	(J) Researcher	Mean Difference (I-J)	Std. Error	Sig.	95% Confidence Interval	
					Lower Bound	Upper Bound
A	B	1,1333	,8960	1,000	-1,984	4,250
	C	-,9000	,8960	1,000	-4,017	2,217
	D	-2,5333	,8960	,133	-5,650	,584
B	A	-1,1333	,8960	1,000	-4,250	1,984
	C	-2,0333	,8960	,318	-5,150	1,084
	D	-3,6667*	,8960	,021	-6,784	-,550
C	A	,9000	,8960	1,000	-2,217	4,017
	B	2,0333	,8960	,318	-1,084	5,150
	D	-1,6333	,8960	,635	-4,750	1,484
D	A	2,5333	,8960	,133	-,584	5,650
	B	3,6667*	,8960	,021	,550	6,784
	C	1,6333	,8960	,635	-1,484	4,750

The mean difference is significant at the 0.05 level.

Figure 3: The comparisons of results of the LV model with an IVSt of 15 mm between the different researchers: A, B, C, and D.

Looking at the comparisons between the researchers of the LV model with an IVSt of 12 mm it can be concluded that there is much interobserver variability between the researchers, except between the researchers A and B and the researchers C and D (figure 4).

Multiple Comparisons						
Dependent Variable: Model_12mm						
Bonferroni						
(I) Researcher	(J) Researcher	Mean Difference (I-J)	Std. Error	Sig.	95% Confidence Interval	
					Lower Bound	Upper Bound
A	B	-,8333	,6096	1,000	-2,954	1,288
	C	2,8000*	,6096	,011	,679	4,921
	D	2,4333*	,6096	,024	,312	4,554
B	A	,8333	,6096	1,000	-1,288	2,954
	C	3,6333*	,6096	,002	1,512	5,754
	D	3,2667*	,6096	,004	1,146	5,388
C	A	-2,8000*	,6096	,011	-4,921	-,679
	B	-3,6333*	,6096	,002	-5,754	-1,512
	D	-,3667	,6096	1,000	-2,488	1,754
D	A	-2,4333*	,6096	,024	-4,554	-,312
	B	-3,2667*	,6096	,004	-5,388	-1,146
	C	,3667	,6096	1,000	-1,754	2,488

The mean difference is significant at the 0.05 level.

Figure 4: The comparisons of results of the LV model with an IVSt of 12 mm between the different researchers: A, B, C, and D.

Situation c

Looking at the results of the statistical analysis it can be concluded that there is no statistically significant difference within groups and between groups for all LV models (figure 5).

ANOVA						
		Sum of Squares	df	Mean Square	F	Sig.
Model_19mm	Between Groups	56,829	3	18,943	2,079	,181
	Within Groups	72,900	8	9,112		
	Total	129,729	11			
Model_15mm	Between Groups	39,080	3	13,027	4,057	,050
	Within Groups	25,687	8	3,211		
	Total	64,767	11			
Model_12mm	Between Groups	4,620	3	1,540	,873	,494
	Within Groups	14,120	8	1,765		
	Total	18,740	11			
Model_9mm	Between Groups	13,370	3	4,457	1,652	,253
	Within Groups	21,580	8	2,698		
	Total	34,950	11			

Figure 5: An one-way ANOVA test is performed to prove if there is inter- and intraobserver variability between the LV models with an IVSt of 9, 12, 15, and 19 mm using a flow of 6.2 L/min.

A graphic visual of the inter- and intraobserver variability for the different situations is given below (figure 6).



Figure 6: The different measurements done by different researchers and the 95% CI. a. Using a flow of 4.0 L/min b. Using a flow of 5.5 L/min. c. Using a flow of 6 L/min.

Bibliography

- [1] Moore KL, Agur AMR, Dalley AF. Clinically Oriented Anatomy. 7th ed. Philadelphia: Lippincott Williams & Wilkins; 2013.
- [2] Agur AMR, Dalley AF. Grant's Atlas of Anatomy, 13th Edition. 13th ed. Philadelphia: Lippincott Williams & Wilkins; 2012.
- [3] El Missiri AM, El Meniawy KAL, Sakr SAS, Mohamed ASE. Normal reference values of echocardiographic measurements in young Egyptian adults. *The Egyptian Heart Journal* 2016;68:209–15. <https://doi.org/10.1016/j.ehj.2016.01.002>.
- [4] Minette MS, Sahn DJ. Ventricular septal defects. *Circulation* 2006;114:2190–7. <https://doi.org/10.1161/CIRCULATIONAHA.106.618124>.
- [5] Park IS, Goo HW. Ventricular septal defect (VSD). In: Park IS, editor. *An illustrated guide to congenital heart disease: from diagnosis to treatment – from fetus to adult*, Singapore: Springer Singapore; 2019, p. 33–56. https://doi.org/10.1007/978-981-13-6978-0_3.
- [6] Saman S JS. Cardiac system 1: anatomy and physiology. *Nursing Times* 2018;114:34–7.
- [7] King J, Lowery DR. Physiology, Cardiac Output. StatPearls, Treasure Island (FL): StatPearls Publishing; 2020.
- [8] Pappano AJ, Gil Wier W. Hemodynamics. *Cardiovascular Physiology*, Elsevier; 2013, p. 119–34. <https://doi.org/10.1016/B978-0-323-08697-4.00006-X>.
- [9] Rodríguez Muñoz D, Moya Mur JL, Moreno J, Fernández-Golfín C, Franco E, Monteagudo JM, et al. Energy dissipation in resynchronization therapy: impact of atrioventricular delay. *J Am Soc Echocardiogr* 2019;32:744-754.e1. <https://doi.org/10.1016/j.echo.2019.01.018>.
- [10] Badeer HS. Hemodynamics for medical students. *Adv Physiol Educ* 2001;25:44–52. <https://doi.org/10.1152/advances.2001.25.1.44>.
- [11] Zhang JXJ, Hoshino K. Microfluidics and micro total analytical systems. *Molecular sensors and nanodevices*, Elsevier; 2014, p. 103–68. <https://doi.org/10.1016/B978-1-4557-7631-3.00003-X>.
- [12] Harris P, Kuppurao L. Quantitative Doppler echocardiography. *BJA Educ* 2015;mkv015. <https://doi.org/10.1093/bjaceaccp/mkv015>.
- [13] Raj MA, Ranka S, Goyal A. Hypertrophic Obstructive Cardiomyopathy. StatPearls, Treasure Island (FL): StatPearls Publishing; 2021.
- [14] Nishimura RA, Seggewiss H, Schaff HV. Hypertrophic obstructive cardiomyopathy: surgical myectomy and septal ablation. *Circ Res* 2017;121:771–83. <https://doi.org/10.1161/CIRCRESAHA.116.309348>.
- [15] Varma PK, Neema PK. Hypertrophic cardiomyopathy: part 1 - introduction, pathology and pathophysiology. *Ann Card Anaesth* 2014;17:118–24. <https://doi.org/10.4103/0971-9784.129841>.
- [16] Hughes SE. The pathology of hypertrophic cardiomyopathy. *Histopathology* 2004;44:412–27. <https://doi.org/10.1111/j.1365-2559.2004.01835.x>.
- [17] Mayo Clinic. Hypertrophic cardiomyopathy 2020. <https://www.mayoclinic.org/diseases-conditions/hypertrophic-cardiomyopathy/symptoms-causes/syc-20350198> (accessed May 4, 2021).
- [18] Wigle ED, Henderson M, Rakowski H, Wilansky S. Muscular (hypertrophic) subaortic stenosis (hypertrophic obstructive cardiomyopathy): the evidence for true obstruction to left ventricular outflow. *Postgrad Med J* 1986;62:531–6. <https://doi.org/10.1136/pgmj.62.728.531>.
- [19] Elliott PM, Anastasakis A, Borger MA, Borggrefe M, Cecchi F, Charron P, et al. 2014 ESC

- Guidelines on diagnosis and management of hypertrophic cardiomyopathy: the Task Force for the Diagnosis and Management of Hypertrophic Cardiomyopathy of the European Society of Cardiology (ESC). *Eur Heart J* 2014;35:2733–79. <https://doi.org/10.1093/eurheartj/ehu284>.
- [20] Ghosh S, Avari JN, Rhee EK, Woodard PK, Rudy Y. Hypertrophic cardiomyopathy with preexcitation: insights from noninvasive electrocardiographic imaging (ECGI) and catheter mapping. *J Cardiovasc Electrophysiol* 2008;19:1215–7. <https://doi.org/10.1111/j.1540-8167.2008.01203.x>.
- [21] Finocchiaro G, Sheikh N, Biagini E, Papadakis M, Maurizi N, Sinagra G, et al. The electrocardiogram in the diagnosis and management of patients with hypertrophic cardiomyopathy. *Heart Rhythm* 2020;17:142–51. <https://doi.org/10.1016/j.hrthm.2019.07.019>.
- [22] Wigle ED. Cardiomyopathy: The diagnosis of hypertrophic cardiomyopathy. *Heart* 2001;86:709–14. <https://doi.org/10.1136/heart.86.6.709>.
- [23] Healio. Hypertrophic Obstructive Cardiomyopathy (HOCM) ECG (Example 1) 2017. <https://www.healio.com/cardiology/learn-the-heart/ecg-review/ecg-archive/hypertrophic-obstructive-cardiomyopathy-hocm-ecg-example-1> (accessed May 4, 2021).
- [24] Parato VM, Antoncicchi V, Sozzi F, Marazia S, Zito A, Maiello M, et al. Echocardiographic diagnosis of the different phenotypes of hypertrophic cardiomyopathy. *Cardiovasc Ultrasound* 2016;14:30. <https://doi.org/10.1186/s12947-016-0072-5>.
- [25] Losi M-A, Nistri S, Galderisi M, Betocchi S, Cecchi F, Olivetto I, et al. Echocardiography in patients with hypertrophic cardiomyopathy: usefulness of old and new techniques in the diagnosis and pathophysiological assessment. *Cardiovasc Ultrasound* 2010;8:7. <https://doi.org/10.1186/1476-7120-8-7>.
- [26] Kwon SH, Gopal AS. 3D and 4D ultrasound: current progress and future perspectives. *Curr Cardiovasc Imaging Rep* 2017;10:43. <https://doi.org/10.1007/s12410-017-9440-2>.
- [27] Nampiaparampil RG, Swistel DG, Schlame M, Saric M, Sherrid MV. Intraoperative Two- and Three-Dimensional Transesophageal Echocardiography in Combined Myectomy-Mitral Operations for Hypertrophic Cardiomyopathy. *J Am Soc Echocardiogr* 2018;31:275–88. <https://doi.org/10.1016/j.echo.2017.11.016>.
- [28] Haland TF, Edvardsen T. The role of echocardiography in management of hypertrophic cardiomyopathy. *J Echocardiogr* 2019;18:77–85. <https://doi.org/10.1007/s12574-019-00454-9>.
- [29] Amano Y, Kitamura M, Takano H, Yanagisawa F, Tachi M, Suzuki Y, et al. Cardiac MR imaging of hypertrophic cardiomyopathy: techniques, findings, and clinical relevance. *Magn Reson Med Sci* 2018;17:120–31. <https://doi.org/10.2463/mrms.rev.2017-0145>.
- [30] Gregor P, Čurila K. Medical treatment of hypertrophic cardiomyopathy - What do we know about it today? *Cor Vasa* 2015;57:e219–24. <https://doi.org/10.1016/j.crvasa.2015.02.003>.
- [31] Fifer MA. Choice of septal reduction therapies and alcohol septal ablation. *Cardiol Clin* 2019;37:83–93. <https://doi.org/10.1016/j.ccl.2018.08.009>.
- [32] Schurmann P, Peñalver J, Valderrábano M. Ethanol for the treatment of cardiac arrhythmias. *Curr Opin Cardiol* 2015;30:333–43. <https://doi.org/10.1097/HCO.0000000000000183>.
- [33] Panza JA, Naidu SS, editors. Hypertrophic Cardiomyopathy, An Issue of Cardiology Clinics, E-book - Srihari S. Naidu, Julio A Panza - Google Boeken. 2019.
- [34] Afanasyev AV, Bogachev-Prokophiev AV, Kashtanov MG, Astapov DA, Zalesov AS, Budagaev SA, et al. Myectomy versus alcohol septal ablation in patients with hypertrophic obstructive cardiomyopathy. *Interact Cardiovasc Thorac Surg* 2020;31:158–65. <https://doi.org/10.1093/icvts/ivaa075>.
- [35] Lakkis NM, Nagueh SF, Dunn JK, Killip D, Spencer WH. Nonsurgical septal reduction therapy

- for hypertrophic obstructive cardiomyopathy: one-year follow-up. *J Am Coll Cardiol* 2000;36:852–5. [https://doi.org/10.1016/s0735-1097\(00\)00767-1](https://doi.org/10.1016/s0735-1097(00)00767-1).
- [36] van der Lee C. Hypertrofische cardiomyopathie . *Cordiaal* 2007;4–8.
- [37] de Jong PL. Myectomy en mitralisklep reparatie n.d. <https://www.erasmusmc.nl/nl-nl/patientenzorg/operaties/myectomy-en-mitralisklep-reparatie> (accessed May 1, 2021).
- [38] Song B, Dong R. Comparison of modified with classic morrow septal myectomy in treating hypertrophic obstructive cardiomyopathy. *Medicine (Baltimore)* 2016;95:e2326. <https://doi.org/10.1097/MD.0000000000002326>.
- [39] Ralph-Edwards A, Vanderlaan RD, Bajona P. Transaortic septal myectomy: techniques and pitfalls. *Ann Cardiothorac Surg* 2017;6:410–5. <https://doi.org/10.21037/acs.2017.07.08>.
- [40] Andrushchuk U, Adzintsou V, Niavyhlas A, Model H, Ostrovsky Y. Early results of optimal septal myectomy using 3-dimensional printed models. *Kardiochir Torakochirurgia Pol* 2019;16:74–80. <https://doi.org/10.5114/kitp.2019.86359>.
- [41] Septal Myectomy 2019. <https://my.clevelandclinic.org/health/treatments/17461-septal-myectomy> (accessed May 2, 2021).
- [42] Douglas JS. Current state of the roles of alcohol septal ablation and surgical myectomy in the treatment of hypertrophic obstructive cardiomyopathy. *Cardiovasc Diagn Ther* 2020;10:36–44. <https://doi.org/10.21037/cdt.2019.07.02>.
- [43] Sherrid MV, Chaudhry FA, Swistel DG. Obstructive hypertrophic cardiomyopathy: echocardiography, pathophysiology, and the continuing evolution of surgery for obstruction. *Ann Thorac Surg* 2003;75:620–32. [https://doi.org/10.1016/s0003-4975\(02\)04546-0](https://doi.org/10.1016/s0003-4975(02)04546-0).
- [44] Evangelista A, Flachskampf FA, Erbel R, Antonini-Canterin F, Vlachopoulos C, Rocchi G, et al. Echocardiography in aortic diseases: EAE recommendations for clinical practice. *Eur J Echocardiogr* 2010;11:645–58. <https://doi.org/10.1093/ejechocard/jeq056>.
- [45] Talreja DR, Nishimura RA, Edwards WD, Valeti US, Ommen SR, Tajik AJ, et al. Alcohol septal ablation versus surgical septal myectomy: comparison of effects on atrioventricular conduction tissue. *J Am Coll Cardiol* 2004;44:2329–32. <https://doi.org/10.1016/j.jacc.2004.09.036>.
- [46] Singh V, Badheka AO, Bokhari SS, Ghersin E, Clark PM, O'Neill WW. Retrograde percutaneous closure of a ventricular septal defect after myectomy for hypertrophic obstructive cardiomyopathy. *Tex Heart Inst J* 2013;40:468–71.
- [47] Kim JH. Tips for Successful Septal Myectomy in Patients with Hypertrophic Cardiomyopathy. *Korean J Thorac Cardiovasc Surg* 2018;51:227–30. <https://doi.org/10.5090/kjtcs.2018.51.3.227>.
- [48] Kuk M, Mitsouras D, Dill KE, Rybicki FJ, Dwivedi G. 3D Printing from Cardiac Computed Tomography for Procedural Planning. *Curr Cardiovasc Imaging Rep* 2017;10:21. <https://doi.org/10.1007/s12410-017-9420-6>.
- [49] Hermesen JL, Burke TM, Seslar SP, Owens DS, Ripley BA, Mokadam NA, et al. Scan, plan, print, practice, perform: Development and use of a patient-specific 3-dimensional printed model in adult cardiac surgery. *J Thorac Cardiovasc Surg* 2017;153:132–40. <https://doi.org/10.1016/j.jtcvs.2016.08.007>.
- [50] Wang Y, Guo H, Wang S, Lai Y. Effectiveness of a patient-specific 3-dimensional printed model in Septal Myectomy of hypertrophic cardiomyopathy. *Pak J Med Sci Q* 2020;36:1678–82. <https://doi.org/10.12669/pjms.36.7.2620>.
- [51] Adhyapak SM. *Hypertrophic Cardiomyopathy: A Practical Guide to Diagnosis and Management* . CRC Press; 2021.
- [52] Menon PG, Rao PV, Adhyapak SM, Yuanchang O, Weeks R. Virtual surgical myectomy as a planning tool for obstructive hypertrophic cardiomyopathy. *J Cardiovasc Magn Reson* 2016;18.

- <https://doi.org/10.1186/1532-429X-18-S1-P46>.
- [53] Füzesi K, Gyöngy M. Comparison of two inexpensive rapid prototyping methods for manufacturing filament target ultrasound phantoms. *Ultrasound Med Biol* 2017;43:712–20. <https://doi.org/10.1016/j.ultrasmedbio.2016.11.006>.
 - [54] Kumar N, Wirekoh J, Saba S, Riviere CN, Park Y-L. Soft miniaturized actuation and sensing units for dynamic force control of cardiac ablation catheters. *Soft Robotics* 2021;8:59–70. <https://doi.org/10.1089/soro.2019.0011>.
 - [55] Holmes III D, Rettmann M, Cameron B, Camp J, Robb R. Developing patient-specific anatomic models for validation of cardiac ablation guidance procedures. In: Miga MI, Cleary KR, editors. *Medical Imaging 2008: Visualization, Image-guided Procedures, and Modeling*, vol. 6918, SPIE; 2008, p. 69181W. <https://doi.org/10.1117/12.773215>.
 - [56] Sasaki K, Kuniyama T, Kasegawa H, Seki M, Seki H, Takada J, et al. Aortic root geometry following valve-sparing root replacement with reimplantation or remodeling: experimental investigation under static continuous pressure. *J Artif Organs* 2021;24:245–53. <https://doi.org/10.1007/s10047-020-01242-4>.
 - [57] Aghababaei A, Kashefi A, Hexamer M. A drive mechanism for a blood pump integrated in an oxygenator. *Current Directions in Biomedical Engineering* 2018;4:45–8. <https://doi.org/10.1515/cdbme-2018-0012>.
 - [58] Mascherbauer J, Schima H, Rosenhek R, Czerny M, Maurer G, Baumgartner H. Value and limitations of aortic valve resistance with particular consideration of low flow-low gradient aortic stenosis: an in vitro study. *Eur Heart J* 2004;25:787–93. <https://doi.org/10.1016/j.ehj.2004.02.011>.
 - [59] Ostadfar A. Biofluid flow in artificial, assistive and implantable devices. *Biofluid Mechanics*, Elsevier; 2016, p. 205–42. <https://doi.org/10.1016/B978-0-12-802408-9.00005-3>.
 - [60] Operation principles of Centrifugal pumps? – Mechanical Engineering n.d. <https://mechaengineerings.wordpress.com/2015/05/14/centrifugal-pumps/> (accessed June 20, 2021).
 - [61] Hoving AM, de Vries EE, Mikhal J, de Borst GJ, Slump CH. A systematic review for the design of in vitro flow studies of the carotid artery bifurcation. *Cardiovasc Eng Technol* 2020;11:111–27. <https://doi.org/10.1007/s13239-019-00448-9>.
 - [62] Anavekar NS, Oh JK. Doppler echocardiography: a contemporary review. *J Cardiol* 2009;54:347–58. <https://doi.org/10.1016/j.jjcc.2009.10.001>.
 - [63] Borazjani I, Westerdale J, McMahon EM, Rajaraman PK, Heys JJ, Belohlavek M. Left ventricular flow analysis: recent advances in numerical methods and applications in cardiac ultrasound. *Comput Math Methods Med* 2013;2013:395081. <https://doi.org/10.1155/2013/395081>.
 - [64] Allen BD, Choudhury L, Barker AJ, van Ooij P, Collins JD, Bonow RO, et al. Three-dimensional haemodynamics in patients with obstructive and non-obstructive hypertrophic cardiomyopathy assessed by cardiac magnetic resonance. *Eur Heart J Cardiovasc Imaging* 2015;16:29–36. <https://doi.org/10.1093/ehjci/jeu146>.
 - [65] End-Diastolic Volume Index - Cardiac MRI n.d. <https://www.cardiacmri.com/analysis-guide/lv-function/end-diastolic-volume/> (accessed June 12, 2021).
 - [66] Myocardial protection and cardioplegia | Thoracic Key n.d. <https://thoracickey.com/myocardial-protection-and-cardioplegia/> (accessed June 12, 2021).
 - [67] Semsarian C, French J, Trent RJ, Richmond DR, Jeremy RW. The natural history of left ventricular wall thickening in hypertrophic cardiomyopathy. *Aust N Z J Med* 1997;27:51–8. <https://doi.org/10.1111/j.1445-5994.1997.tb00914.x>.

- [68] Redondo E, Ng S, Muñoz J, Pumera M. Tailoring capacitance of 3D-printed graphene electrodes by carbonisation temperature. *Nanoscale* 2020;12:19673–80. <https://doi.org/10.1039/d0nr04864j>.
- [69] Peel B, Voyer-Nguyen P, Honjo O, Yoo S-J, Hussein N. Development of a dynamic Chest Wall and operating table simulator to enhance congenital heart surgery simulation. *3D Print Med* 2020;6:12. <https://doi.org/10.1186/s41205-020-00067-4>.
- [70] Dragon Skin™ 10 NV Product Information | Smooth-On, Inc. n.d. <https://www.smooth-on.com/products/dragon-skin-10-nv/> (accessed June 12, 2021).
- [71] Riedle H, Molz P, Franke J. Determination of the mechanical properties of cardiac tissue for 3D printed surgical models. 2018 IEEE-EMBS Conference on Biomedical Engineering and Sciences (IECBES), IEEE; 2018, p. 171–6. <https://doi.org/10.1109/IECBES.2018.8626728>.
- [72] Hiesinger W, Brukman MJ, McCormick RC, Fitzpatrick JR, Frederick JR, Yang EC, et al. Myocardial tissue elastic properties determined by atomic force microscopy after stromal cell-derived factor 1 α angiogenic therapy for acute myocardial infarction in a murine model. *J Thorac Cardiovasc Surg* 2012;143:962–6. <https://doi.org/10.1016/j.jtcvs.2011.12.028>.
- [73] Iliina A, Lasso A, Jolley MA, Wohler B, Nguyen A, Scanlan A, et al. Patient-specific pediatric silicone heart valve models based on 3D ultrasound. *Proc SPIE* 2017;10135. <https://doi.org/10.1117/12.2255849>.
- [74] Elenkov M, Ecker P, Lukitsch B, Janeczek C, Harasek M, Gföhler M. Estimation Methods for Viscosity, Flow Rate and Pressure from Pump-Motor Assembly Parameters. *Sensors* 2020;20. <https://doi.org/10.3390/s20051451>.
- [75] Saczkowski R, Maklin M, Mesana T, Boodhwani M, Ruel M. Centrifugal pump and roller pump in adult cardiac surgery: a meta-analysis of randomized controlled trials. *Artif Organs* 2012;36:668–76. <https://doi.org/10.1111/j.1525-1594.2012.01497.x>.
- [76] Critoph CH, Patel V, Mist B, Elliott PM. Cardiac output response and peripheral oxygen extraction during exercise among symptomatic hypertrophic cardiomyopathy patients with and without left ventricular outflow tract obstruction. *Heart* 2014;100:639–46. <https://doi.org/10.1136/heartjnl-2013-304914>.
- [77] Cristancho D, Delgado D, Martínez F, Fakhree M, Jouyban A. Volumetric properties of glycerol + water mixtures at several temperatures and correlation with the Jouyban-Acree model. *Rev Colomb Cienc Quim Farm* [Online] 2011;40:92–115.
- [78] Cardiac Output | Michigan Medicine n.d. <https://www.uofmhealth.org/health-library/tx4080abc> (accessed June 12, 2021).
- [79] Formlabs. Form 3 2021. <https://formlabs.com/eu/3d-printers/form-3/> (accessed June 17, 2021).
- [80] 3D Printer Solutions. Ultimaker S5 2021. <https://www.3dprintersolutions.nl/ultimaker-s5.html> (accessed June 17, 2021).
- [81] Bennett SC. Mechanical circulatory support in lung transplantation: Cardiopulmonary bypass, extracorporeal life support, and ex-vivo lung perfusion. *World J Respirol* 2015;5:78. <https://doi.org/10.5320/wjr.v5.i2.78>.
- [82] MAQUET GG. Pompen . HL 30 V2.3, Gebruiksaanwijzing. NL-09, Rastatt Germany: MAQUET Cardiopulmonary AG; 2012, p. 25–45.
- [83] Ritchi AC. Extracorporeal Artificial Organs. *Biomaterials Science*, Elsevier; 2013, p. 827–41. <https://doi.org/10.1016/B978-0-08-087780-8.00072-3>.
- [84] Centrifugal pumps - IB Pompen n.d. <https://ib-pompen.nl/products/centrifugal-pumps/> (accessed June 20, 2021).
- [85] Geske JB, Cullen MW, Sorajja P, Ommen SR, Nishimura RA. Assessment of left ventricular

outflow gradient: hypertrophic cardiomyopathy versus aortic valvular stenosis. *JACC Cardiovasc Interv* 2012;5:675–81. <https://doi.org/10.1016/j.jcin.2012.01.026>.

- [86] Mandeş L, Roşca M, Ciupercă D, Popescu BA. The role of echocardiography for diagnosis and prognostic stratification in hypertrophic cardiomyopathy. *J Echocardiogr* 2020;18:137–48. <https://doi.org/10.1007/s12574-020-00467-9>.
- [87] Weissler-Snir A, Crean A, Rakowski H. The role of imaging in the diagnosis and management of hypertrophic cardiomyopathy. *Expert Rev Cardiovasc Ther* 2016;14:51–74. <https://doi.org/10.1586/14779072.2016.1113130>.

